Master Thesis Report

Lifting Gantries: A Study On The Structural Behaviour & Design Method

May 29, 2016

Author

Steven Oomen MSc.

Graduation Committee

Prof. Dr. M. Veljkovic	TU Delft
Dr. Ir. M.A.N. Hendriks	TU Delft
Dr. Ir. R. Abspoel	TU Delft
Ir. L.J.M. Houben	TU Delft
Dr. Ir. M. Cristutiu	Mammoet
Ir. W. de Jong	Mammoet

Preface

This report contains my master thesis, the final stage of the Master's programme Civil Engineering at Delft University of Technology. I carried out the research project in conjunction with Mammoet, a leading company in engineered heavy lifting and transport services. The subject of the thesis is related to lifting gantries, a piece of equipment frequently used by Mammoet and well suited for a study in the area of interest of my master track Structural Engineering.

During the project I had a lot of support. I would like to thank my committee members affiliated with the university, Prof. Dr. M. Veljkovic, Dr. Ir. M.A.N. Hendriks and Dr. Ir. R. Abspoel, for their guidance during our meetings. Also, I would like to thank my colleagues at Mammoet for their support. Special gratitude goes out to Dr. Ir. M. Cristutiu, Ir. W. de Jong and and Ir. L. Oorschot for their time and efforts regarding my thesis.

Steven Oomen,
Delft, May 29, 2016

Abstract

Several topics related to lifting gantries have been studied. These are the modelling of the structure, the structural behaviour of the gantry, the input parameters of the model and the standards used for the design. A hand calculation model, based on the analysis of built-up compression members in EN 1993-1-1, has been developed that describes the behaviour of a portal like gantry structure. The model executes geometrically non-linear calculations, that take into account the second order effects from the deformation of the gantry, and determines the resistance of the gantry based on the axial forces in its chords and on stability checks. Three different mast sections, out of which the gantry columns are made, have been investigated: MSG, DS and NYW. The latter is currently under developed by Mammoet and is called a New York Wheel mast section. The focus is on the application of this section type.

The gantry in the model is subject to a vertical load from the self-weight of the mast sections, a vertical load from the weight of the payload and a horizontal point load at the top of the gantry. The latter accounts for operational loads and wind loads on both the structure and the payload. In the model the horizontal load is expressed as a percentage of the weight of the payload.

The resistances obtained from the hand calculation model are within 5% of the resistances obtained from a numerical benchmark model, for the gantry configurations considered. Therefore, the model is considered accurate enough for a preliminary design. It is able to represent a rigid and a flexible foundations, as well as a hinged and a rigid connection between the columns and beam(s) of the gantry.

From the calculations with the hand calculation model several conclusions were drawn. The horizontal load is of large influence for the maximum payload, much larger than the influence of the global imperfection. The difference can easily be between 10-to-30% for the NYW mast sections, between 2% and 4% horizontal load. Also, the influence is larger for a gantry with a rigid beam-column connection than for a hinged connection. Calculating with a different imperfection, for example no imperfection instead of 1/250 of the gantry height, result in a 6-to-10% resistance difference.

The resistance of a gantry with a rigid connection at the top is considerably larger than for a hinged connection, for an asymmetric section like the NYW mast sections. A rigid connection yields a 1.5 to 4 times higher resistance than a hinged connection, when NYW sections are used on a rigid foundation.

The resistance for the three mast section types under consideration has been compared for a rigid foundation. It turns out that for both a hinged and a rigid beam-column connection the NYW sections can bear the highest payload, by far. The resistance to tensile forces, mostly governed by the strength of the connections, is much lower for the MSG sections than for the DS sections. Also, a rigid connection significantly improves the asymmetrical DS sections. For relevant gantry heights the MSG sections can bear a payload that is roughly 50% of the payload that the DS sections can carry, for a hinged top connection. For a rigid connection it is around 30%. The DS sections can carry 15-to-25% of the load the NYW sections can carry, for a hinged connection. For a rigid connection it is 25-to-35%.

The stiffness of the foundation has been modelled with the method of Pais and Kausel (1988). It appeared that the stiffness of the foundation can have a significant influence on the resistance of the

gantry. The MSG sections are more susceptible to a flexible foundation, because of their relatively small base frame. This results in a much smaller rotational stiffness at the bottom of the gantry columns. A foundation on dense sand leads to a resistance decrease around 5% for the NYW sections and around 35% for the MSG sections.

One of the goals of this thesis was to incorporate the use of guy lines into the model and to investigate their influence on stability, stiffness and ultimately resistance. A preliminary study showed great potential for the use of guy lines. The buckling length can be reduced by around 50%, almost to the point where a column with a fixed end at the top is resembled. Also, the first order deflection can be reduced significantly, as over 75% of the horizontal load is taken by the guy lines. This means that the second order effects are drastically reduced. The reduction also has a positive effect on the first order bending moments in the column. A guy line that is installed under a 60° angle with the foundation turns out to be effective in both supporting the column and minimizing the gantry footprint.

The behaviour of guy lines is highly non-linear. Therefore, it was found challenging to incorporate them in the final hand calculation model accurately. However, the evidence from the preliminary design leads to the recommendation to further investigate the application of guy lines.

Several standards have been studied for the design of the gantry. It was concluded that the European crane standard EN 13001-1 is best suited to take into account the loads on the structure and that the structural behaviour of the gantry is best described using the European building standard EN 1993-1-1.

The global imperfection of the gantry is a parameter of interest. Mammoet wants to calculate with an imperfection that equals one thousandth of the height of the gantry, since they believe their gantries can be erected with such high precision. The standards under consideration prescribe a larger imperfection, typically 1/500. The fabrication and erection tolerances are however much tighter for the mast sections than provided by the standards. Therefore, a smaller imperfection (1/1000) can be justified, except for very tall gantries and gantries in storm conditions.

The horizontal load on the gantry varies between 2.5% and 4% of the weight of the payload, depending on the direction, the weight of the payload and whether or not skidding of the load is involved. A larger portion of the horizontal load comes from wind loads, of which the load on the object to be lifted is a substantial part. It is therefore recommended to further investigate the wind load.

Contents

List of Figures

List of Tables

List of Abbreviations

Abbreviation	Meaning
AISC	American Institute of Steel Construction
ANSI	American National Standards Institute
ASCE	American Society of Civil Engineers
ASD	Allowable Stress Design
CDF	Cumulative Density Function
CEN	European Committee of Standardization
DS	Double Stacked mast sections
EN	Series of 10 European standards (1990-1999)
FEM	Finite Element Method
KNMI	The Royal Netherlands Meteorological Institute
LRFD	Load and Resistance Factor Design
MSG	Mammoet Sliding Gantry mast sections
NEN	NEderlandse Norm
NYW	New York Wheel mast sections
PDF	Probability Density Function
RHS	Rectangular Hollow Section
SEI	Structural Engineering Institute
Te	Metric tonnes
ULS	Ultimate Limit State

List of Symbols

Symbol	Unit	Description	Standard
α	$^\circ$	Strand angle	
Δ	m	Gantry deflection (for tailing)	
η_i	m	Lateral displacement due to imperfections	
λ	m/s	Weibull scale parameter	
ν	-	Poisson ratio	
Φ	rad	Rotation	
σ	N/mm^2	Prestress level	
B	m	Foundation width	
d	m	Offlead	
D_i	m	Centre-to-centre distance of the mast section chords	
E	kN/m^2	Young's modulus	
E_{eff}	kN/m^2	Effective Young's modulus	
EI	kNm^2	Flexural stiffness	
F_{cr}	kN	Elastic critical buckling force	
F_H	kN	Horizontal load	
F_V	kN	Vertical load	
F_w	kN	Wind on payload	
f_y	kN/m^2	Yield strength	
G	kN	Self-weight	
G	-	Shear modulus	
H	m	Gantry height	

Symbol	Unit	Description	Standard
$H_{w,\%}$	%	Wind on payload as a percentage of the payload mass	
H_s / $H_{strands}$	m	Length of the strands (for tailing)	
k	-	Weibull shape parameter	
k	kN/m	Gantry stiffness (for tailing)	
k_r	kNm/rad	Rotational stiffness	
k_{yy} / k_{zz}	kNm/rad	Rotational stiffness of foundation	
k_s	kN/m	Strand stiffness	
L	m	Foundation length	
L	m	Horizontal strand span	
L_1	-	Load group 1: 0 to 1600 Te	
L_2	-	Load group 2: 1600 to 2400 Te	
L_3	-	Load group 3: 2400 to 3200 Te	
L_s	m	Strand length	
n	-	Number of strands	
N_{chord}	kN	Axial force in the chord	
$N_{Rd,c}$	kN	Compression resistance	
$N_{Rd,t}$	kN	Tension resistance	
q	kN/m	Distributed load	
Q	kN	Total distributed load	
S_v	kN	Shear stiffness	
w	N/mm^3	Unit weight of strands	
x	-	Ratio of horizontal over vertical load	
χ_{LT}	-	Lateral torsional buckling coefficient	EN 199-
α	-	Imperfection factor	EN 199-
$\bar{\lambda}$	-	non-dimensional slenderness	EN 199-
χ	-	Flexural buckling coefficient	EN 199-
δ_i	m	First order lateral deflection of the gantry	EN 199-
γ_{M1}	-	Material resistance factor	EN 199-
γ_G	-	Self-weight load factor	EN 199-
γ_Q	-	Variable load factor	EN 199-
Φ	-	factor that depends on imperfection factor and slenderness	EN 199-
A	m^2	Cross-sectional surface	EN 199-
C_m	-	Modification factor	EN 199-
k_{zy} / k_{yz}	-	Interaction factors	EN 199-
M_{Ed}	kNm	Design moment	EN 199-
M_{Rk}	kNm	Characteristic moment resistance	EN 199-
n	-	Elastic instability factor	EN 199-
N_{cr}	kN	Elastic critical buckling force	EN 199-
N_{Ed}	kN	Design normal force	EN 199-
N_{Rk}	kN	Characteristic normal force resistance	EN 199-
W	m^3	Section modulus	EN 199-
R_u	*	Required strength	ANSI/AISC
R_n	*	Nominal strength	ANSI/AISC
α	-	ASD/LRFD force level adjustment factor	ANSI/AISC
β	-	Initial out-of-plumbness factor	ANSI/AISC
Δ	m	Nodes out of place	ANSI/AISC

Symbol	Unit	Description	Standard
δ	m	Member out of straightness	ANSI/AISC
ϕ	-	Resistance factor	ANSI/AISC
τ_b	-	Stiffness reduction parameter	ANSI/AISC
B_1	-	Multiplier to account for P-Δ effects	ANSI/AISC
B_2	-	Multiplier to account for P-δ effects	ANSI/AISC
D	kN	Dead load	ANSI/AISC
EI^*	kNm^2	Reduced flexural stiffness	ANSI/AISC
K_1	-	Buckling length factor	ANSI/AISC
L	kN	Live load	ANSI/AISC
L_H	kN	Horizontal load	ANSI/AISC
L_V	kN	Vertical load	ANSI/AISC
M_{lt}	kNm	First order moment due to lateral translation only	ANSI/AISC
M_{nt}	kNm	First order moment while structure restraint against lateral translation	ANSI/AISC
M_c	kNm	Moment resistance	ANSI/AISC
M_r	kNm	Required moment resistance	ANSI/AISC
N_i	kN	Notional load at level i	ANSI/AISC
P_{el}	kN	Elastic critical buckling force	ANSI/AISC
P_{lt}	kN	First order axial force due to lateral translation only	ANSI/AISC
P_{nt}	kN	First order axial force while restraint against lateral translation	ANSI/AISC
P_c	kN	Normal force resistance	ANSI/AISC
P_r	kN	Required normal force resistance	ANSI/AISC
Y_i	kN	Gravity load at level i	ANSI/AISC
$\bar{v}$	m/s	10 min. Average wind speed	EN 1300-
$q_w(z)$	N/m^2	Wind pressure	EN 1300-
$v(z)$	m/s	3 second gust wind speed	EN 1300-
z	m	Altitude	EN 1300-

***** Multiple units possible

EN 199- Refers to Eurocode (EN 1990[2]), Eurocode 1 (EN 1991[3]) and Eurocode 3 (EN 1993[5],[6])

EN 1300- - Refers to the European crane safety standards[8]

ANSI/AISC Refers to the US steel structures standards ANSI/AISC 360-10[12]

1 Introduction

Lifting gantries are, often temporary, structures consisting of masts and beams used for the lifting and installing of heavy loads. In this thesis, very tall and slender gantries are considered (Figure 1). Due to this geometry and these heavy loads, over 100 meter high and lifting several thousands of tonnes, gantries exhibit a very specific structural behaviour. A gantry is used when a crane does not suffice, which could be due to the available space or because the load is too large or too heavy.

(a) Image **(b)** Schematisation

Figure 1: An example of a lifting gantry structure (Mammoet).

The research in this thesis report has been carried out in association with Mammoet, a Dutch company specialized in heavy lifting. It operates world wide, executing operations on land and on water. At Mammoet lifting gantries are used quite often, mainly for the installation and removal of heavy vessels (e.g. reactors, absorbers, condensers, crackers), for companies in the petrochemical industry. The gantries are made out of mast sections and beams. Currently, a couple of mast section types are used to build gantries, the most common of which is the Mammoet Sliding Gantry (MSG) type. As Mammoet is seeking to enlarge its lifting capabilities, a new type of sections is under development, called the New York Wheel (NYW) mast section. This type will also be used in the erection of a giant ferris wheel in New York City, hence the name. The main focus in this thesis report is on the application of both these sections. Although, the use of so called Double Stacked (DS) sections, from Mammoet's largest crane, is considered as well.

In order to analyze the behaviour of the gantry, a hand calculation model is developed. The aim is to be

able to determine the resistance of the gantry for a preliminary design, with this model. As the gantry is very tall and slender, the structural stability and deformations are of great importance. These deformations play a major role in second order effects. Parameters of interest are, among others, the global imperfection of the gantry columns and the horizontal forces on the structure. Also, the influence of the stiffness of the foundation on which the gantry is placed, as well as the connection between columns and gantry beam are analyzed. In order to increase stability and stiffness, guy lines can be attached to the gantry. These are prestressed steel cables connected to both the structure, at a certain height, and an anchor point at foundation level. The influence of such structural elements is also considered.

Another central topic of this thesis is the way standards deal with gantries. A lifting gantry looks like a structure, but it carries out tasks like a crane. Also, as the structure is very slender, one could argue that it acts like a tower or a mast. Therefore, different engineers use different engineering standards and different clients demand the use of different standards. The standards on crane safety (EN 13001-series[9]), the general design rules and rules for buildings for steel structures (EN 1993-1-1[5]) and the steel structures design rules for towers, masts and chimneys (EN 1993-3[6]) could all be used for the design of a gantry in Europe. As Mammoet is planning to use some of the equipment under consideration in this thesis in the United States as well, it also of interest to look at the American standard on steel structures (ANSI/AISC 360-10[12]).

Therefore, part of the research focuses on the different design methods in these standards and the ideas behind them.

1.1 Literature

Previously, a "study on the load carrying capacity of unguyed gantry systems"[24] was carried out. The columns of the gantries in the thesis were made of MSG mast sections. Multiple configurations were analyzed for a range of gantry heights, using finite element calculations, and a rigid connection between columns and beam was selected to be the best way to improve the resistance of the gantry. The thesis report served as an inspiration for the configurations of the gantry models and for the hand calculation models in this thesis.

For the development of the hand calculation models the critical buckling load was essential. A reader on elastic stability of structure of Hartsuijker and Welleman[20] has been instrumental in determining the (approximate) elastic buckling loads. Timoshenko and Gere[21] have written a world renowned book on elastic stability as well, that gives insight in the stability of structures. The stiffness of the foundation has been incorporated in the hand calculation model by means of the "Approximate formulas for dynamic stiffnesses of rigid foundations" of Pais and Kausel (1988[18]). Soil properties for this stiffness have been taken from "Design of Steel Structures" by Subramanian (2011[17]).

Several sources have been used for the analysis of the lateral loads on the gantry in Section 6. The basis of design[16] for Mammoet's PTC DS crane served as a starting point for the analysis. An article on "Wind Speed Over Short Periods of Time" by Durst (1960[25]) and a master thesis report by Rodenburg (2015[23]) were considered for the wind load calculations.

Furthermore, multiple European and American standards were considered, for the design of the gantry. More details on these standards are given in Section 8.

1.2 Research Objectives

The objectives of this thesis can be divided into three major parts. The first is related to the model development, while the second part concerns the structural behaviour of the gantry. The last part is about the input of the model and the standards under consideration. Three standard based hand calculation models are developed. Their performance is tested using a benchmark model, based on finite element calculations. This model is thought to represent reality well enough to serve as a benchmark for the other models. One standard based model is chosen to go forward with, to describe the structural behaviour of the gantry.

Model

- How well do the hand calculation methods under consideration perform, when compared to the benchmark model? Which method is most suitable to go forward with?
- How well do the results from the final hand calculation model resemble those from the benchmark model?

Gantry Behaviour

- How large is the influence of the amount of horizontal loading on the allowable payload?
- How large is the influence of the global imperfection on the allowable payload?
- How large is the influence of the foundation stiffness on the allowable payload?
- How large is the difference in allowable payload between the NYW, MSG and DS sections?
- How does the type of beam-column connection influence the allowable payload?
- Can the model take into account the application of guy lines? What is the contribution of these guy lines to the stability and stiffness of the gantry?

Model Input & Standards

- How do the different standards deal with the loads on the structure?
- What global imperfection is prescribed by the standards and what is a realistic imperfection for the gantry columns?
- What are realistic horizontal loads, related to the load that is lifted by the gantry, and what are the major contributors to the horizontal load on the structure?

1.3 Structure of the Report

The flowchart in Figure 2 shows the structure of the remainder of this report. After the introduction, the set-up and components of the gantry are explained in Section 2. Section 3 treats four different models. These have been developed to describe the structural behaviour of the gantry structure. The first two hand calculation models are based on the Eurocode. The third hand calculation model is based on the American ANSI/AISC standard. The fourth and last model is a numerical model and serves as a reference, to see how the three hand calculation models perform. From the results in this section, one model is chosen to go forward with.

Section 4 describes this model in detail, as well as the benchmark model, and in Section 5 the results are discussed. Two important input parameters for the model are the horizontal load that acts on the gantry and the global initial imperfection of the structure. Both play a significant role in the second order deflections and bending moments. In Section 6 the horizontal load is discussed, while Section 7 treats the imperfection. The differences between the standards treated in the thesis are discussed in Section 8. In Section 9 the application of guy lines and its influence on the structural behaviour of the gantry are treated.

Conclusions are drawn in Section 10 and recommendations given in Section 11. Finally, a list of references and the appendices to the report can be found.

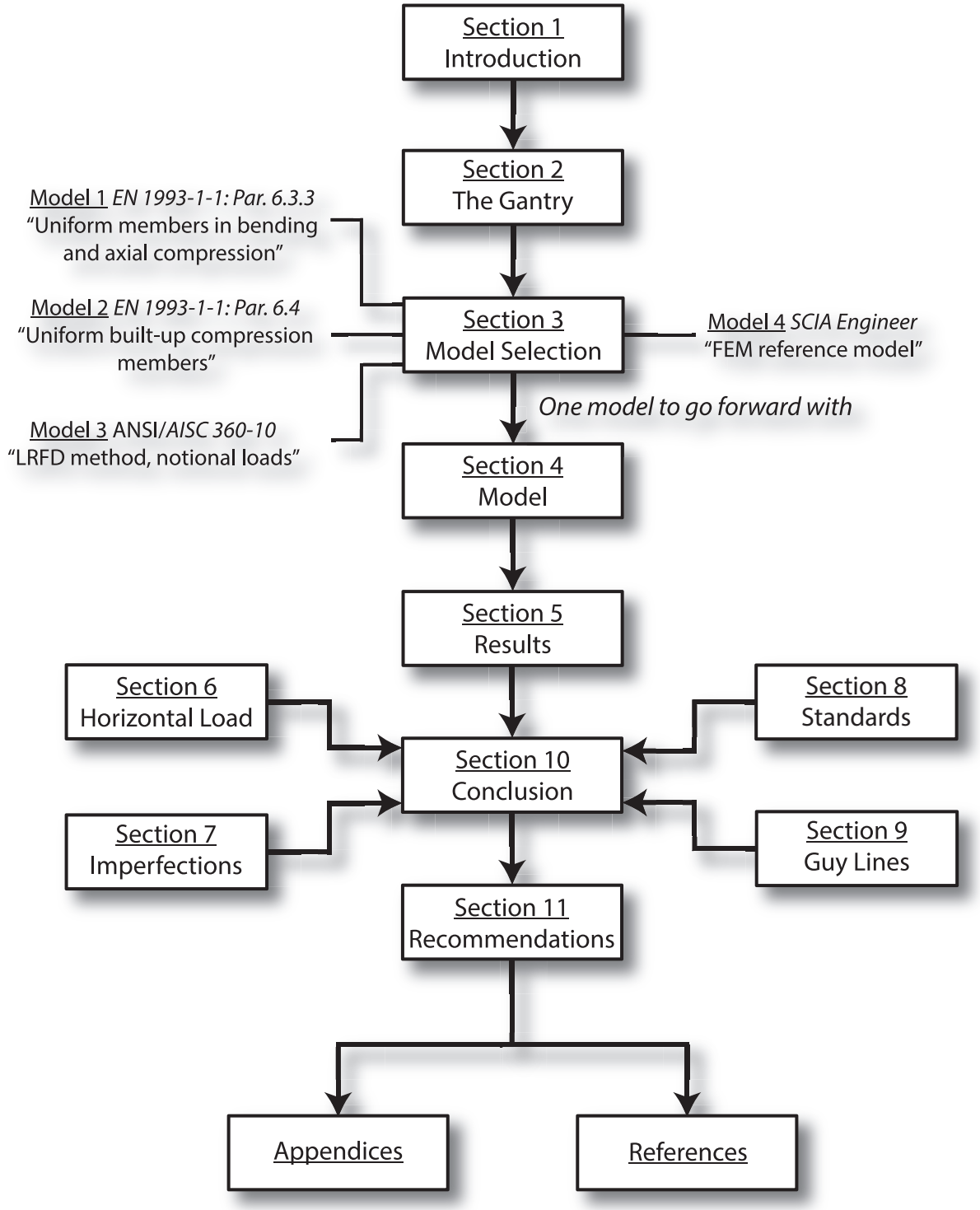

Figure 2: Flowchart of the report structure.

2 The Gantry

Lifting gantries are used in many different configurations and in numerous different situations. A distinction is made between three-dimensional, frame like gantries (Figure 3a) and two-dimensional gantries that look like a simple portal structure (Figure 3b). The subject of this thesis is the portal like gantry. This section treats the pieces of equipment that together form the gantry. In Section 2.1 the structure is described and the different components are listed. In the subsequent sections these components are discussed in more detail.

(a) 3D gantry **(b)** Portal gantry

Figure 3: Gantry layouts (Mammoet).

2.1 Structure

A sketch of the gantry is shown in Figure 4, while Figure 5 shows several details of the structure. The

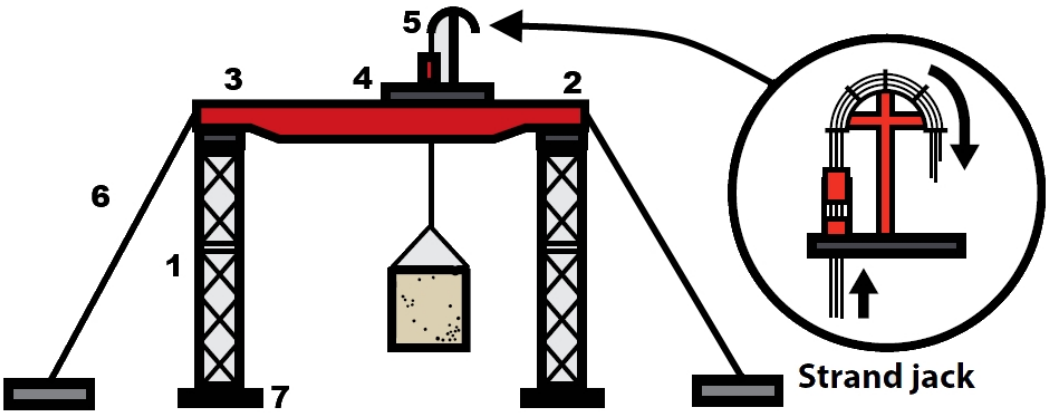

Figure 4: Gantry structure (Mammoet).

gantry columns, made out of mast sections, are indicated with [1]. The gantry beam is denoted by [3] and the connection between column and beam by [2]. Such an interface is shown in Figure 5c. Gantries are possibly equipped with a skidding system [4], on top of the gantry beam, that enables the horizontal shift of the payload that hangs from the gantry. An example of such a system, on top of gantry beams, is shown in Figure 5b. On top of the beam or this skidding system strand jacks [5] are placed to lift the

load (Figure 5a). In order to increase the lifting capabilities of the gantry, guy lines [6] might be included in its design. Figure 5d shows the application of guy lines at the top of the gantry, while Figure 5f shows the foundation of a guy. The foundation of the gantry [7] is another topic of interest. Figure 5e shows a base frame of a gantry column, on top of a concrete foundation slab.

(a) Strand jacks

(b) Skidding system

(c) Mast-beam interface

(d) Guy line

(e) Mast foundation

(f) Guy foundation

Figure 5: Gantry parts (Mammoet).

Gantries typically lift very heavy and tall loads, like reactors and vessels. These objects are installed into, or removed from, a vertical position, while transported horizontally. For the transition from one orientation to the other, equipment is used to aid the gantry. This can be done with an assist crane

(Figure 6a), using SPMT (Self-Propelled Modular Transporter) units (Figure 6b), or using a second gantry structure on top of a skidding system. All of these are able to tail the load, such that the transition is realized without introducing too much horizontal forces.

(a) Using a crane.

(b) Using SPMT's with a tailframe.

Figure 6: Manners of tailing the lift load (Mammoet).

2.2 Mast Sections

The gantry masts are built out of mast sections, stacked on top of each other. The three types are discussed hereafter.

2.2.1 Mammoet Sliding Gantry (MSG)

The MSG mast sections (Figure 7) are widely used within Mammoet to build lifting gantries. The chords ([1] in Figure 7) are made out of S690 Q quality steel, whereas the other members are of S355 J2H. Member [2] is a RHS 140 x 140 x 7.1 profile, [3] is a RHS 140 x 140 x 5 profile and the cross-section of member [4] is a RHS 100 x 100 x 8. The outer dimensions of the cross-section of the mast section measure 2430 mm by 2570 mm, while a section is 5700 mm long. One section weighs 7.1 metric tonnes. The sections are pinned together using coupling blocks.

2.2.2 Double Stacked (DS)

The second section under consideration is the DS (Double Stacked) mast section. The section has four rectangular chords ([1] in Figure 8) (300 x 340 x 25 mm) of steel grade S690 QL. All members indicated with [2] are made of RSH 140 x 140 x 7.1 profiles and of steel grade S355 J2H. The members in the plane of the cross-section that are indicated by [3] are of the RHS 100 x 100 x 6.3 type and of steel grade S355 J2H. The section is 11400 millimeters long and has a 4300 by 2130 millimeter cross-section. It weighs 17 Te. The DS sections are used in the boom of Mammoet's largest ring crane, but could also be used in a gantry.

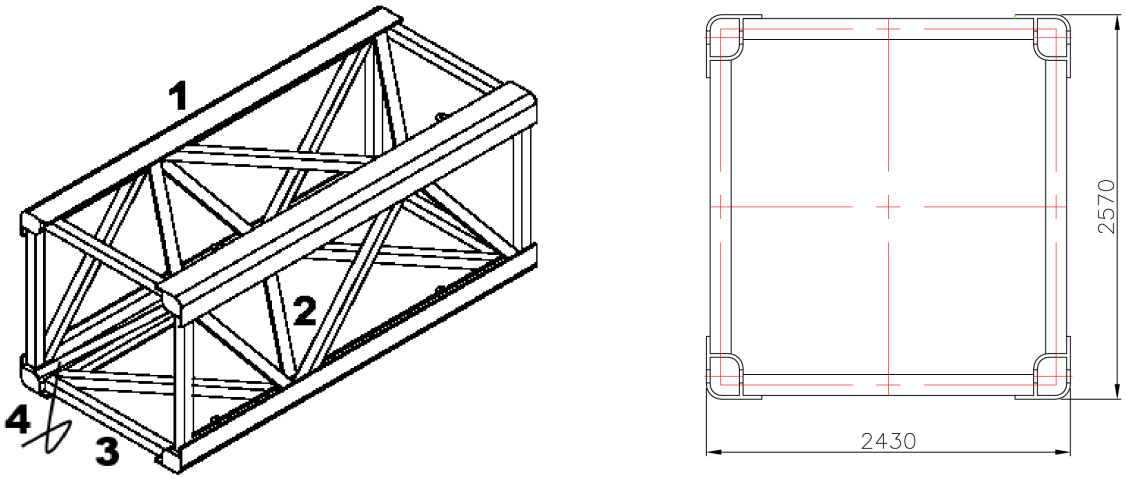

Figure 7: MSG mast section (Mammoet).

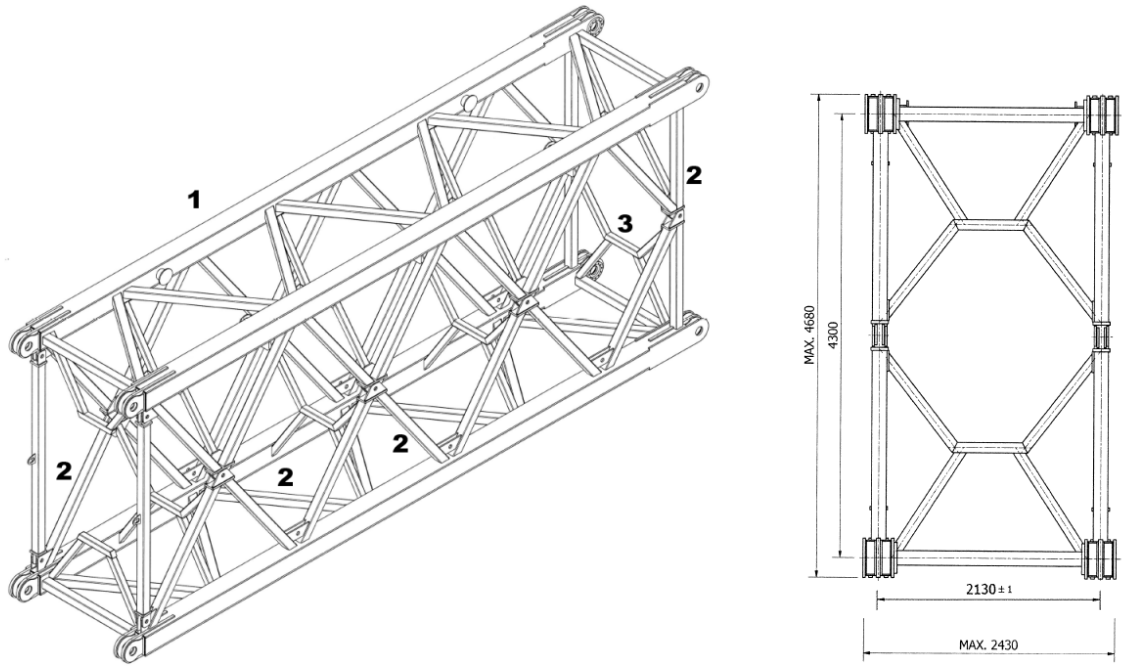

Figure 8: DS mast section (Mammoet).

2.2.3 New York Wheel (NYW)

In addition to the MSG and DS sections, there is a new section type under development by Mammoet, called the New York Wheel mast section. This section is 11800 millimeters long (11000 mm center to center distance between the holes at chord ends) and has a 8000 by 4000 millimeter cross-section. One mast section weighs around 39 metric tonnes. All members in this truss frame are linked using pinned connections. The chords, indicated with [1] in Figure 9, are square hollow sections (400 x 400 x 30 mm) and made of steel grade S690 QL. This means that it is quenched and tempered steel, suitable for low temperature environments and with a minimum yield strength of 690 N/mm^2. Member [2] in Figure 9 is a tubular section with diameter 323.9 mm and thickness 10 mm, steel grade S355 J2H. The same holds

for [5]. Diagonal members like the one indicated with [3] in Figure 9 are tubular members with diameter 323.9 mm and thickness 12.5 mm, steel grade S355 J2H. This also holds for [6]. Member [4] is a tubular section with diameter 273 mm, thickness 10 mm and steel grade S355 J2H.

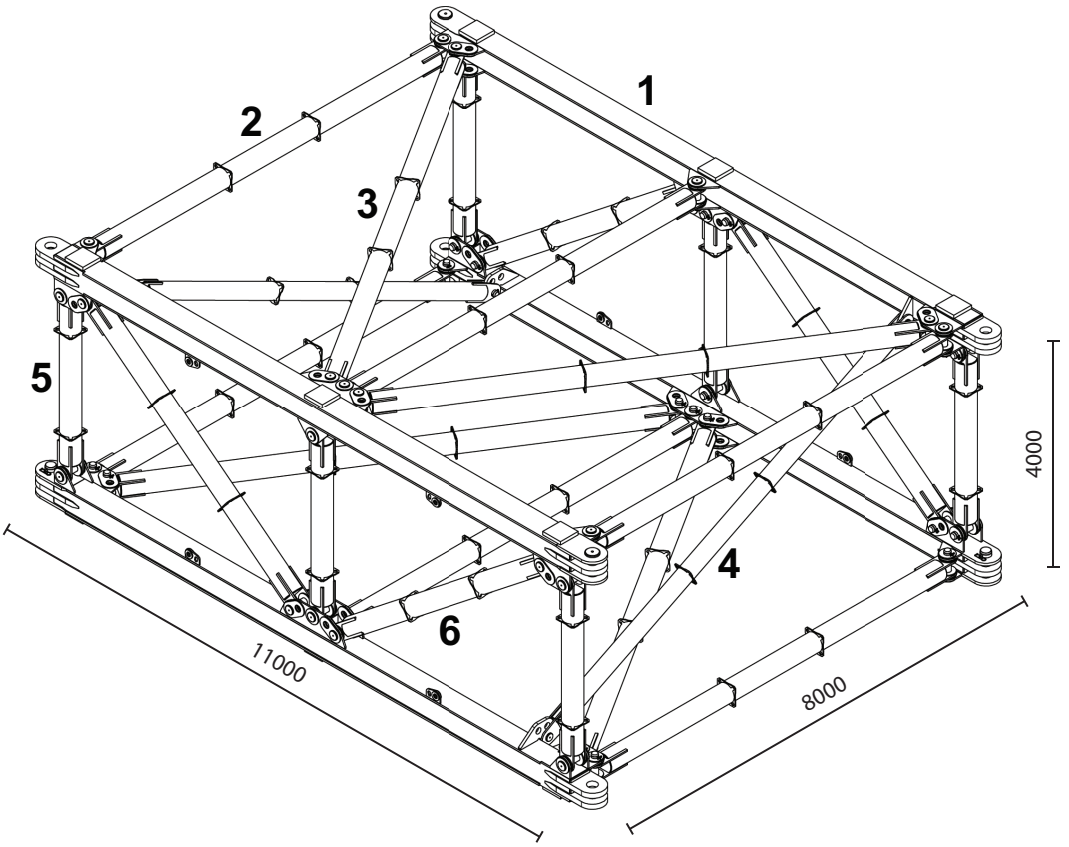

Figure 9: New York Wheel mast section (Mammoet).

2.3 Gantry Beam

A beam is placed on top of the columns and connected to them. The dimensions of the top beam depend, among other things, on the required span of the gantry and the lift load. It is therefore in this thesis assumed that the beam suffices and its weight, as it varies with the dimensions of the beam, is not taken into account. **This weight should thus be subtracted from the maximum load the gantry can lift.** Care should be taken with the load factors, since the self-weight of the beam and the payload are factored differently. Therefore, a simple subtraction is not possible. Of course, if one wants the top connection to provide rotational stiffness the properties of the top beam are of importance. The finite element calculations are carried out with a gantry beam that is currently under development by Mammoet and is to be used in combination with the New York Wheel mast sections. Again, its weight is not included, but its stiffness is. The approximate moment of inertia for bending around the strong axis of this beam equals 1.78 m^4 and 0.34 m^4 over the weak axis. The gantry beam under development roughly weighs 200 Te, for a reasonable length. A beam that is often used in combination with the MSG mast sections weighs roughly 100 Te.

2.4 Column-Beam-Connection

As indicated earlier in the report, the connections between the masts and the top beam ([2] in Figure 4) are usually executed in such a way that they can be regarded as hinged connections. This ensures that the top bending moments in the mast sections are as small as possible. However, it also limits the stiffness and stability of the structure. Therefore, the situation where these connections provide a non-zero rotational stiffness is also investigated.

2.5 Base Frame & Foundation

A base frame is used to transfer the loads in the bottom mast section to the foundation. The dimensions of this base frame are of importance for the rotational stiffness at the bottom of a gantry column. The influence of the foundation stiffness is discussed in Section 4.1.1, where the rotational stiffness at the bottom of the column is related to the soil stiffness and the footprint of the base frame. The base frame considered for the MSG sections is the frame of type 1 in Appendix A.1 and has a footprint of 4710 by 2730 mm. For the New York Wheel sections a 20 x 10 m base frame is under development. For the DS sections no base frame is used within this thesis. That means that no calculations are executed for a gantry from DS sections on a flexible foundation.

2.6 Guy Lines & Strand Jacks

The load is lifted by means of strand jacks (Figure 5a), a hydraulic lifting device. The load is carried by multiple strand wires, clamped by two gripping heads. A hydraulic cylinder moves one head with respect to the other, lifting the load. Strand jack systems are also used as guy lines. Strand wires are connected to both the top of the gantry and the foundation. These strands are then prestressed, forming flexible lateral supports for the gantry columns.

Appendices A.2, A.3 and A.4 show the properties of the three strand jack systems considered in this thesis, for the realization of guy lines. The maximum load in the system, as well as the properties of and the number of strands is shown.

2.7 Skidding System

Sometimes the lift is carried out next to the final position of the load. Using a skidding system on top of the gantry beam, the load is then shifted sidewards. The strand jacks rest on top of this system, that uses a hydraulic push-pull cylinder to move a skidshoe over a skidtrack. The skid actions can introduce extra horizontal forces. In some cases the system is even placed underneath the gantry itself to be able to shift the whole structure. That situation is not considered within this thesis.

3 Hand Calculation Models

The purpose of this section is to compare three hand calculation models with a reference model, to determine which model to go forward with and to find out how well this model resembles the behaviour of the gantry system. A typical gantry layout, with two cantilever columns, a gantry beam on top and a hinged beam-column connection (Figure 10 (a)), is investigated. The resistance is calculated for an ultimate limit state (ULS) situation. A horizontal load in only one direction, one of the two principal directions of the mast sections, is considered. This means that the model considers bending over either the strong or the weak axis of the mast section. For the gantry in Figure 10 (a), with a hinged connection at the top, the weak axis is always governing.

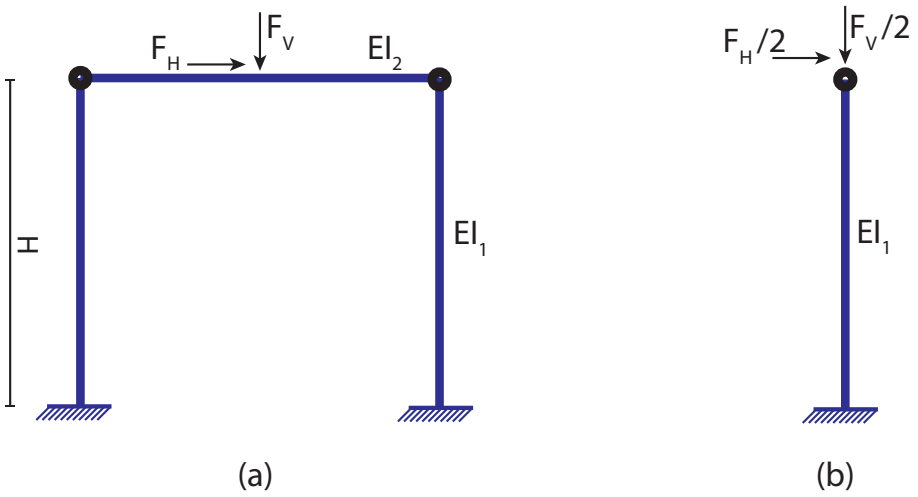

Figure 10: Structural gantry model and simplified column model.

The live load, as well as the horizontal load, is considered to be applied in the middle of the top beam. Thus 50% of both loads is carried by every column. The bending moments and normal forces in a column (Figure 10 (b)) are calculated.

The governing situation is considered the situation where the gantry is susceptible to its self-weight, to the live load and to a horizontal load. The self weight is taken from the weight of the respective sections. The horizontal load is considered to cover possible tailing and skidding loads, as well as wind loads, and is expressed as percentage of the live load. The partial safety factors to be used in the load combination depend on the calculation method that is used. In addition, the imperfection of the column is taken into account.

The mast sections discussed in Section 2 are considered in the study. Section 3.1 deals with the stiffness of the mast sections, while the models are presented in Section 3.2. Results are discussed in Section 3.3 and the model selection in Section 3.4.

3.1 Column Stiffness

The stiffness of the mast sections is an important input parameter for the models. Therefore, the theoretical bending and shear stiffness have been calculated for the three mast sections under consideration.

The deflections of a free standing column subject to a horizontal load have been calculated with these stiffnesses and compared to the deflections from finite element calculations in SCIA Engineer[15]. In this software package the mast sections have been modelled with their actual members. It turned out that the shear stiffness needs not to be taken into account in a preliminary design, since its influence is relatively small. The stiffness is based on the moment of inertia of the chords of the sections. The analysis is carried out in Appendix B.

3.2 Design Verification

In Section 3.2.1 a ULS check for a simple column according to EN 1993-1-1 is carried out. In Section 3.2.2 a check for Build-up Compression Members from EN 1993-1-1 is performed. The third method, in Section 3.2.3, uses the direct analysis approach from the American AISC standard. The fourth and last method considers a second order non-linear analysis using the software package SCIA Engineer[15], as explained in Section 3.2.4.

3.2.1 Method 1: EN 1993-1-1, Paragraph 6.3.3

This method relies on the buckling resistance analysis for single members in bending and axial compression, in section 6.3.3 of EN 1993-1-1 (equation 6.61 and 6.62). As the chords are closed hollow sections, the sections are not susceptible to lateral torsional buckling. Therefore χ_{LT} equals one. The cross-section is class 3, which means that ΔM_{Ed} is zero. Only one direction is considered at a time, such that the interaction factors k_{zy} and k_{yz} can be set to zero. This leaves the design check formulated in Equation 1, that performs a check in the cross-section just above ground level and is used for both directions. N_{Ed} is the design compression force and N_{Rk} the characteristic resistance against compression, defined as the product of the cross-sectional surface and the yield strength $A \times f_y$.

$$\frac{N_{Ed}}{\chi N_{Rk}/\gamma_{M1}} + k\frac{M_{Ed}}{\chi_{LT} M_{Rk}/\gamma_{M1}} \leq 1 \tag{1}$$

The partial factor for resistance of members to instability assessed by member checks γ_{M1} is equal to one. The design value of the bending moment M_{Ed} is based on a first order calculation that takes into account the influence of imperfections, in accordance with the Eurocode. The first order moment, determined in the undeformed state, is as shown in Equation 2.

$$M_{Ed} = F_H H + F_V \eta_1 + G\eta_2 = F_V x H + F_V \eta_1 + G\eta_2 \tag{2}$$

In this equation F_H and F_V represent the horizontal and vertical force at the top of the column, H is the gantry height and G is the total self-weight of the column. The imperfections at the top and in the middle of the column are indicated with η_1 and η_2 respectively. The design compression force N_{Ed} equals the sum of the factored vertical load F_V and self-weight G. M_{Rk} is the product of section modulus and yield strength $W \times f_y$. The interaction factor k should be determined using either one of the two methods given in the standard. The method in Appendix B of EN 1993-1-1 is chosen. This means Equation 3 should be used.

$$k = C_m\Big(1 + 0.6\bar{\lambda}\frac{N_{Ed}}{\chi N_{Rk}/\gamma_{M1}}\Big) \leq \Big(1 + 0.6\frac{N_{Ed}}{\chi N_{Rk}/\gamma_{M1}}\Big) \tag{3}$$

In this equation C_m is roughly 0.6, since the moment at the bottom is much larger than at the top. The reduction factor for flexural buckling χ is defined in Equation 4.

$$\chi = \frac{1}{\Phi + \sqrt{\Phi^2 - \bar{\lambda}^2}} \ \ with \ \ \chi \leq 1 \tag{4}$$

The factors in this equation are as follows:

$$\Phi = 0.5[1 + \alpha(\bar{\lambda} - 0.2) + \bar{\lambda}^2] \tag{5}$$

$$\bar{\lambda} = \sqrt{\frac{Af_y}{N_{cr}}} \ \ for\ class\ 1, 2, 3\ cross\text{-}sections, \tag{6}$$

where α is an imperfection factor that depends on the applicable buckling curve and the critical elastic buckling force. The buckling length for the structure under consideration is two times the column height. In accordance with table 6.2 of EN 1993-1-1, buckling curve c is chosen, for welded box sections with relatively thick welds. This table is meant for single member, not for built-up members. Curve c was chosen, since the chords of the mast sections are welded boxes with thick welds. The crane standard, EN-13001-3[11], comes to the same buckling curve.

The design normal force and bending moment are obtained by multiplying the characteristic loads with the partial safety factors. The self-weight load factor is 1.35 and the live load factor, that is thus also applied to the horizontal load, equals 1.5. The factors are obtained from EN 1990 Table NB.4 - A1.2(B).

Apart from the design validation check in Equation 1, the stability of the column is assessed. Therefore, the combined effect of the load at the top and the self-weight of the column is considered. The critical elastic buckling force for a point load at the top of the column in Figure 10 (b) is $F_{cr} = 2.46 \times EI/H^2$ and $Q_{cr} = 8.30 \times EI/H^2$ for a distributed load q that equals Q/H. This means that the buckling force is 3.17 times higher for the distributed load. Therefore, the stability check in Equation 7 is carried out. The critical elastic buckling force for the distributed load is derived in Appendix D.2 (Model a), for the point load in Appendix D.3 (Model a).

$$F_V + \frac{G}{3.17} \leq \frac{2.46 \times EI}{H^2} \tag{7}$$

Where the influence of the self-weight is reduced by the factor 3.17. This is allowed since the critical Euler buckling forces are obtained from a linear differential equation, allowing for superposition of the loads. The check considers the combined effect of the payload and the self-weight in the column.

3.2.2 Method 2: Built-up Compression Members from EN 1993-1-1

In section 6.4 of Eurocode 3 EN 1993-1-1 a method for ultimate limit state calculations on uniform built-up compression members is presented. The column is then considered as a two-dimensional truss model in the direction under consideration (Figure 11). The horizontal force is again a percentage of the vertical force, through the parameter x. The design value of the bending moment M_{Ed} in the bottom of the column is based on a second order calculation. The second order bending moment is presented in Equation 8. The first term represents the first order bending moment due to the horizontal load.

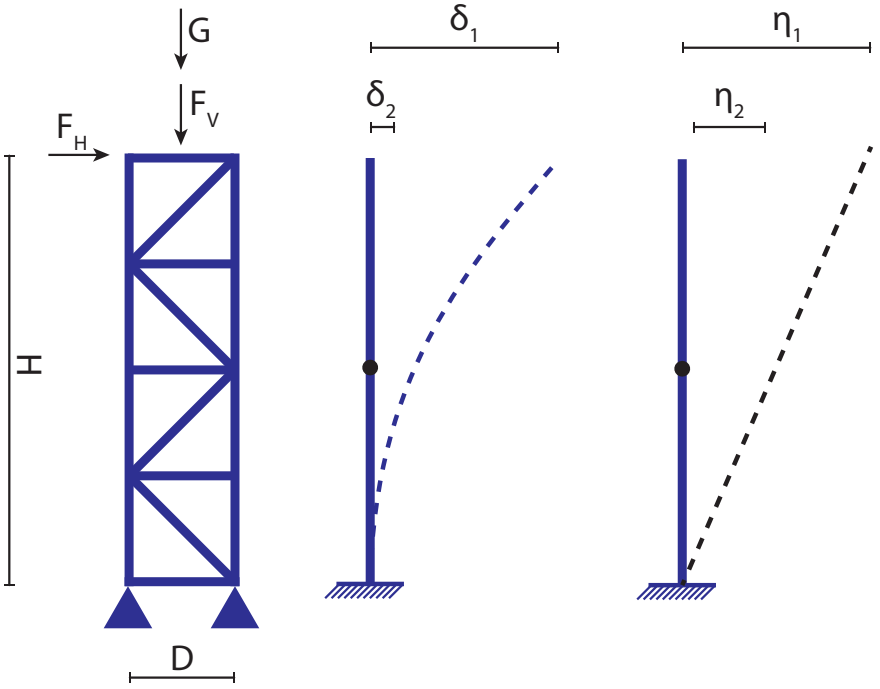

Figure 11: Model for method 2: Left the truss model, in the middle the first order deflection δ_1 & δ_2, on the right the imperfections η_1 & η_2.

The second term is associated with the second order moment due to a combination of the first order deflections, imperfection and payload. This term consists of four contributors. The first two contributors take into account the second order bending moments as a result of the deflections and the forces from the payload and the self-weight, where the total self-weight is thought to act halfway the column. The third and fourth contributor represent effects involving the sway imperfection of the column. Since the effect of the second order moments strengthens itself, these moments are multiplied by the factor $\frac{n}{n-1}$. In analogy with Equation 7, $n = \frac{N_{cr}}{F_V + G/3.17}$ is the minimum force amplifier to reach the elastic critical buckling. This amplification factor describes the geometrically non-linear behaviour of the structure. N_{cr} is the critical elastic buckling force. The multiplication factor is derived in Appendix D.5.

$$M_{Ed} = F_H H + \frac{n}{n-1}\Big(F_V\delta_1 + G\delta_2 + F_V\eta_1 + G\eta_2\Big) = F_V x H + \frac{n}{n-1}\Big(F_V\frac{F_V x H^3}{3EI} + G\frac{5F_V x H^3}{48EI} + F_V\eta_1 + G\eta_2\Big) \tag{8}$$

In this method, a check is performed on the resistance of the section chords in compression. The self-weight and payload results in compression, which means that the chords in compression are more heavily loaded than the ones in tension. The tensile strength is not considered in the model selection process, because it is about the modelling and not so much about the exact resistance. The section is thought to take the bending moment in the critical cross-section, just above ground level, by means of normal forces in the chords. The design load on one chord is thus a combination of the normal force and the moment in the column (Equation 9).

$$N_{chord} = \frac{F_V + G}{4} + \frac{M_{Ed}}{2D} \tag{9}$$

The design check comes down to the check on the compression resistance of a single chord in the bottom section of the column ($N_{chord} \leq N_{Rd,c}$). For the three section types, $N_{Rd,c}$ is calculated as 80% of their

characteristic normal force resistance. The reduction is applied to account for flexural buckling of the chord member. The New York Wheel section chord resistance is then 24 000 kN and for the DS and MSG sections 16 000 kN is found. These values have been compared to the ones used by Mammoet and are found to represent the compression resistances well.

The stability is checked by means of the check in Equation 7, just like for the first method.

3.2.3 Method 3: AISC Notional Loads

In the US standard on steel structures design in accordance with two different provisions, the LRFD method and the ASD method, are allowed. Within this thesis, the LRFD method is considered. It has to be noted that this standard uses symbols that differ substantially from those in the Eurocode. The LRFD approach states that the required strength R_u shall not exceed the design strength $\phi \times R_n$ (Equation 10).

$$R_u \leq \phi R_n \tag{10}$$

In this equation ϕ is the resistance factor and R_n the nominal strength. The design for stability is carried out following the Direction Analysis Method of Design. The initial imperfection of the structure is taken into account by means of notional loads N_i (Equation 11).

$$N_i = \beta \alpha Y_i \tag{11}$$

The factor β represents the initial out-of-plumbness of the structure and is by default 1/500 (0.002), as specified in the AISC Code of Standard Practice [14]. For the analysis in this report an out-of-plumbness of 1/250 (0.004) and 1/1000 (.001) is considered as well. For the LRFD approach $\alpha = 1.0$ and Y_i represents any gravity load applied to the structure. The gravity load for the dead load D of the structure is considered, as well as the gravity load due to the live load L (Equation 12).

$$N_D = \frac{1}{2}\beta 1.2D \tag{12a}$$

$$N_L = \beta 1.6L \tag{12b}$$

The factors 1.2 and 1.6 represent the partial safety factors for the dead load and live load respectively, in accordance with paragraph 2.3 of ASCE/SEI 7-10 [13]. As the dead load acts approximately halfway the height of the structure, the influence of the out-of-plumbness in combination with this load is considered smaller than for the live load, that acts on the structure at the top. Therefore, a factor $\frac{1}{2}$ is applied to N_D. Apart from the notional loads, a dead load, a vertical live load and a horizontal live load act on the structure. The horizontal load is expressed as a fraction x of the vertical live load ($L_H = x \times L_V$). This results in the situation depicted in Figure 12. The loads combination is as shown in Equation 13. For the notional loads the load factors are already in the loads, as shown in Equation 12.

$$1.2D + 1.6L + N = 1.2D + 1.6(L_V + L_H) + (N_D + N_L) \tag{13}$$

The strength of the structure is checked using equation (H 1-1a) in ANSI/AISC 360-10 [12], for symmetric members subject to flexure and compression. This check is shown in Equation 14.

$$\frac{P_r}{P_c} + \frac{8}{9}\frac{M_r}{M_c} \leq 1.0, \tag{14}$$

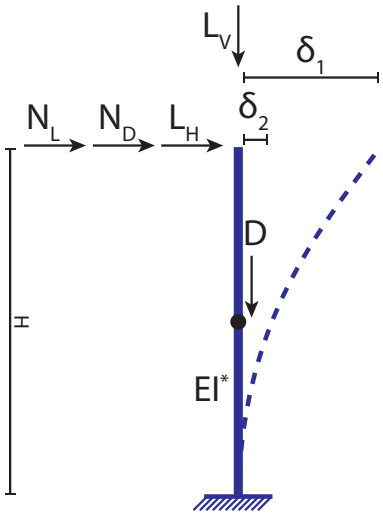

Figure 12: Model for method 3.

where M_r is the required flexural strength and P_r is the required axial strength. The design axial strength P_c equals the resistance for compression times the nominal compression strength $\phi_c P_n = \phi_c A F_y$, where $\phi_c = 0.9$. The design flexural strength M_c is $\phi_b M_n$, where $\phi_b = 0.9$ and M_n the nominal flexural strength. The required axial and flexural strength are calculated using the approximate second-order analysis in Appendix 8 of the AISC standard (Equation 15).

$$P_r = P_{nt} + B_2 P_{lt} \tag{15a}$$

$$M_r = B_1 M_{nt} + B_2 M_{lt} \tag{15b}$$

The parts M_{lt} and P_{lt} account for moments and axial forces due to lateral translations only, while M_{nt} and P_{lt} represent the moments with the structure restrained against translation. In this case $P_{lt} = 0$ and B_1 effects are neglected, as this concerns local member imperfections. B_2 accounts for global amplification effects and is calculated in accordance with Equation 16.

$$B_2 = \frac{1}{1 - \alpha \frac{P_r^*}{P_{el}}} \geq 1 \tag{16}$$

P_{el} represent the elastic critical buckling strength, as given in Equation 17 and where EI^* represent the reduced flexural stiffness of Equation 18. In analogy with the two previous methods, $P_r^* = L_V + D/3.17$.

$$P_{el} = \frac{\pi^2 EI^*}{(K_1 H)^2} \tag{17}$$

$$EI^* = 0.8 \times EI \times \tau_b \tag{18}$$

The reduction factor τ_b relies on the ratio of required axial strength P_r and the axial yield strength P_y, as in Equation 19.

When $\alpha P_r / P_y \leq 0.5$

$$\tau_b = 1.0$$

(19)

When $\alpha P_r / P_y > 0.5$

$$\tau_b = 4(\alpha P_r / P_y)[1 - (\alpha P_r / P_y)]$$

3.2.4 Method 4: Benchmark calculations

The results of the three standard based methods are compared to the results found from finite element calculations in SCIA Engineer[15], a method that serves as a benchmark. Where the three previous methods calculate the results for a one-dimensional beam element, the SCIA calculations rely on a model that consists of all the members of the mast sections. A non-linear calculation is carried out, including a global imperfection of the column. Using the built-in stability package, the first few buckling modes are determined. The first mode corresponds with the lowest buckling force around the weak axis of the sections and is used as the shape of the imperfection, where the maximum deflection equals 1/250, 1/500 and 1/1000 respectively.

The live load and horizontal load are applied at the top, just as in the other methods, while self-weight is calculated through the program and acts on the elements in the structure. The self-weight that is calculated by the program is somewhat lower than the actual weight of the sections, because the connections are not modeled. Therefore, the self-weight is multiplied by a factor (NYW: 1.356, DS: 1.043, MSG: 1.069). The column rests on four hinged supports. As the lateral translation and the rotation of the top of the column are not restrained in both horizontal directions, the weaker axis of the cross-section will be governing for the resistance. Therefore, only the resistance for this side is calculated, where the resistance is determined by checking the compression force in the bottom chord against the chords resistance determined in Section 3.2.2 and by checking for global stability.

The load factors of the Eurocode, $\gamma_G = 1.35$ and $\gamma_Q = 1.5$, are used. It is computationally expensive to determine the resistance of the gantry for all heights, section types, percentages of horizontal load and imperfections. Therefore, only a couple of relevant gantry heights are analyzed using the FEM package.

3.3 Results

Results are obtained for four different horizontal load percentages. The models are used for horizontal loads equal to 0%, 2%, 4% and 6% of the vertical live load. Also, four different amounts of imperfection are considered: H/250, H/500, H/1000 and no imperfection. This means sixteen sets of parameters for each height.

The gantry height and the capacities presented here are not completely continuous. The resistance is only evaluated for physically possible heights, multiples of the section heights. The resistance is determined by executing the checks for a range of live loads, with step size 100 metric tonnes for calculations with the benchmark model. Using smaller step sizes would be very time-consuming. The other methods are evaluated for a step size of one metric tonne.

In Figure 13 the results for one particular case are considered, in an absolute sense. Figure 14 shows the resistance from methods 1,2 and 3 as a percentage of the resistance that follows from the benchmark model. Both graphs show the resistance for the New York Wheel sections, for 2% horizontal load and a 1/250 imperfection.

For very low heights the first and third method yield a significantly higher resistance than the second method. For more realistic heights, where the fourth method is also present, the second method states a

higher resistance for the gantry. The first and third method yield much lower and almost equal results, for these heights. Since the first method is meant for single members, one might argue that buckling curve c is not suitable. However, using curve a or b does not yield very different results. It is concluded that this method is not suitable for the built-up mast sections.

The fourth method, based on a second order finite element calculation, is considered most accurate. Therefore, it serves as a check for the other method. It is clear from both graphs that the second method best resembles the finite element calculations. The differences are very small. Similar results are obtained for the other section types, for different amounts of horizontal load and other imperfections.

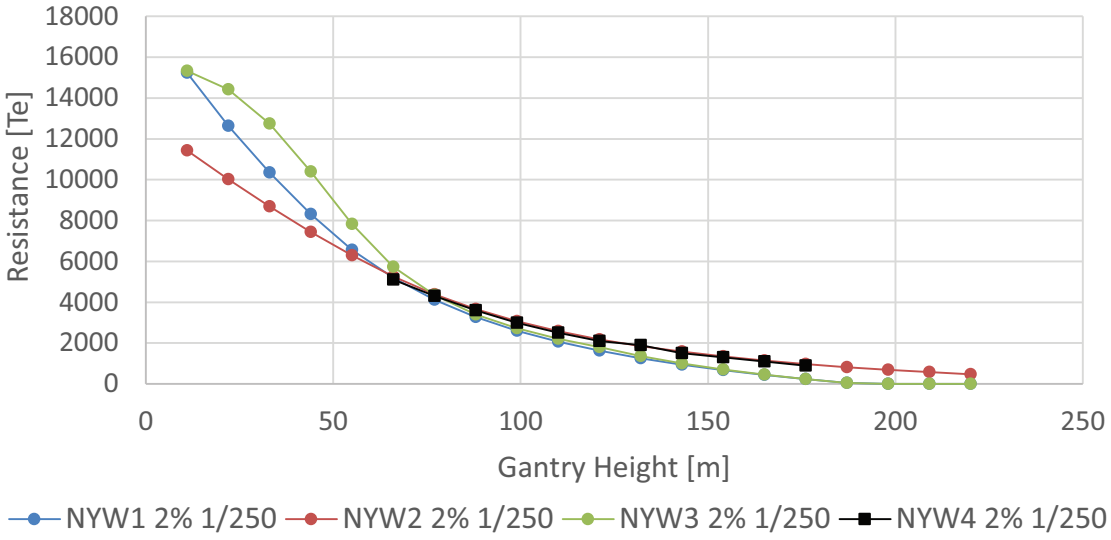

Figure 13: Resistance versus Height for 2% horizontal load and 1/250 imperfection, for New York Wheel sections and according to method 1, 2, 3 and 4 (benchmark model).

3.3.1 Second Order Versus First Order Calculations

The calculations with methods 2 and 3 are based on a second order moment. This is done to account for geometrical non-linear behaviour of the gantry. Here, the difference between a first order and a second order calculation, for the second method, is analyzed. Also, the results from method 4 are shown. In Eurocode 3, EN 1993-1-1[5], paragraph 5.2 it is stated that for an elastic analysis a first order analysis may be used if Equation 20 is satisfied.

$$n = \frac{N_{cr}}{N_{Ed}} \geq 10 \tag{20}$$

This means that the elastic critical buckling force should be ten or more times larger than the design normal force. A quick check learns that this is far from reality for the gantry system under consideration, if one looks at reasonable heights and loads close to the limits of the structure. The figures in Appendix C.1 show the difference in resistance between a first order and a second order calculation, for a 1/250 imperfection and for the New York Wheel mast sections. Figure 46 shows the first order as well as the second order resistance, for all horizontal load percentages under considerations.

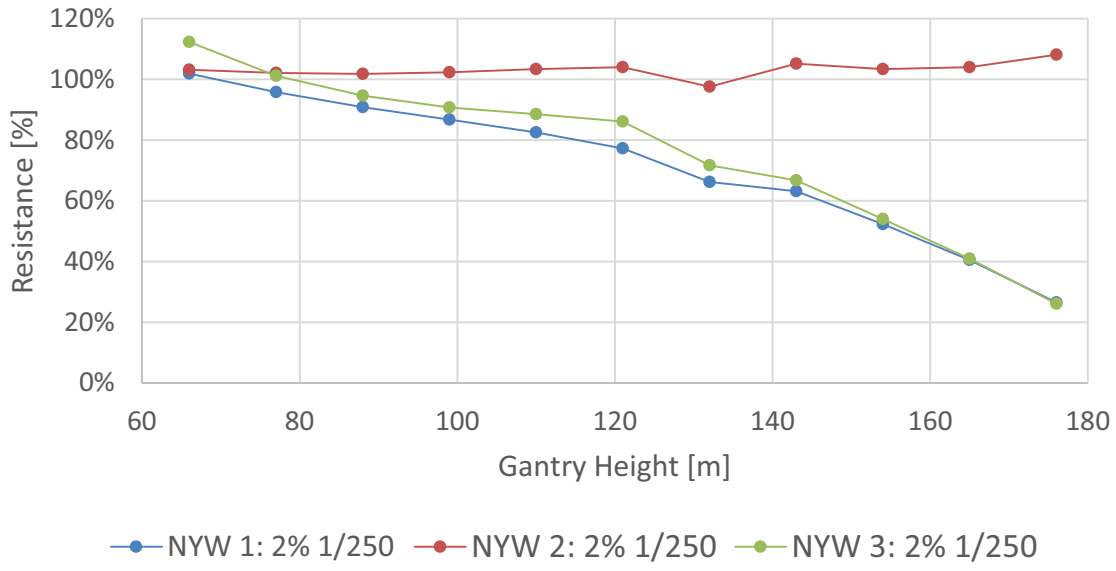

Figure 14: Resistance versus Height for 2% horizontal load and 1/250 imperfection, for NYW sections: The resistances for methods 1,2 and 3 as a percentage of the resistance that follows from the benchmark model.

The graph in Figure 47 represents the ratio of first order to second resistance. It is clear that for a gantry that is subjected to a larger horizontal load the difference is larger. Also, the maximum difference between first and second order calculations is then reached at higher altitudes. The overestimation of the resistance, with the use of a first order calculation, first increases with height (it is already 10% or more for all load percentage categories at a height of 50 m). It reaches a peak, after which the difference decreases again. The difference remains significant at large heights for all horizontal load categories (10% for 0% horizontal load and even around 65% for 6% horizontal load. It is thus clear that a first order calculation, where the second method is used, is not applicable.

The relation between height and difference in resistance can be explained. At low heights the second order effects are small, as one might expect. The absolute deflection at the top, due to both the imperfection and the horizontal load, increasing with increasing height. This means that the second order moments also increase. At very large heights the difference decreases, due to two phenomenon. The self-weight of the structure becomes very important, limiting the live load and thus the horizontal load. This means that the deflection is also limited, reducing second order effects. Also, due to large height of the structure, not so much the the chords resistance but the overall buckling stability of the structure becomes governing.

For the other section types and amounts of imperfection and horizontal load similar results were found.

3.4 Model Selection

The results in Section 3.3 suggest that method 2 is best suitable to describe the behaviour of a gantry that is subjected to both a vertical and a horizontal load. Therefore, this method is chosen to go forward with in the remainder of this report.

4 Model

In Section 3 it was decided to go forward with method 2, that is based on the analysis of built-up compression members in Eurocode 3. In that section the behaviour of one column, subject to a horizontal load from one direction, was analyzed.

In this section, the gantry is analyzed for a combination of horizontal loads in both principal directions of the mast sections. That means that bending is taken into account over both the strong (y) and the weak (z) axis. The horizontal load can be equal in both directions, a 45° load angle, but it can also differ. Various angles of the horizontal load are shown in Figure 15 (a), where the gantry is looked at from above. The horizontal and vertical load are applied to the structure in the middle of the gantry beam. Due to the symmetry of the structure, it suffices to look at load angles between 0° and 90°. Figure 15 (b) shows how the horizontal load, depending on the load angle, is divided over the two principal axes of the section.

For the resistance of the gantry, the normal force and bending moment in one of the two gantry columns is considered. The resistance is determined for an Ultimate Limit State (ULS), based on the axial forces in the chords and the total axial forces in the gantry columns. The shear forces in the chords are not taken into account, as preliminary checks show that they only result in small stresses. A shear stress larger than 1% of the yield stress is hardly ever found in the chords. In a final design this should of course be taken into account, as well as the forces in the braces of the mast sections. The Serviceability Limite State (SLS) is not considered. All horizontal loads are represented by a single point load at the top of the gantry. This load represents actions from skidding and tailing, wind on the payload, wind on the gantry beam(s) and wind on the mast sections. In reality the wind on the mast sections does of course not act at the top of the gantry. The horizontal point load, as well as the weight of the payload, acts in the middle of the gantry beams. Different positions, for example due to skidding of the payload, are not considered. The calculations are based on the situation where the gantry lifts the payload. Storm conditions are not considered.

4.1 Calculation Method

It is assumed that both the vertical and horizontal force are divided equally over the two columns. The weight of the payload, the self-weight of the columns and the horizontal load are included. The weight of the gantry beam is excluded, since it depends on both the span of the gantry and the weight of the payload. The resulting resistance should be corrected for the self-weight of the beam, where the load factors are taken into consideration. Figure 16 (a) provides a front view of the gantry and a top view of the foundation layout. In Figure 16 (b) the column that is analyzed is shown, together with the boundary conditions of column models 1, 2, 3 and 4.

The columns rest on a base frame, as described in Section 2.5, that is either placed on a rigid or a flexible foundation. The connection between the columns and the gantry beam can be either hinged or rigid. The spring at the top (k_{r2}) can thus either have zero or infinite stiffness, corresponding with a hinged and a rigid connection at the top. Also, the foundation stiffness (k_{r1}) can either be infinite (rigid

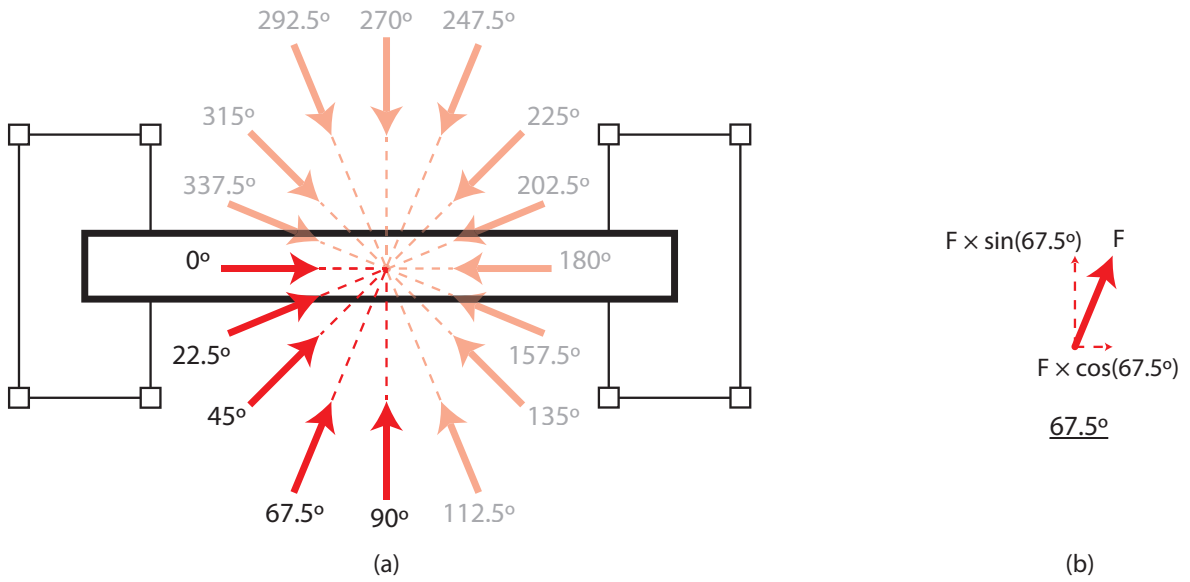

Figure 15: Horizontal load on the gantry: (a) Horizontal loading under an angle (view from above), (b) Horizontal load decomposed, for a 67.5° load angle.

foundation) or finite (flexible foundation). Combinations of these situations lead to models 1 to 4 and are shown in Table 1. For example, for a gantry on a rigid foundation and with a rigid connection between

Table 1: Gantry configurations and models: Column models, for both directions, for the gantry configurations.

Beam - column connection	**Foundation**	**Y**	**Z**
Hinged	Rigid	1	1
Hinged	Flexible	3	3
Rigid	Rigid	1	2
Rigid	Flexible	3	4

columns and beam corresponds with model 2 for bending over the y-axis and model 1 for bending over the z-axis. This is the case because the rigid connection only works for bending over the y-axis. The load distribution between the two columns and the rigidity of the top connection only hold if the gantry beam is much stiff than the gantry columns. This is the case for high gantries with a relatively small span. The gantries studied in this thesis generally fulfill that requirement.

The Buckling load, for a point load as well as a distributed load, and the first order deflections of the four column models are summarized in Figure 48, in Appendix D. These results are derived in detail in that appendix. From these results, the second order bending moment in both directions can be calculated (Equation 21).

$$M_{i,Ed} = M_{1,i} + \frac{n_i}{n_i - 1}(F_V w_{1,i} + G w_{2,i} + F_V \eta_{1,i} + G\eta_{2,i}), \quad for \;\; i = y, z \tag{21}$$

The first order moment $M_{1,i}$, the elastic instability factor n_i and the first order deflections $w_{1,i}$ and $w_{2,i}$ depend on the direction under consideration and on the gantry set-up. The factor n_i is derived in

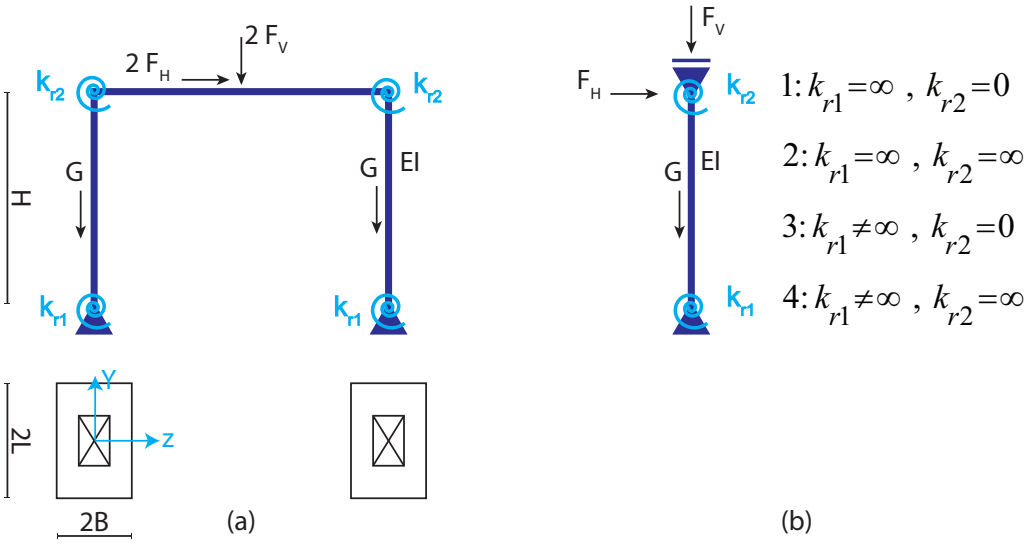

Figure 16: Gantry model, for different set-ups: (a) Front view of the gantry and top view of the foundation layout, (b) Gantry column, with the boundary conditions of models 1, 2, 3 and 4.

Appendix D.5 and takes into account the elastic buckling load. The parameters $\eta_{1,i}$ and $\eta_{2,i}$ represent the imperfections at the top and halfway the column. These imperfections cause bending moments, due to the presence of the payload and the self-weight of the column. The elastic instability factor n_i is derived in Appendix D.5. The flexural stiffnesses of the respective mast section types are derived in Appendix B.

The resistance of the gantry is based on the four checks in Equation 22. The checks in Equation 22a and 22b check the normal force in the chords against the compression and tension resistance of the chords. These resistances are given in Table 2. The tension resistance is not as much limited by the chords themselves as it is by the connection between the chords of different mast sections. These checks are performed just above the foundation, in the chords that are loaded most heavily in compression respectively tension. Bending in both directions is combined with the normal force in the column. The bending moment is taken by axial forces in the chords. Equation 22d and 22c perform buckling checks for the column for buckling over both principal axes. If the instability factor is smaller than one, the buckling load is smaller than the actual load, thus the structure becomes unstable.

$$N_{chord} = \frac{F_V + G}{4} + \frac{M_{y,Ed}}{2D_z} + \frac{M_{z,Ed}}{2D_y} \leq N_{Rd,c} \tag{22a}$$

$$N_{chord} = \frac{F_V + G}{4} / \frac{M_{y,Ed}}{2D_z} / \frac{M_{z,Ed}}{2D_y} \leq N_{Rd,t} \tag{22b}$$

$$n_y \geq 1 \tag{22c}$$

$$n_z \geq 1 \tag{22d}$$

4.1.1 Soil Stiffness

The base frame of the gantry legs, an example of which is shown in Figure 17, can rotate if the foundation is flexible. The first mast section is still rotationally fixed connected to the base frame.

Table 2: Compression and tension resistance of the chords of the mast sections: Resistance in kN.

	MSG	DS	NYW
Compression	16000	16000	24000
Tension	3000	12500	16200

Figure 17: Base frame on foundation (Mammoet).

The static rotational stiffness of the subsoil is calculated using the equations formulated by Pais and Kausel (1998[18]). These equations are wildly used in practice and are also the recommended in[19], a report on the soil-structure interaction for building structures. The paper of Pais and Kausel (1998[18]) describes the translational and rotational stiffness of the foundation, using the shear modulus and the poisson ratio of the soil and the dimensions of the foundation. These equations are based on the assumption of a rigid structure on soil. For the purpose of this thesis, the rotational stiffness in both bending directions of the columns is of interest. The formulas for bending about the strong (z) and the weak (y) axis, as indicated in Figure 18, are given in Equation 23 and 24 respectively.

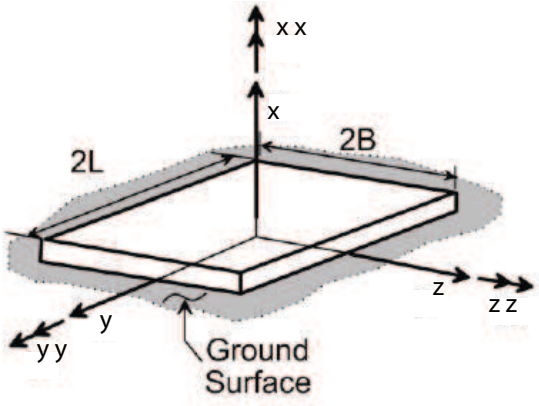

Figure 18: Foundation in coordinate system: Pais and Kausel (1988[18]).

$$k_{zz} = \frac{GB^3}{1-\nu}\left[3.73\left(\frac{L}{B}\right)^{2.4} + 0.27\right] \tag{23}$$

$$k_{yy} = \frac{GB^3}{1-\nu}\left[3.2\left(\frac{L}{B}\right) + 0.8\right] \tag{24}$$

The moment in the flexible support M_{ii} is related to the angle of rotation ϕ_{ii} and the rotational stiffness of the subsoil, k_{yy} or k_{zz} (Equation 25).

$$M_{ii} = k_{ii} \times \phi_{ii}, \quad for \;\; i = y, z \tag{25}$$

The soil properties vary wildly for different types of soil and even within the soil types. Therefore, a thorough investigation of the subsoil is always necessary when the gantry is placed directly on the ground. Table 3 shows some typical values for the Young's modulus and poisson ratio, taken from a book on the Design of Steel Structures[17]. These values will be considered in this thesis.

Table 3: Typical values for the Young's modulus and the poisson ratio, for different soil types[17].

Type of soil	ν [-]	$\times 10^3$ **E [kN/m^2]**
Sand: Loose	0.3	17
Sand: Dense	0.3	64.5
Sand and Gravel: Dense	0.3	146
Rigid Foundation	0.3	1.00E+10

Information on the dimensions of the base frame of the respective mast section types is to be found in Section 2.5. With these measures the rotational stiffness can be calculated, for both bending around the y-axis and the z-axis.

4.2 Benchmark Model

The results from the model described in Section 4.1 are compared to the results from a finite element model in SCIA Engineer[15]. In that program, the mast sections are modelled using one dimensional beam elements, with the mechanical properties of the real mast sections. That means that all pinned connections in the sections are modelled as hinges, the elements in the mast sections have the correct mechanical properties and the self-weight of the sections is correct. To achieve this the self-weight has to be adjusted by a factor, to account for the weight of connections. The play in the pinned connections is not modelled. For the New York Wheel sections this weight correction factor equals 1.356. The load factors, 1.35 for the self-weight and 1.5 for the payload and horizontal load, are the same as in the model in Section 4.1. Figure 61, in Appendix E, shows a partial rendered view of a mast section in SCIA Engineer. The hinges are not visible in this image. An example of a complete gantry is shown in Figure 19.

The gantry is modelled with two adjacent gantry beams (green) on top of the columns, connected by means of dummy elements (red). Both the weight of the payload and the horizontal load are applied in the middle of the beams. Both beams take half the load. Figure 64, in Appendix E, shows the hinged connection between one column and the two beams. Figure 63, in the same appendix, shows a rigid column-beam connection. The beams are 40 m long and have a moment of inertia of 1.78 m^4 over its strong axis and 0.34 m^4 over its weak axis.

Geometrically non-linear calculations are executed, that take into account the first buckling shape as the imperfection of the structure, with an amplitude equal to 1/500 of the height. The overall stability

is checked, as well as the maximum compression and tension force in the chords of the mast sections. The benchmark results presented in Section 5 are limited to the New York Wheel mast sections and to gantry heights of 88, 110, 132, 154 and 176 m.

The base frame under the bottom mast section is modelled by means of very stiff dummy elements. In the middle of these elements, indicated in red in Figure 62 in Appendix E, a support with a rotational stiffness is placed. An infinite rotational stiffness corresponds with a rigid foundation, a finite stiffness with a flexible foundation. The results from the benchmark model are based on a rigid foundation and on a foundation on loose sand. Between the chords of the bottom section and the base frame hinges are placed, such that only normal forces are present in the chords.

This model is thought to represent reality well, under the given loads. The finite element method, as well as the calculation method in Section 4.1, does not take into account play in the connections between the members of the mast sections.

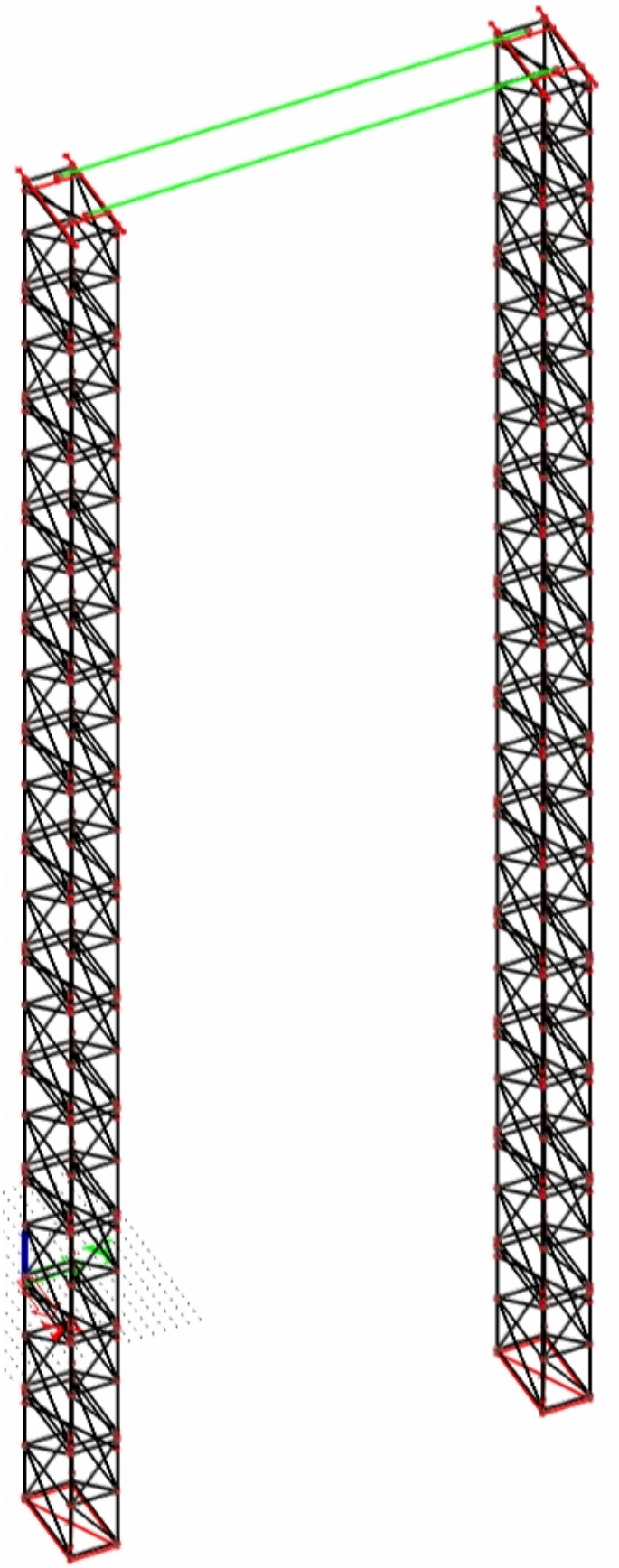

Figure 19: Benchmark model in SCIA Engineer[15]

5 Results

Here, the results from the model in Section 4.1 are compared to the results from the benchmark model in Section 4.2. This comparison, executed in Section 5.1, gives a view on the performance of the model.

Also, the influence of the horizontal load percentage (Section 5.2), load angle (Section 5.3), imperfection (Section 5.4), soil stiffness (Section 5.5) and type of mast section (Section 5.6) are discussed. These are all considered for the model of Section 4.1 only.

Unless stated otherwise, all calculations are based on the New York Wheel mast sections.

5.1 Model Performance

For an imperfection of 1/500 the resistance has been determined for both models. This has been done for a rigid and a flexible (on loose sand) foundation and for a hinged and a rigid connection between column and beam. This results in four different gantry configurations. The results have been obtained for a 45° load angle, where the horizontal load equals 2% in both directions. The results are shown in Figure 20.

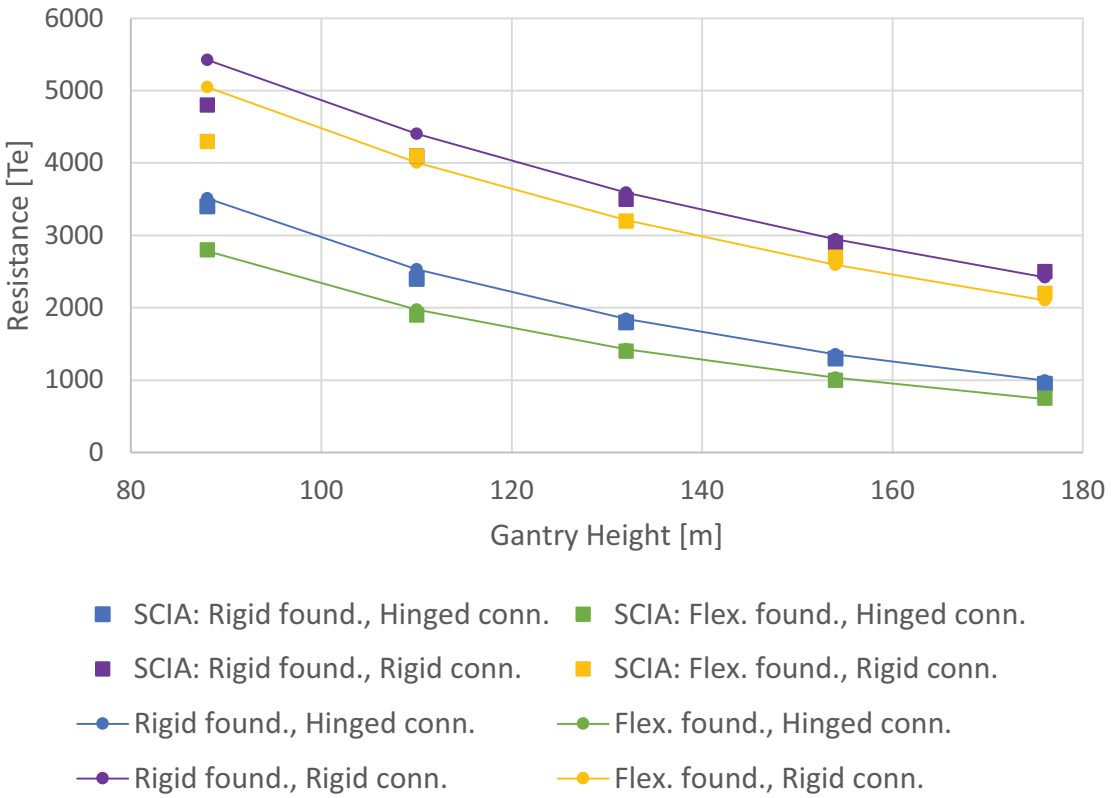

Figure 20: Resistance of New York Wheel mast section gantry: For both the calculation model and the benchmark model, for 2% horizontal load in both directions and a 1/500 imperfection. Results for both a rigid foundation and a foundation on loose sand, for a hinged and a rigid top connection.

It seems that, except for the relatively low gantry with 88 m high columns, the model behaves a expected. Except for these observations, the difference between calculation model and benchmark model is equal to or below 5%. If the gantry is relatively low, two phenomena can negatively influence the performance

of the model. The shear deformation of the NYW mast sections is relatively large for these heights. The hand calculation model does not take into account the shear deformation and might therefore overestimate the resistance of the gantry. Also, the assumption of an equal load distribution between the two columns might be too far from reality. The gantry with a rigid connection between beams and columns is a statically indeterminate structure. Therefore, the ratio of stiffness between the gantry beam and the columns influences the load distribution. The assumption of an equal load distribution is justifiable as long as the gantry beam is much stiffer than the columns. If the columns are very short, this is not the case anymore. These two phenomena might explain the larger discrepancy between the results of the two models for an 88 m high gantry.

To see if the accuracy of the model depends on the horizontal load, the resistance has been determined for 0%, 1%, 2%, 3%, 4%, 5% and 6%. This has been done for a 132 m high gantry, for a 1/500 imperfection and for both a hinged and a rigid connection at the top. It has only been done for a rigid foundation. Again the load angle is 45°, which means that both directions experience the load described above.

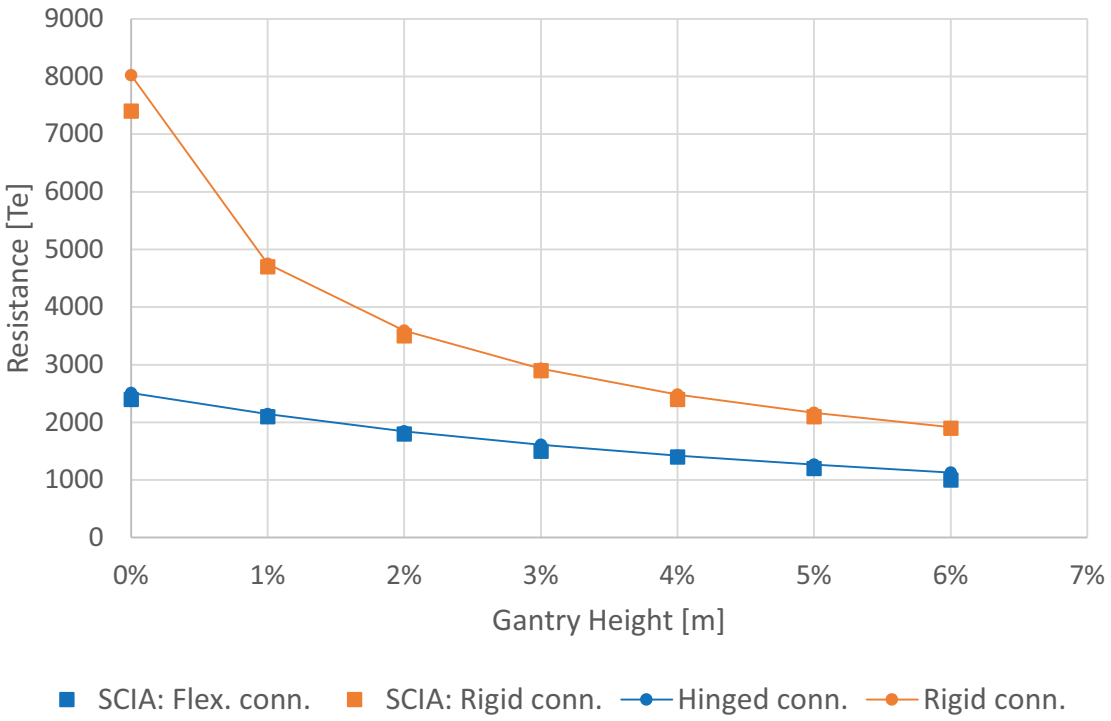

Figure 21: Resistance of New York Wheel mast section gantry for different horizontal loads: For both the calculation model and the benchmark model, for a 45° load angle and a 1/500 imperfection. Results for a rigid foundation, for a hinged and a rigid top connection.

Figure 21 shows that the model does very well under all horizontal loads under consideration, except for the situation with a rigid beam-column connection and without a horizontal load. It is concluded that the model performs reasonably well. Therefore, it is used in the next sections.

The hand calculation model performs checks on the compression and tension resistance of the chords just above ground level. For all calculations performed with the benchmark model in SCIA Engineer [15]

the chords of the bottom mast sections were found to be governing as well.

5.2 Load Percentage

It is interesting to see how sensitive the maximum payload in a gantry is to the percentage of horizontal load that is applied. Therefore, the resistance has been calculated for a horizontal load equal to 0%, 2%, 4% and 6%, in both directions. This means that the load angle is 45°. The imperfection is 1/500. Appendix F.1 shows graphs with the results of these calculations, for a rigid foundation and a hinged as well as a rigid beam-column connection. These graphs show the results in an absolute as well as a relative sense, where the resistance is plotted as a percentage of the resistance for a 0% horizontal load.

The graphs show a resistance that decreases for a larger horizontal load, for realistic gantry heights. The relative difference first increases and then decreases again. Second order effects become more important with height, but as height increases the payload decreases and so do the horizontal load and the instability factor.

The graphs show that the resistance depends on the percentage of horizontal load heavily. The difference can easily be between 10-to-30% between 2% and 4% horizontal load, for the NYW mast sections. Thus, it is important to know what a realistic load percentage is.

5.3 Critical Angle of Horizontal Load

The horizontal load on the gantry can act on the structure from many directions, since the horizontal loads in the two directions do not necessarily have to be equal. In the previous results the angle was assumed 45°. In this section, the influence of the load angle is analyzed. In Figure 15, a top view of the gantry is shown, where the horizontal load is applied under different load angles. The resistance is calculated for both the New York Wheel and the MSG mast sections, for a rigid foundation and for both a hinged and a rigid connection between column and gantry beam. This is done for a 3% horizontal load and for a 1/500 imperfection. The resistances, as a function of the load angle and for four different heights, are shown in Appendix F.2. The critical load angle is defined as the angle for which the maximum allowable playload is lowest.

No dependence emerges between the gantry height and the critical load angle, for both mast section types and configurations. For the New York Wheel sections and a hinged connection at the top the critical angle lies around 12°. For a rigid connection it lies around 40°, making the resistance more symmetrical. This is as expected, since the rigid connection increases the stiffness and buckling resistance around the weak axis. For the MSG sections the critical load angle for a hinged top connection is 45°. This was also to be expected, as these mast sections have almost symmetrical properties. For a flexible foundation the results would probably be a bit different, since the dimensions of the MSG base frame are far from symmetric. For a rigid top connection the angle is around 70°, as one of the directions has become much stiffer. Similar results are found for different amounts of horizontal load.

For the New York Wheel mast sections it is quite efficient to have a rigid connection at the top if the horizontal load is similar in both principal directions of the mast sections. For the MSG sections the

situation is quite different.

5.4 Imperfection

The influence of the imperfection is considered for the New York Wheel mast sections, for a gantry on a rigid foundation and for both a hinged and a rigid connection between beam and column. This is done for 3% horizontal load and for four different amounts of imperfection: 1/250, 1/500, 1/1000 and no imperfection. The resistances are shown in the graphs in Appendix F.3, both in an absolute and a relative sense.

The influence of the imperfection is much smaller than that of the horizontal load percentages that were used in Section 5.2, for both a hinged and a rigid connection between beam and columns. A resistance difference over 5%, that is for example found between a 1/250 and a 1/1000 imperfection, is however still significant. The resistance is of course larger for a smaller imperfection. The difference first increases with height, due to the growing importance of second order effects. Afterwards it stabilizes, to grow again and very large heights. This is due to a change in failure mechanism. For these large heights the tension resistance becomes governing, where the compression resistance is governing for lower heights.

5.5 Soil Stiffness

In this section the influence of the foundation stiffness is considered, for both the MSG and the New York Wheel sections. The DS sections are not treated. Appendix F.4 shows the resistance for a rigid foundation and for a foundation on the soil types given in Section 4.1. The results are based on 3% horizontal load, under a 45° angle, and for a 1/500 imperfection.

The results show that the soil stiffness can have a significant effect on the gantry resistance, especially for a hinged connection at the top. The effect is stronger for the MSG sections, because the base frame is relatively tiny for these sections. The resistance can be increased if a larger area of soil is activated, by means of a larger base frame. For dense sand and for a hinged connection at the top the resistance for New York Wheel mast sections is 5 to 10% lower than for a rigid foundation. For a rigid beam-column connection the decrease is 5% for large heights. For the MSG sections the reduction is around 40% for a hinged connection and around 30% for a rigid connection, at reasonable heights. The resistance for a rigid connection shows strange behaviour at very low heights. For these heights the approximate buckling resistance is not accurate, which results in unexpected and unreliable results.

5.6 Mast Section Type

It is of interest to see the difference in resistance between the different mast section types. Therefore, the resistance is calculated for the three mast section types, for a rigid foundation and for both types of beam-column connection. The results are based on 3% horizontal load at a 45° load angle and on a 1/500 imperfection.

Figure 22 shows that for a hinged beam-column connection the resistance of the New York Wheel sections is much larger than that of the other two types. The DS and MSG sections give a similar

resistance for low heights, but for more reasonable heights the DS sections give a higher resistance. This is a result of the fact that the tension resistance of the chords of the MSG sections is much lower than for the DS sections. At low heights the compression resistance is governing for both section types. At larger heights compression is still governing for the DS sections, but tension becomes governing for the MSG sections. This explains the change in the course of the resistance for the MSG sections in the graph.

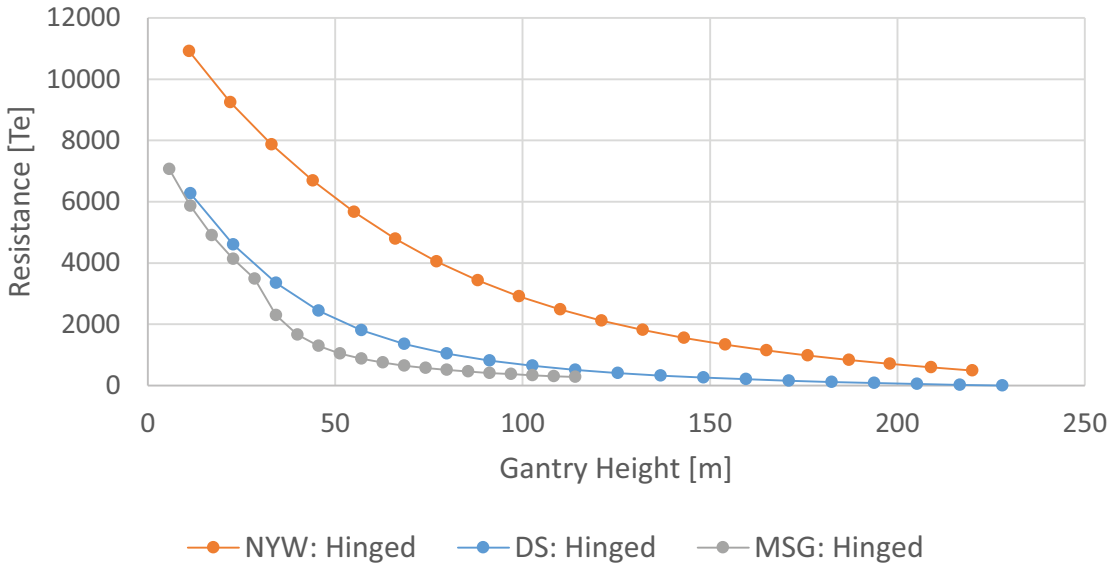

Figure 22: Resistance of the respective mast sections: For a rigid foundation, a hinged connection a the top, 3% horizontal load at a 45° and a 1/500 imperfection.

The results for a rigid top connection are given in Figure 23 and again show a resistance that is much larger for the New York Wheel sections that for the other two types. The DS sections now can carry a significantly larger payload than the MSG sections, because the weak axis of these sections is reinforced by the rigid connection at the top. This makes the resistance of these sections much more symmetrical.

For relevant gantry heights the MSG sections can bear a payload that is roughly 50% of the payload that the DS sections can carry, for a hinged top connection. For a rigid connection it is around 30%. The DS sections can carry 15-to-25% of the load the NYW sections can carry, for a hinged connection. For a rigid connection it is 25-to-35%.

Overall, the compression check is governing up to a certain height. As the maximum allowable payload becomes lower for increasing height, the share of the bending moment in the axial forces in the chords becomes bigger. The tensile check becomes governing because the tensile resistance is lower than the compression resistance. The tensile resistance is limited by the resistance of the connections. The tensile check is positively influence by the compression from the weight of the payload and the columns. Therefore, one could argue that for a detailed design the tensile check should be executed with a load factor that does not positively influence the check as well.

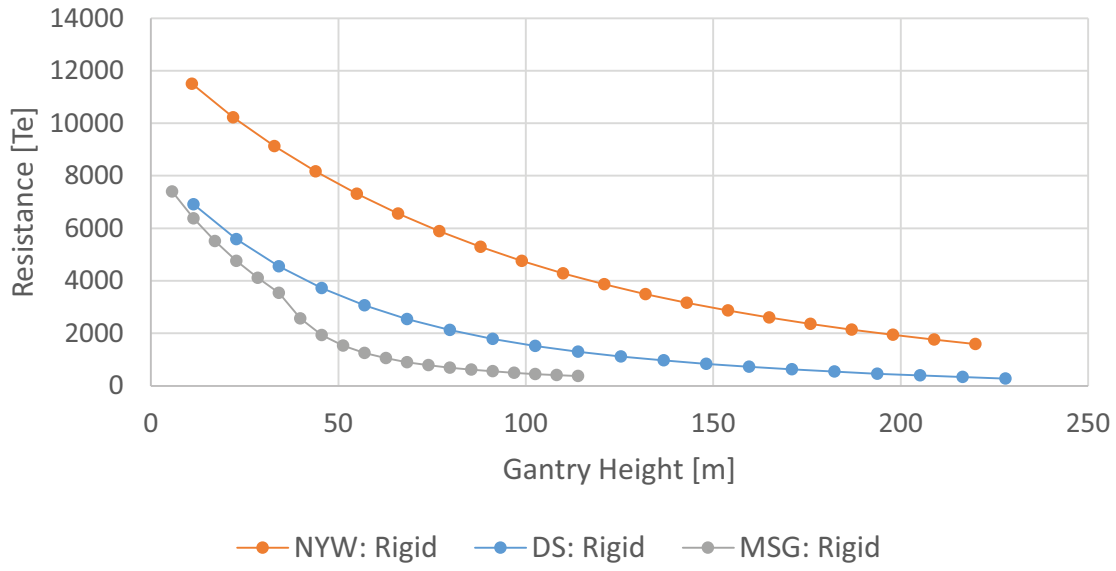

Figure 23: Resistance of the respective mast sections: For a rigid foundation, a rigid connection a the top, 3% horizontal load at a 45° and a 1/500 imperfection.

6 Horizontal Load On The Gantry Structure

In previous sections, calculations were carried out using different percentages of horizontal load, modelled as a point load at the top of the gantry. Within this section, the origin of these percentages is investigated. The goal is to find realistic horizontal loads, to assess the consequences of these loads for the feasibility of the gantry structure and to identify the contributors to these loads. From previous results, it has become clear that the resistance of the gantry depends heavily on the percentage of horizontal load that is taken into account. Therefore, it is very relevant to have a closer look at the horizontal loads on the structure.

Four different contributors to the total horizontal load are identified:

- The wind load on the gantry structure, both on the columns and on the gantry beams
- The wind load on the payload that is lifted by the gantry
- The loads that can result from skidding the payload along the gantry beam
- The loads that can results from tailing of the payload

The calculations carried out in this section concern a gantry on a rigid foundation, made out of NYW mast sections, with a hinged connection at the top and for a 30 m span. Two beams are applied next to each other. In the remainder of this section the transverse and longitudinal beam axes are used extensively to indicate the direction of the load. The transverse axis (or direction) refers to the direction perpendicular to the gantry beams, while the longitudinal axis (or direction) refers to the direction along the gantry beams (Figure 24).

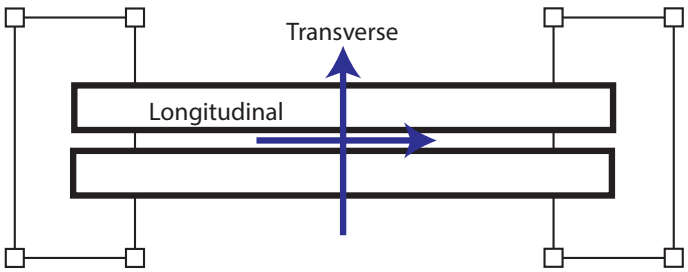

Figure 24: Top view of the gantry, longitudinal and transverse beam axis indicated.

First, wind speeds and pressures are treated in Section 6.1. Afterwards, the four load contributions are discussed. Finally, the total horizontal load (Section 6.6), that results from combinations of the four contributions, and the results (Section 6.7) are treated.

6.1 Wind Actions

Gantries are designed to operate under predefined wind conditions, just like cranes. One difference between the two is that a crane can often be configured or put in a position such that it catches much less wind than during operation, whereas this is not possible (in time) for a gantry. That means that storm

conditions are more important for a gantry than for most cranes.

The wind pressure $q_w(z)$ at altitude z is calculated in accordance with EN-13000:2010[8], as shown in Equation 26.

$$q_w(z) = 0.625 \times v(z)^2, \tag{26}$$

where $v(z)$ is the 3 second gust wind speed at altitude z. This speed is used to calculate the wind pressure at the top of the gantry. In weather forecasts, usually the 1 hour average wind speed $\bar{U}$ 10 m above the ground is cited. Therefore, the 3 second gust wind speed needs to be related to the 1 hour average wind speed. Equation 27 shows the exponential function that relates the 3 second gust wind speed at altitude z to the 10 min. average wind speed 10 m above the ground $\bar{v}$. Again, this is in accordance with EN-13000:2010[8]. It describes a fully developed wind profile.

$$v(z) = ((z/10)^{0.14} + 0.4) \times \bar{v} \tag{27}$$

The relation is shown in Figure 25 for three different 10 min. wind speed averages. It is indicated in the graph that a 3 second gust wind speed of 14 m/s at 100 m altitude corresponds with 7.9 m/s (4 Bft) 10 min. average wind speed at 10 m.

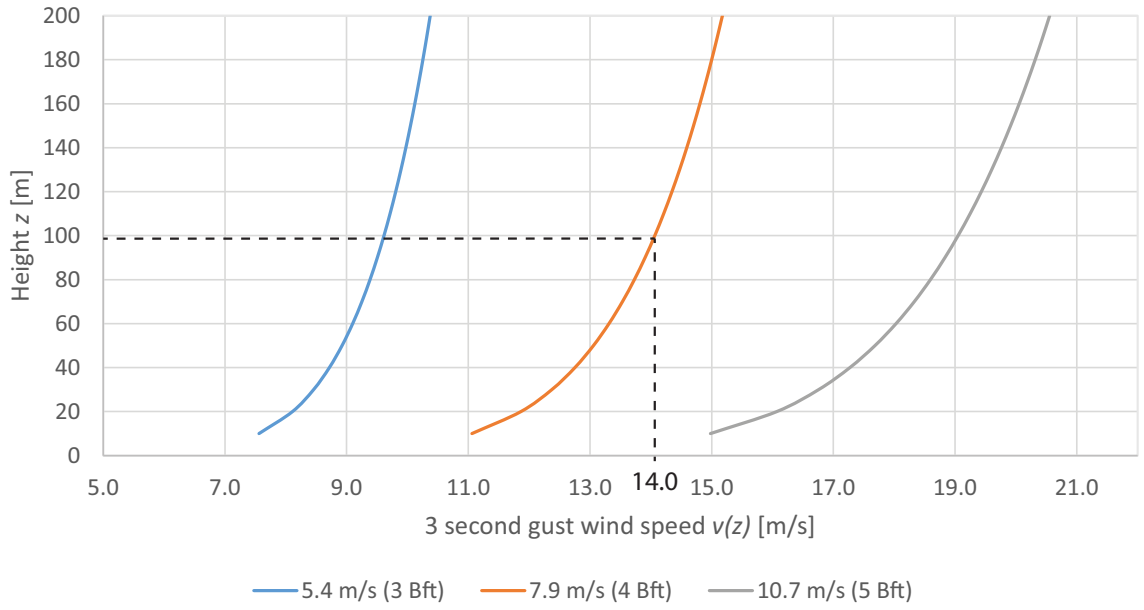

Figure 25: Wind over height: Relation between height above the ground and 3 second gust wind speed, for three different 10 min. average wind speeds. Calculated in accordance with EN-13000:2010[8].

The 10 min. average wind speed can be related to the 1 hour average wind speed using the Durst Curve[25]. This curve allows to convert average wind speeds to different durations. It shows that that the 10 min. speed is 1.07 times the 1 hour speed.

The wind speed that is taken into account in the design of the structure depends, among other things, on the probability that this speed is exceeded. If the operational conditions of the gantry are exceeded with high frequency, a lot of working days go to waste. The probability distribution that is most

commonly used for wind speeds is the Weibull distribution. The probability density function (PDF) is defined by a shape parameter $k > 0$ and a scale parameter $\lambda > 0$ and is given in Equation 28.

$$f(x, \lambda, k) = \begin{cases} \frac{k}{\lambda}\left(\frac{x}{\lambda}\right)^{k-1} e^{-(x/\lambda)^k} & x \geq 0 \\ 0 & x < 0 \end{cases} \tag{28}$$

From the cumulative distribution function (CDF), the amount of inoperable days, on average and within a certain period, can be found. The amount of inoperable days equals the probability that a wind speeds is exceeded times the working period in days. Both the PDF and CDF are plotted in Figure 26, for $k = 2.1$ $[-]$ and $\lambda = 8.89$ $[m/s]$. The value of for the shape parameter is typical for the Dutch coastal area, according to The Royal Netherlands Meteorological Institute (KNMI[22]). The scale parameter can be approximated as 1.125 times the 1 hour average wind speed[23]. This means that 8.89 corresponds with a wind speed of 7.9 m/s, which is equivalent to 4 Bft.

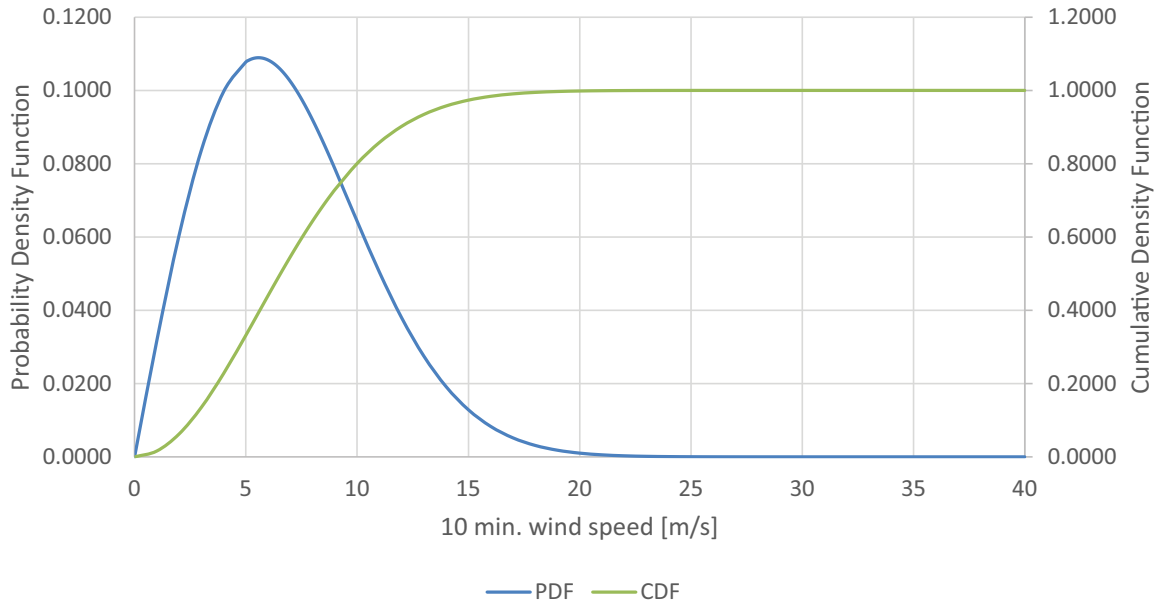

Figure 26: Weibull distribution: PDF and CDF for shape factor $k = 2.1$ and scale factor $\lambda = 8.89\ m/s$.

In conclusion, the following procedure can be followed to determine the amount of operable days in a certain period:

1. Set the design 3 second gust wind speed at the top of the gantry (used to determine the horizontal load and ultimately the resistance of the gantry).
2. Using Equation 27, determine the 10 min. average wind speed 10 m above ground level.
3. Transform the 10 min. average wind speed to a 1 hour average wind speed, using the Durst Curve[25].
4. Use the Weibull distribution to find the probability that the the 1 hour average wind speed is not exceeded. The parameters of the Weibull distribution can be determined from wind data of the project region or from literature.
5. Determine the amount of operable days: multiply the probability with the proposed period of time.

6.1.1 Amount of Working Days and Storm Probabilities

The procedure in Section 6.1 is followed for a 3 second gust wind speed at the top of the gantry of 10 m/s and 14 m/s. The expected amount of operable days is calculated for a gantry height of 60,100,140 and 180 m. For the Weibull distribution $k = 2.1$ $[-]$ and $\lambda = 8.89$ $[m/s]$ are used. The results in Table 4 show that if only a 10 m/s gust wind speed is taken into account, which is equivalent to 3 Bft, the amount of operable days is very limited. For very tall gantries operation is expected to be possible on less than one out of five days. A 14 m/s gust wind speed, equivalent to 4 Bft, means that on over 40% of the days operations can be carried out.

Table 4: Amount and percentage of operable days per year, for different wind speeds: for 10 m/s and 14 m/s gust wind speed at the top of the gantry.

Height [m]	10 m/s operable days per year	10 m/s % operable days	14 m/s operable days per year	14 m/s % operable days
60	112	31%	191	52%
100	101	28%	177	48%
140	94	26%	166	45%
180	62	17%	159	43%

Not only the in-service wind is important. The occurrence of more extreme wind speeds is of interest for survival of the gantry, when it is out-of-service. Two storm wind speeds are considered, in accordance with region D (32 m/s) and E (36 m/s) of annex N.3 in EN-13000:2010[8]. Region D refers to, among others, the Dutch coastal area. Table 5 shows the amount of days per year these speeds are not exceeded and the % of days these speeds are exceeded, for the same Weibull distribution that is used for the in-service wind speeds. For tall gantries, the 32 m/s speed is expected to be exceeded on 5% of the days and the 36 m/s speed only on 2% of the days.

Table 5: Amount and percentage of days per year the storm wind speed is not exceeded, for different wind speeds: for 32 m/s and 36 m/s gust wind speed at the top of the gantry.

Height [m]	32 m/s Days not exceeded per year	% of days 32 m/s is exceeded	36 m/s Days not exceeded per year	% of days 36 m/s is exceeded
60	358	2%	362	1%
100	353	3%	361	1%
140	353	3%	361	1%
180	347	5%	358	2%

6.2 Wind on the Payload

For the design of their PTC 140 DS crane (Figure 28), Mammoet carried out research into the wind on the payload. This study is used in the Basis of Design[16] of the crane. The payload usually has a substantial surface, which means that is able to catch a lot of wind. The load is transferred to the gantry through the strands from which it hangs (Figure 27).

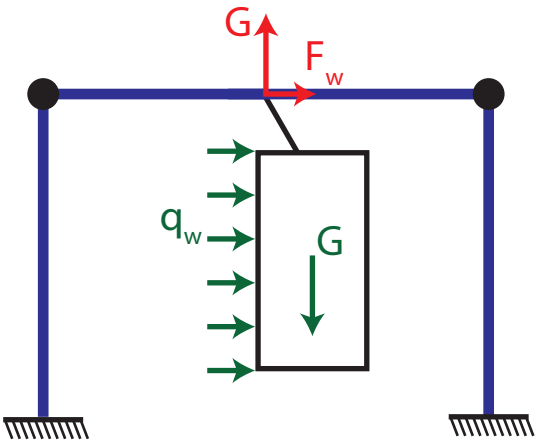

Figure 27: Wind on the payload: Horizontal load on gantry, due to wind on the payload.

The wind load on the payload is calculated using Equation 29, where q_w is obtained from the wind speed at the top of the gantry and is applied over the complete surface of the payload. The shape of the payload, and thus the surface, is not known when the crane is designed. The crane is just designed to lift a certain mass, independent of its shape. For the analyses in this thesis the same holds.

$$F_w = mass \times (area\text{-}mass\text{-}factor \times shape\text{-}coefficient) \times q_w/1000 \tag{29}$$

This corresponds with a percentage of horizontal load due to wind $H_{w,\%}$ as stated in Equation 30.

$$H_{w,\%} = (area\text{-}mass\text{-}factor \times shape\text{-}coefficient) \times q_w/(1000 \times 9.81), \tag{30}$$

In these equations, *mass* is defined as the mass of the payload in metric tonnes (Te). The mass is converted into an area using the *area-mass-factor*, unit m^2/Te. The *shape-coefficient* is assumed 1.20, for the lift of a vessel. This coefficient needs to be adjusted for loads with different shapes. Finally, $q_w(z)$ stands for the dynamic wind pressure at height z, in N/m^2, as a result of the prevailing wind speed. This pressure is calculated at the top of the gantry and applied over the complete payload, which overestimates the actual wind load. The *area-mass-factor* and *shape-coefficient* differ for different standards, but their product is very similar. In EN 13001[9] the product comes down to 1.20.

The standards considered by Mammoet all use an area-mass factor that is independent of the mass of the payload. However, from their track record in lifting heavy objects, using data of both crane and gantry lifts, Mammoet found a relation between the two.

The area of the payload is roughly related to a square of the main dimensions ($A \sim d^2$), the mass to a cubic ($m \sim d^3$). The mass thus grows faster than the area, with the main dimensions. Three load groups (L_1, L_2, L_3) where introduced and area-mass-factors determined (Table 6). The shape-coefficient was assumed equal to 1.2. A light-weight load can correspond with a higher factor, but really heavy loads always experience a lower area-mass factor, as expected.

The same load groups, area-mass factors and shape coefficient are used for the calculations in this section. The percentage of horizontal load can then be calculated using Equation 30.

Figure 28: PTC 140 DS Crane (Mammoet)

Table 6: Area-mass factor for different load groups.

load group	load P	area-mass factor $[m^2/Te]$	shape-coefficient [-]	product $[m^2/Te]$
L_1	$0 < P \leq 1600$	1.31	1.2	1.57
L_2	$1600 < P \leq 2400$	0.90	1.2	1.08
L_3	$2400 < P \leq 3200$	0.65	1.2	0.78

6.3 Wind on the Structure

Apart from the payload, the structure itself is susceptible to wind as well. Therefore, the wind on the masts and the top beam is considered, in accordance with the method for lattice structures in Annex A of EN 13001-2[10]. The wind is applied at a 90° angle with respect to mast section. This method takes into account area of the members, the solidity of the mast section and the aerodynamics of the section. The wind pressure at the top of the gantry is applied uniformly over the entire column, which is a conservative approach. Since the horizontal load is represented by a point load in the gantry model, the distributed load on the column is transformed into a quasi-equivalent point load (Figure 29). This point load is calculated as the force that results in the same displacement at the top as the distributed load (Equation 31).

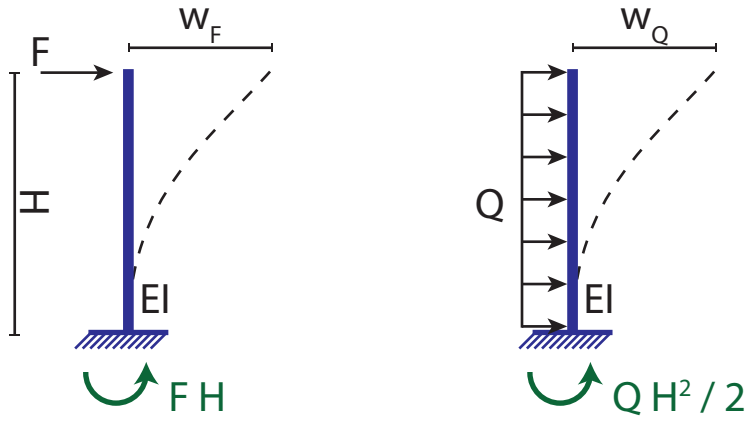

Figure 29: Column deformation: point load versus distributed load.

$$w_F = w_Q \rightarrow \frac{FH^3}{3EI} = \frac{QH^4}{8EI} \rightarrow F = \frac{3QH}{8} \tag{31}$$

The bending moment at the bottom is not equal for this point load, which is why its called a quasi-equivalent load. The bending moment for the point load is $3QL^3/8$, for the distributed load $QH^2/2$.

6.4 Loads From Skidding

If the load is skidded horizontally by means of a skid system on top of the gantry beams, this can result in extra horizontal forces, due to the inertia of the payload. It is standard practice within Mammoet to take into account 2% of the wind of the payload in the skid direction and 1% in the other direction.

6.5 Loads From Tailing

The actual lifting of the object typically includes the transition from a horizontal position of the object to a vertical position. This transition is aided by a tailing crane, a second (and much smaller) gantry structure or a tailing frame (Figure 6b). Here, the aid by a tailing frame is considered. The gantry lifts the object from the top, while the frame pushes its bottom forward. Figure 30 shows two phases of the lifting process, representing the two extremes of possible positions and orientations.

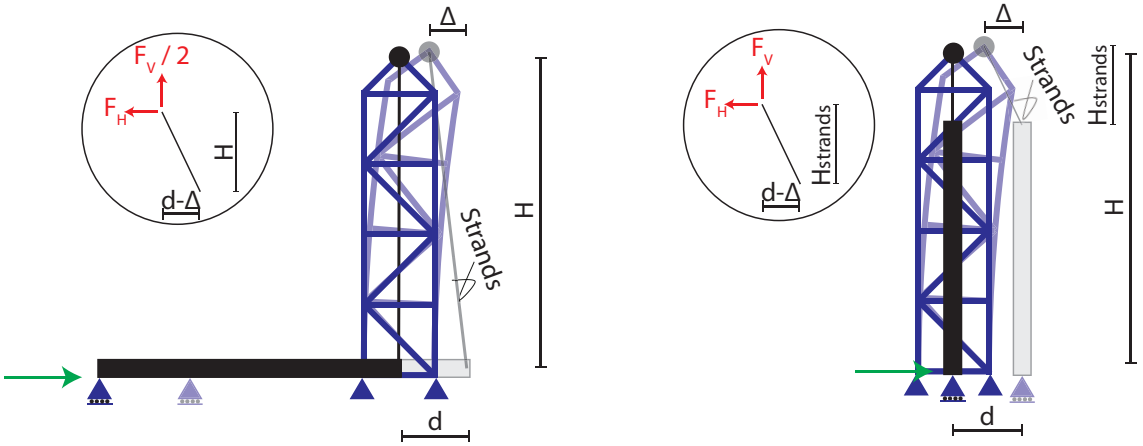

Figure 30: Tailing with a tailing frame, two phases: (almost) vertical and horizontal.

A good coordination between the lifting and the tailing process is essential. If tailing speed falls short or is too large, additional horizontal forces act on the gantry. The left side of Figure 30 shows the very beginning of the process, where the load hangs from the gantry and is supported by the tailing frame. In this case it is assumed that both the tailing frame and the gantry take 50% of the weight of the load. In the second phase, depicted on the right side of Figure 30, the load hangs vertically from the gantry. In this situation the gantry carries the complete weight of the load.

The additional tailing load is usually taken into account by adding a horizontal load equal to 1% of the vertical load in both horizontal directions. Whether or not this can be justified is of interest.

For both positions of the payload an off lead of 1% is considered in the direction of movement. This means that F_H in Figure 30 equals $0.01 \times F_V$. For the horizontal position, the first case, the length of the

strands is considered equal to the gantry height. For the vertical position, the second case, the length is taken as 10 m. The horizontal load from tailing is considered for gantries with a height of 50, 100, 150 and 200 m. This results in the values for the misalignment of the strands d that are given in Table 7.

If the gantry is infinitely stiff, the horizontal tailing load stays 1%, but it is not. The horizontal load results in a displacement Δ of the top of the gantry (Figure 30). This leaves a different horizontal load, as the angle of the strands has changed (d has become $d-\Delta$). Equation 32 describes the horizontal force in all strands combined (from geometry).

$$F_H = (F_V \times x) \times \frac{d-\Delta}{H_S}, \tag{32}$$

where x represents the percentage of payload that is taken by the gantry (50% for the first case and 100% for the second case) and H_S is the length of the strands. The deformation of the gantry Δ depends on the horizontal force F_H and the gantry stiffness $k = 6 \times EI/H^3$. This stiffness describes two adjacent cantilever columns. The percentage of extra horizontal load is calculated by solving Equation 33, which leaves Equation 34.

$$\frac{F_H}{F_V} = x \times \frac{d-\Delta}{H_S} = x \times \frac{d - F_H/k}{H_S} \tag{33}$$

$$\frac{F_H}{F_V} = x \times \frac{d \cdot k}{H_S \cdot k + F_V} \tag{34}$$

Thus, for an infinitely large stiffness this percentage is independent of the load F_V and is simply equal to $x \times d/H_S$. Equation 34 also shows that the percentage of horizontal load decreases with increasing payload, if the gantry is not infinitely stiff. This means that the percentage is closer to 1% for a lighter payload. A payload close to the limit of the gantry was used, for the heights under considerations.

For the first phase, the left side of Figure 30, the load percentage is always close to one. For the second situation however, a higher gantry results in a larger load decrease. The flexibility of the gantry, in combination with a relatively small off lead (0.1 m versus 1,2,3 or 4 m), makes sure that the horizontal force from off lead is reduced significantly. This is a good thing, as it gives some margin in the final phase of the lift. It has to be noted though that taller gantries are also more susceptible to second order effects from the deflection of the gantry structure, effects that are not taken into account here. The much smaller value of d for the vertical position is justified by the fact that the last phase of the erection is carried out much slower, as the operators know that this is the most critical phase.

Overall, as long as one takes great care in the execution of the last phase of the erection, an extra horizontal load of 1% seems sufficient.

Table 7: Tailing load, for different gantry heights and load positions.

		Horizontal (Hs = H)			Vertical (Hs = 10 m)		
H [m]	Load [Te]	d [m]	Stiff	Flexible	d [m]	Stiff	Flexible
50	4000	1	1.00%	0.99%	0.1	1.00%	0.88%
100	2000	2	1.00%	0.97%	0.1	1.00%	0.65%
150	1000	3	1.00%	0.97%	0.1	1.00%	0.52%
200	400	4	1.00%	0.98%	0.1	1.00%	0.53%

6.6 Total Horizontal Load

The four influences described are combined into three different load cases. Tailing and skidding are mutually exclusive, since they are not carried out simultaneously. Not all gantries have a skid system on top of the beam(s). Therefore, the results for cases 1 and 2 are calculated for both skidding and tailing. If skidding is involved, this action is governing.

Case 1: in-service

The combined effect of in-service wind (14 m/s at the top) and skidding/tailing is considered in this case. The in-service wind acts on the mast sections, the gantry beams and the payload. The wind loads are expressed as a percentage of the weight of the payload. The skidding/tailing loads are already expressed in percentages. The sum of the loads gives a horizontal load as a percentage of the weight of the payload.

Case 2: Emergency in-service wind

In this case the weather conditions become more severe during the lift operation. Therefore, the operation is suspended. The payload is however still hanging from the gantry. This combination only considers the emergency in-service wind. The goal of this combination is to find out how much extra wind pressure can be allowed, because of the absence of the operational actions from skidding/tailing. The emergency in-service wind acts on the mast sections, the gantry beams and the payload. The wind loads are again expressed as a percentage of the weight of the payload. The ratio between the total load in Case 1 and the total load in this case is calculated. This ratio gives the allowed increase in wind pressure. Any increase below 40% is considered too low to make a difference. A 40% increase in pressure roughly equals 20% increase in wind speed. This increase too little to distinguish the speed, due to large variations in (gust) wind speed.

Case 3: Emergency out-of-service wind

The emergency out-of-service wind (36 m/s at the top) acts on the gantry. This is a survival case, where no payload is hanging from the gantry. Thus, the emergency out-of-service wind acts on the mast sections and the gantry beams alone. The load is expressed in kN and applied to the gantry in the calculation model of Section 4.1. The gantry, not carrying a payload, is checked in this model. The load factor for the wind load is set to 1.2, instead of 1.5, since it is an extreme event. The check is performed with a load factor on the self-weight of 1.35 and 0.9. The reason is that the self-weight of the gantry can possibly have a positive influence on the tension check.

In Case 1 the horizontal load is expressed as a percentage of the weight of the payload, while Case 2 and 3 do not give a load percentage. Therefore, the load cases are considered as separate results. No comparison between the cases is made.

6.7 Results & Conclusion

For every load case and group the loads have been calculated for different gantry heights and payloads. Two wind directions are considered, one along the longitudinal axis of the gantry beam and one along

the transverse direction (Figure 24). Tables 15, 16, 17 and 18 show the results for cases 1 and 2, for the longitudinal respectively the transverse gantry beam direction and for skidding respectively tailing. These results are presented for a 88, 110, 132, 154 and 176 m high gantry.

The results for Case 1 show that the percentage of horizontal load is always biggest for the longitudinal direction, for skidding. For tailing, the opposite is true. Also, the percentage of horizontal load increases with height and decreases with payload. There is a significant difference in percentage between the respective load groups. A closer look at the percentages from Case 1 shows that between 40 and 75 percent of the horizontal load is due to wind. The share of the wind load decreases with an increasing payload and increases with height. Also, the majority comes from wind on the payload. Therefore, it is very useful to take the shape of the payload into consideration.

The reverse wind speed capacity, calculated in Case 2, is reasonable for both directions and for both skidding and tailing. An exception, where it is lower than 40%, is found for low payload weights (800 Te and lower). this means that in case of a sudden worsening of the weather situation, there is no margin left for these weights. Also, the reserve wind pressure increases with increasing payload and decreases with increasing height.

Table 8 shows an overview of percentages that are representative for both directions and operations (skidding/tailing). Case 3 has been considered for an emergency out-of-service wind in accordance with

Table 8: Overview of horizontal load percentages (Case 1): Overall percentage per load group, for both directions and for both tailing and skidding.

	0 to 1600 Te (L_1)	1600 to 2400 Te (L_2)	2400 to 3200 Te (L_3)
Skidding: Longitudinal	5.0%	4.0%	3.5%
Skidding: Transverse	4.0%	3.0%	2.5%
Tailing: Longitudinal	4.0%	3.0%	2.5%
Tailing: Transverse	4.0%	3.0%	2.5%

both region D (32 m/s) and region E (36 m/s), for both a hinged and a rigid beam-column connection. For both connection types a rigid foundation is used. The table shows up to which height the gantry does not fail under the influence of the emergency out-of-service wind on the gantry columns and beams. The

Table 9: Results for Case 3: Heights up to which the gantry does not fail, for both a hinged and a rigid connection between beam and column and for both a load factor of 0.90 and 1.35 on the self-weight.

	Rigid: 32 m/s	Rigid: 36 m/s	Hinged: 32 m/s	Hinged: 36 m/s
Load factor 1.35	154 m	154 m	132 m	121 m
Load factor 0.90	154 m	154 m	132 m	121 m

results indicate that that very tall gantries may not be able to bear the emergency out-of-service wind. Therefore, special attention should be paid to this load situation, for those high gantries. The effect is stronger for a hinged connection than for a rigid connection. It is probably even more severe for a flexible foundation.

7 Imperfections

The global imperfection of the gantry is one of the key input parameters of the calculation model, where it is taken into account as a sway imperfection. In the benchmark model, used to make finite element calculations, the first buckling mode is used to take the imperfection into account. Due to the large vertical load that the gantry has to carry, an imperfection results in serious extra bending moments. The local member imperfection of the chord is taken into account in the calculation of the compressive resistance $N_{Rd,c}$ and is thereby not considered here. The results in Section 5 show that the resistance is influenced more by a change in horizontal load than it is by using a different amount of imperfection, for the horizontal load percentages and imperfections under consideration. However, these results also show that calculating with a different imperfection can increase the resistance by 6-to-10% percent. It is thus very relevant to consider what imperfection to use.

A gantry column that is made out of pinned components, such as the New York Wheel Wheel mast sections, can have an out-of-plumbness due to several sources in the components and their connections. Where measures deviate from their nominal values, due to the fabrication tolerances, the mast sections and their connections can become skewed. Also, play in the connections can cause the columns to be imperfect. Mammoet desires to calculate the resistance with a 1/1000 imperfection and such precision needs justification. Unfortunately, Mammoet has no record of the actual precision of the gantries after erection.

Section 7.1 treats the sources of imperfection, while measurements on the fabrication precision of the mast sections are discussed in Section 7.2. Section 7.3 deals with theoretical imperfections. Conclusions are drawn in Section 7.4. The imperfection that needs to be taken into account in calculations, following the standards under consideration, is discussed in Section 8.1.

7.1 Sources of Imperfection

Since the members of MSG sections, shown in Figure 7, are all welded together, there is only play in the connection between two sections. The DS sections exist of two pieces that are connected using pins in the longitudinal direction of the sections (Figure 8), which leaves room for play within the sections as well. The situation of the New York Wheel mast sections is much more complicated, since all members are pinned together (Figure 31). There is play in these connections, which allows for a skewed mast section as well.

Thus, several things can contribute to an imperfect mast section, but in the MSG and DS sections not all of these are relevant. Hereafter, sources of imperfection relevant for the New York Wheel mast sections are discussed.

Foundation If the foundation is not completely level, the base frame of the column can be placed under angle. This means that the column suffers from a sway imperfection. However, base frames are generally positioned very accurately using shims and level apparatus.

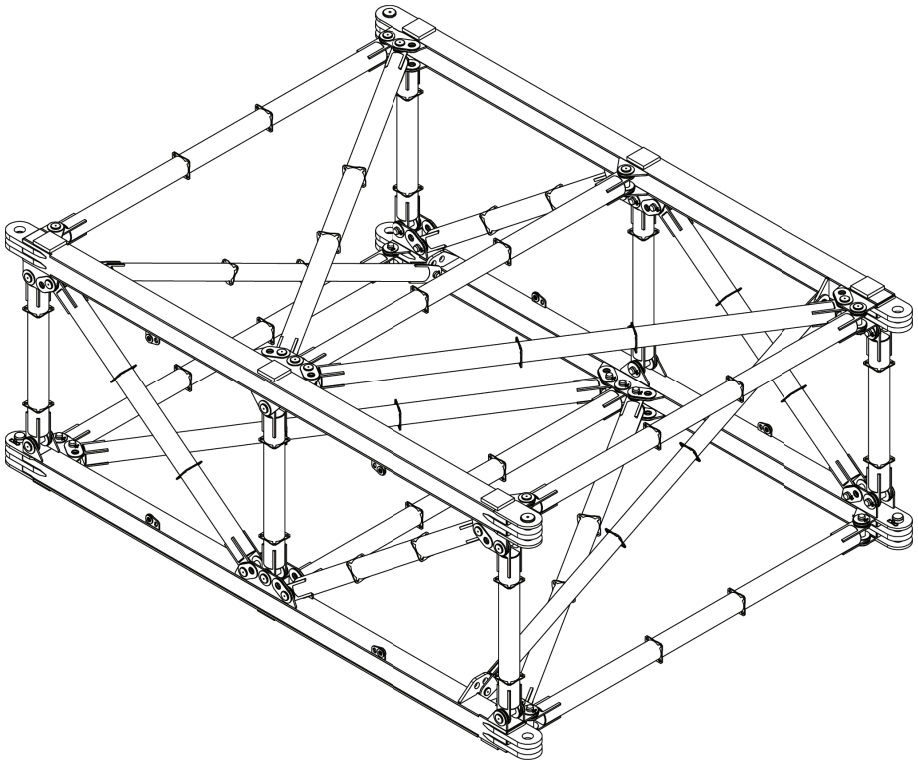

Figure 31: New York Wheel mast section (Mammoet).

Member lengths Due to the fabrication tolerances of the members, the length of the members of the mast sections varies. This can cause the mast sections to be skewed. The length of the chords can have an influence on the angle of the connection between successive mast sections in case of full contact connections. This is the case for the MSG sections, but not for the DS and NYW sections.

Position of the holes at the end of the members The members are connected via pin-hole connections. If the holes are misplaced, the section can become skewed and the connection can be under a (larger) angle.

Play in the pin-hole connections Even if all pins and holes are exactly fabricated as on the drawing, there is play in the connections. This allows for skewed sections and connections under an angle.

Pin hole diameter The holes are machined with a certain precision. If these are larger than intended, additional play in the connections is available. This gives the mast section the opportunity to become more skewed. Also, additional play in the connection between successive section can cause this connection to be under a (larger) angle.

Pin diameter The influence is similar to that of the pin hole diameter. If the pins are smaller than intended, the play becomes larger.

Figure 32 gives a 2D view of the connection between to successive NYW mast sections, for both compression (a) and bending (b). The rotation of the connection θ is influenced by the play in the pin-hole connections. This play is influenced by the nominal diameter of the holes and the pins as well as by the tolerances on these measures. The precision on the position of the holes is not included in this figure.

The largest connection angle for the compression case is found for a maximum hole and minimum pin on one side and the opposite on the other site. For the bending case, where one chord is in compression and one is in tension, a maximum hole and minimum pin on both sides results in the largest angle. In this case the connection opens up and the play is utilized. This results in a much larger angle than the compression case, where the rotation is only caused by the manufacturing tolerances on the pins and holes.

Under lifting conditions the wind load is moderate. This means that the bending moments are not very large. Also, the weight of the object that is lifted results in compression in the chords. Therefore, the bending situation is not present over the entire height of the column, as in part of the column all chords are loaded in compression. In storm conditions the situation is quite different. No payload is present to ensure compression in the chords and the wind load is much larger. This means that the region in which the bending case is present is much larger. However, after the storm the gaps of the pin-hole connections close again. In the storm situation the second order effects are much smaller, in absence of the weight of the payload. Very tall gantries can only lift a limited payload. This means that little weight is available to ensure compression in the chords, which results in a relatively large bending length. The imperfection is then possibly relatively large.

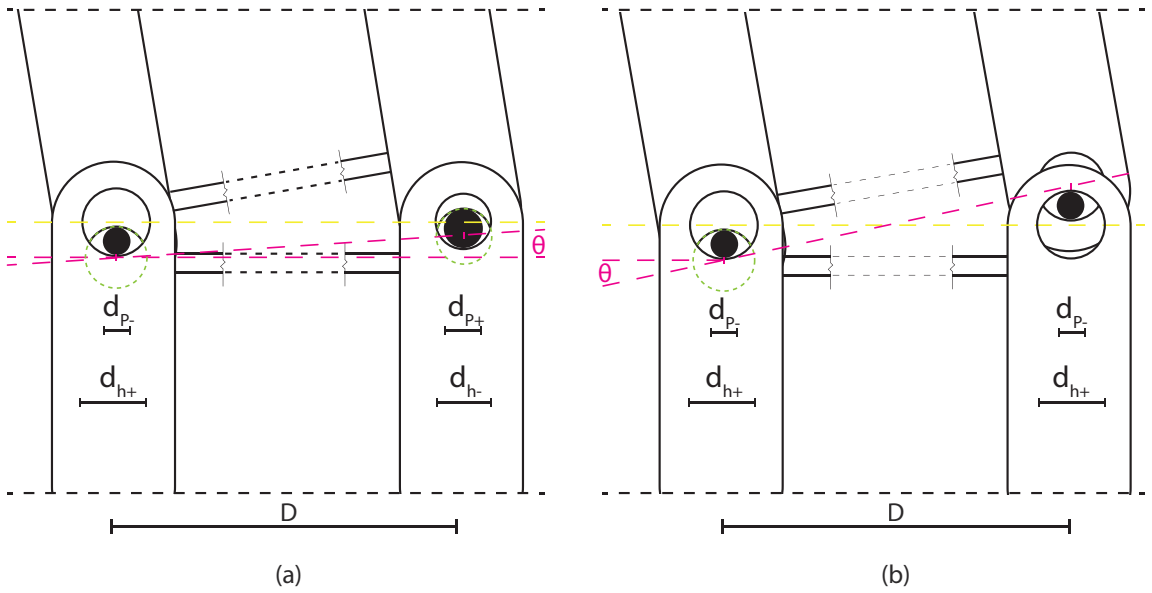

Figure 32: 2D view of connection between two successive NYW mast sections: (a) connection in compression, (b) connection in bending.

It stands to reason that it is hard to theoretically analyze the influence of the play and tolerances in the mast section, as it is a three-dimensional problem with many variables. One could start a statistical exercise on this, but that is deemed out of scope for this thesis. A simplified, two-dimensional analysis has however been executed by Mammoet. Section 7.3 deals with this analysis, but first the actual fabrication precision is considered.

7.2 Measurements

As stated earlier, within Mammoet no consistent record of the actual global imperfections of gantries exists. However, for both the MSG and DS sections measurements have been carried out on actual mast sections. Within this section, a so called Manufacturing Record Book is considered. This document, written by Hollandia, concerns measurements on the actual dimensions of DS mast sections that were built for Mammoet. The dimensions of nine mast sections, consisting of a top and a bottom part, are considered. An example of the documented values, on which also the nomenclature used in this section is shown, is given in Appendix H. Seven different types of dimensions are recognized to be of interest, all of which are shown in Table 19, in the same appendix.

Three of these measures, the the L,D and B-series, show very little variation and are thus not considered any further. From the other four, three sets of holes and a set of distances, a total of 320 observations has been recorded. Unfortunately, no data on the pins is available. Figures 85, 86, 87 and 88 in Appendix H show these observations. It is clear that the sections are fabricated well within the specified tolerances. Records on the MSG sections show similar results. For these sections data is also available on the pins. That data shows that the pins are fabricated very accurately as well.

From the records on the DS and MSG sections it is concluded that the most important source of imperfection for the mast sections is the play in the connections.

7.3 Global Imperfection for New York Wheel Sections

The New York Wheel mast sections contain many pinned connections, all with play in them. The pin diameter at the chords ends is 170 +0.0/-0.1 mm. The minimum pin diameter is thus 169.9 mm and the maximum is 170.0 mm. For the hole it is 171 -0.1/-0.4 mm. This corresponds with a minimum hole diameter of 170.6 mm and a maximum of 170.9 mm. This leaves a maximum play of 1 mm, a minimum of 0.6 mm and an average of 0.8 mm. This is similar to the DS sections.

As indicated before, it is very hard to find out the exact influence of the play and tolerances on the possible out-of-straightness of a gantry column. Also, the gantry contains two interacting columns, which makes an overall imperfection even harder to analyze. Nevertheless, since the mast sections are disassembled for transport, an analysis was carried out to assess the influence of the play and tolerances on the ease of assembly and on the imperfection of a column. This analysis is very much simplified, as only a single plane was considered. The assembly and the imperfection require opposite characteristics of the play and tolerances. For the assembly large play is preferred, while it is preferred to have small play for limiting the imperfection.

Although it is not of much interest here, it was concluded that assembly is always possible if the members are fabricated within the specified tolerances. The calculation of the imperfection includes the play in the pin-hole connections between mast sections and the play in the pin-hole connections between chords and braces. A global imperfection around 1/250 is found if it is assumed that every section-to-section connection is in bending. That seems quite dramatic, but in reality chords in tension are not present over the entire height of the column. When only half the column contains chords in tension,

which seems a much more realistic assumption for a lifting situation, an imperfection around 1/1000 is found. When all connections are in compression, an imperfection way smaller than 1/1000 is found.

7.4 Conclusion

The results in this section suggest that the mast sections can be fabricated with very high accuracy. However, the play in the connections of the mast sections can allow for a serious global imperfection. This imperfection is biggest when the gantry columns are in bending over a large portion of their height, which is the case for a relatively big horizontal load. Such a load can be found for very tall gantries and for storm conditions and can cause an imperfection between 1/250 and 1/500. In a lifting situation and for gantries with moderate heights the weight of the payload ensures compression in the chords over a large portion of the gantry columns. That means that a smaller global imperfection is found ($\approx$ 1/1000). Just after erection, in the absence of large horizontal loads, the column is in compression over its entire length and the imperfection is much smaller than 1/1000.

8 Comparison of Methods and Standards

Several standards are considered within the context of this thesis. Two European standards on steel structures, a European crane standard and an American standard for structural steel building. EN 1993-1-1[5] "General Rules and Rules for Buildings" focuses on the structural design of buildings, while EN 1993-3-1[6] "Towers and Masts" is specifically intended for the structural design of lattice towers and guyed masts and is used as a supplement to the buildings standard. One might also argue that a gantry should be designed along the guidelines of EN 13000[8] "Cranes - General Design", since the gantry executes crane like operations. The ANSI/AISC 360-10[12] "Specification For Steel Structure Buildings" standard is the American counterpart of EN 1993-1-1[5].

These standards differ on many aspects, such as the initial imperfection (Section 8.1), the loads on the structure (Section 8.2) and the application of guy lines (Section 8.3).

8.1 Imperfections

The various standards prescribe an amount of imperfection that shall not be exceeded:

EN 1993-1-1[5] This standard considers a sway imperfection for frames that equals $\phi = \frac{1}{200}\alpha_H\alpha_m$, where $\alpha_H = \frac{2}{\sqrt{H}}$ and $\frac{2}{3} \leq \alpha_H \leq 1$. The factor α_m takes into account the number of columns that are placed next to each other in the frame and equals $\alpha_m = \sqrt{0.5(1 + \frac{1}{m})}$. For the gantry under consideration $m = 2$ and H is such that $\alpha_H = 2/3$. This means that $\phi \approx \frac{1}{350}$. The imperfection may also be modelled directly using the buckling shape of the structure or by means of equivalent horizontal loads, similar to the AISC method of notional loads.

A 1/350 imperfection seems rather large, but it has to be noted that this is based on fabrication and erection tolerances used in the building industry. The standard relies on EN 1090-2[1] for the fabrication and erection tolerances. This standard prescribes a nominal pin-hole clearance of 3 mm for holes with a diameter larger than 27 mm. This clearances is reduced to 2.5 mm for towers and masts. The NYW mast sections and the DS mast sections are fabricated with a nominal pin-hole clearance of 1 mm. The hole tolerance that is prescribed in the standard is ± 0.5 mm, while it is -0.1/-0.4 mm for the NYW and DS sections. The mast sections are thus fabricated much more precise than is prescribed by the standard.

EN 1993-3-1[6] The towers and masts standard states that a maximum displacement of the tower top of lattice towers not larger than 1/500 is recommended. It also states that the national annex may give further information. In the Dutch national annex no such information is given. For the incorporation of the imperfection into calculations reference is made to the elastic global analysis in EN 1993-1-1.

The structures dealt with in this standard are slender structures, but they carry a limited vertical load. Therefore, second order effects are limited and not specified by this standard. These masts and towers are typically subject to substantial horizontal (wind) loads.

EN 13001-1[9] The crane standard does not provide any values for the global imperfection whatsoever.

ANSI/AISC 360-10[12] In the American steel structures standard two approaches are allowed. The first involves direct modelling of the imperfection, using the buckling shape or actual imperfections (if known). The second approach makes use of so called notational loads, fictitious lateral loads that result in extra displacements. The AISC Code of Standard Practice[14] prescribes a maximum column out-of-plumbness of 1/500. This is equivalent to a notional load $N = 0.002 \times F_V$, where F_V is the vertical load on the column.

Thus, different standards allow for different (methods to include) imperfections, with a maximum out-of-plumbness of 1/350 and a minimum of 1/500. Of course, Mammoet wants to keep the imperfections as tight as possible, since this allows for a larger payload or a lighter structure. In fact, Mammoet aims at an imperfection as tight as 1/1000. They state that they can build their gantries as accurate as that, but this is not supported by any standard nor by any consistent measurements in the field.

8.2 Loads & Resistance

The model is subject to three loads: The self-weight of the mast sections, the weight of the payload that is lifted by the gantry and the horizontal load on the gantry. The standards use different load and resistance factors for the structure.

EN 1993-1-1[5] divides the resistance by a material factor of 1.0. The self-weight of the structure is taken into account with a partial factor of 1.35 and all variable loads are factor by 1.5. The load factors can be found in table NB.4-A1.2(B) of EN 1990[2]. The standard refers to EN 1991-1-4[4] for wind calculations

EN 1993-3-1[6] divides the resistance by a material factor of 1.0. The gantry falls into reliability class 3, which means that the consequences of failure are likely to be high. The load factors can be found in table A.2 of EN 1993-3-1. The partial factor on self-weight is 1.2 and on variable loads 1.6. This standard refers to EN 1991-1-4[4] for wind calculations, but includes specific guidelines for wind loads on lattice structures as well. For the calculation of the structural resistance reference is made to EN 1993-1-1.

ANSI/AISC 360-10[12] determines the required strength for a load and resistance factor design (LRFD) by multiplying the characteristic strength by the resistance factor. This factor equals 0.9 for tension, compression and flexure. The load combinations are obtained from ASCE/SEI 7-10[13] "Minimum Design Loads for Buildings and Other Structures". This standard gives a load factor of 1.2 for the dead load (self-weight) and 1.6 for the live load (variable load). If notional loads are used, they are factored by 1.0.

EN 13001-1[9] divides the strength by a material factor of 1.1, which is equivalent to the 0.9 factor of the AISC. The load factors depend on the load combinations in which they are used and are to be found in EN 13001-2[10]. Load combinations A cover regular loads under normal operations, load combinations B cover regular loads combined with occasional loads and load combinations C cover

a selection of regular loads combined with occasional and exceptional loads. The partial factors for the loads on the gantry are shown in Table 10.

Table 10: Partial safety factors according to EN 13001-2 Table 12 (CEN).

	A	B	C
Dead load	1.22	1.16	1.10
Hoist load	1.35	1.22	1.10
Horizontal load	1.35	1.22	1.10
Wind load	-	1.22	1.10
Exceptional load	-	-	1.10

The table shows that when more loads are taken into account the load factors may be reduced. The load factor on in-service wind equals 1.22 (load combination B). The emergency in-service and out-of-service wind factors are 1.1. This standard is much better suited to account for controlled lifting conditions than the building standard EN 1993-1-1, since it better covers the operational aspects of lifting.

The load and resistance factors of the standards are summarized in Table 11, for the dead load and variable (lift) load. The material and resistance factors are given, as well as the load factors. The total load factors, that correct for different material and resistance factors, are also given. The crane standard (EN 13001-1) also applies a dynamic lift factor.

Table 11: Summary of partial safety factors for the standards under consideration.

	EN 1993-1-1	EN 1993-3-1	EN 13001-1	AISC-LRFD
Material factor γ_m	1.0	1.0	1.1	-
Resistance factor	-	-	-	0.9
Dead load factor	1.35	1.20	1.22	1.20
Variable (lift) load factor	1.50	1.60	1.35	1.60
Dynamic lift factor	-	-	1.11	-
Total dead load factor	1.35	1.20	1.34	1.33
Total variable (lift) load factor	1.50	1.60	1.65	1.78

The table shows that the AISC-LRFD (Load and Resistance Factor Design) appplies a much larger load factor to the live load than the other standards. Also, the crane standard allows for a relatively low load factor on the lift load, but the material and dynamic load factor make sure that the total load factor is not smaller than found from the building standard.

8.2.1 Wind Load

The wind load is calculated from a wind profile over height in all standards under consideration. Ultimately, the 3 second gust wind speed is calculated and then used to calculate a wind pressure. The load factor on wind is 1.5 for EN-1993-1-1, but the gantry is a temporary structure. EN 1991-1-4[4] prescribes that a reduction on the wind speed may be applied. For a period longer than three months but shorter

than a year a return period of 10 years is prescribed. This results in a reduction factor on the wind speed of 0.9, corresponding with a factor 0.81 on the wind pressure. This leaves a load factor $1.5 \times 0.81 = 1.22$. The load factors on emergency in-service and out-of-service wind are 1.1 for EN 13001-1. This is a bit lower, but the crane standard applies a material factor of 1.1, while EN 1993-1-1 applies 1.0. This leads to a factor of $1.1 \times 1.1 = 1.21$. In the American AISC standard a load factor of 1.6 is applied to wind. But in this standard the wind speed may be reduced by a factor 0.8 for structures active between six weeks and one year. Also, a factor 0.9 is applied to the resistance side of the check. This leaves $1.6 \times 0.8^2/0.9 = 1.14$.

Therefore, it is concluded that the partial factor on wind loads is very similar for the standards under consideration.

8.3 Guy Lines

EN 1993-1-1 refers to EN 1993-1-11[7] "Design of Structures With Tension Components" for the design of guy lines. This standards takes into account the catenary effect, as explained in Section 9.1, that reduces the effective stiffness of the guy lines. EN 1993-3-1 gives specific guidelines for guyed masts, including the effect of wind and ice.

8.4 Conclusion

In conclusion, the hand calculation method from the building standard, as described in Section 4.1, is best suited to describe the behaviour of the gantry. Where the building standard is preferable for the model, it seems that the crane standard best takes into account the operational aspects of lifting. It allows for different load factors for in-service and out-of-service wind loads and takes into account the dynamic effects of lifting the payload.

The imperfection that is prescribed by the respective standard, and in particular the imperfection prescribed by the European standards EN 1993-1-1 and EN 1993-3-1, seems too conservative for the gantry structure. The fabrication and erection tolerances used in these standard are much bigger than the actual fabrication tolerances of the mast sections.

9 Guy Lines

The resistance and second order deflections of the gantry are greatly influenced by the buckling resistance and stiffness of the gantry columns. One way to improve these involves the application of guy lines, bundles of prestressed, high strength, steel strands. Those guys are realized using strand jack systems (Figure 33) and provide a flexible lateral support at the top of the gantry columns.

It is difficult to study the behaviour of a gantry provided with guy lines. It is very hard to find the buckling resistance of the columns analytically, when a translational spring at the top of the column is introduced. Also, since the stiffness of the guy lines depends on the stress level in the strands, as is explained in Section 9.1, the calculation of the force distribution between column and guy lines involves non-linear behaviour. It is thus very complicated to find the reaction forces and the deflections of the column.

Therefore, the influence of the application of guy lines is analyzed only in a preliminary sense, using linear (stability) calculations in SCIA Engineer. The results give an indication of what is to gain by adding guy lines to a gantry design. This section treats three strand jack systems currently in use by Mammoet and investigates the influence of the application of these systems on the buckling resistance and first order deflections of the columns. Only the buckling resistance against a point load, not against a distributed load, is considered here. Also, the fraction of the horizontal load the guy lines bear is analyzed. The amount of prestressing and the angle of the guy lines are parameters of interest, as well as the stiffness of the strands.

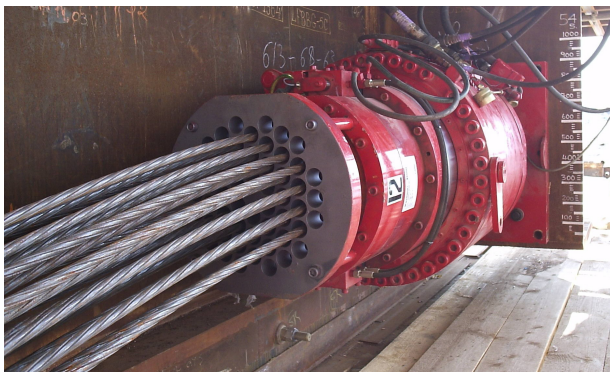

Figure 33: Application of a strand jack (Mammoet).

Four guy lines in both horizontal directions are considered, between the top of the gantry (Figure 5d) and the foundation (Figure 5f) level. These are indicated in blue in Figure 34, where the horizontal span L and the guy line angle α are shown as well. The angle is assumed to be the same for both directions. Of course, in practice these angles can differ.

The strand angle α determines the horizontal strand span, for a given gantry height, and has great influence on its effectiveness. A strand under a smaller angle is longer and therefore less stiff than a steeper strand. Another disadvantage of a shallow angle is the increase in footprint of the gantry. However, since its trajectory is more horizontal, its lateral stiffness is higher. Also, a steeper guy line introduces a larger

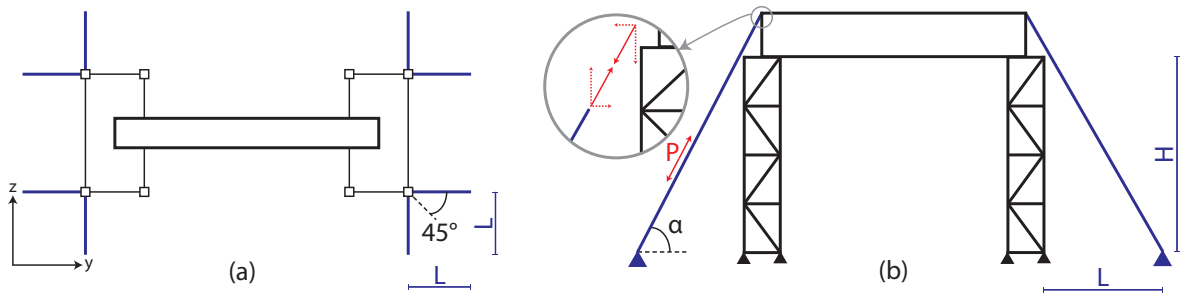

Figure 34: Gantry with guy lines: Top view (a) and side view (b). The gantry height H, horizontal strand span L and strand angle α are indicated.

vertical prestress force into the columns, as shown in Figure 34 (b).

The influence of the guy lines is considered for the four column models in Figure 35, where k_s represents the stiffness of the strands. These columns correspond with the models of Figure 48, in Section 4. Model (a) represent a single freestanding column, whereas model (b) represents a freestanding column on a flexible foundation, with rotational stiffness k_r. Models (c) and (d) show columns that are restrained against rotations at the top, with a rigid and flexible foundation respectively.

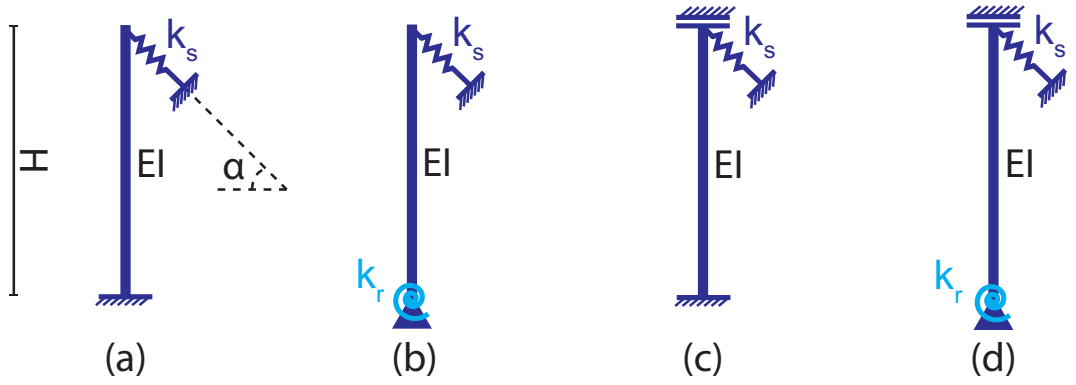

Figure 35: Column models, including guy lines.

The strand jack systems are discussed in Section 9.1, while the column models of Figure 35 are treated in Section 9.2 and the strand angles in Section 9.3. Section 9.4 deals with the results.

9.1 Strand Jack Systems

Two strand jack systems used by Mammoet to facilitate guy lines are considered, one that can take a maximum load of 100 Te and one with a maximum of 300 Te. A third system, with a maximum load of 600 Te, is also looked at. This system might be of use for the New York Wheel mast sections, since the gantries made out of these sections can be much higher than MSG gantries. These systems use bundles of 18 mm diameter strands. In the 100 Te system 7 strands are used, in the 300 Te system 18 and in the 600 Te system 36. The nominal Young's modulus of these strands equals 200 MPa. The effective Young's modulues E_{eff} $[N/mm^2]$ depends on the nominal modulus E $[N/mm^2]$, the unit weight of a strand w $[N/mm^3]$, the horizontal span of the strand L $[m]$ and the stress in the strand σ $[N/mm^2]$.

This is due to the catenary effect, caused by the self weight of the strand (Equation 35). This relation is described in EN 1993-1-11[7], the European standard for steel structures with tension components. More information on the strand jack systems can be found in Appendices A.2, A.3 and A.4.

$$E_{eff} = E \Bigg/ \left(1 + \frac{w^2 L^2 E}{12\sigma^3}\right) \tag{35}$$

The presstress level usually lies between 30% and 50% of the maximum load in the strand system and the strand angle commonly is around 60°. A minimum prestressing is necessary to keep the guys in tension and thus provide support for the columns. The stress level in the strands, necessary for determining the effective modulus, can be found by dividing the prestress force by the the total area of all strands. Figure 36 shows the effective Young's modulus as a function of the amount of prestressing (as a percentage of the maximum load in the system), for the 100 Te, 300 Te and 600 Te system. The effective modulus is shown as a percentage of the nominal modulus. For the 100 Te system the effective modulus is over 90% of the nominal modulus for 25% prestressing or more and over 95% for 30% or more. For the 300 Te and 600 Te systems these effective moduli are found for 20% and 25% respectively.

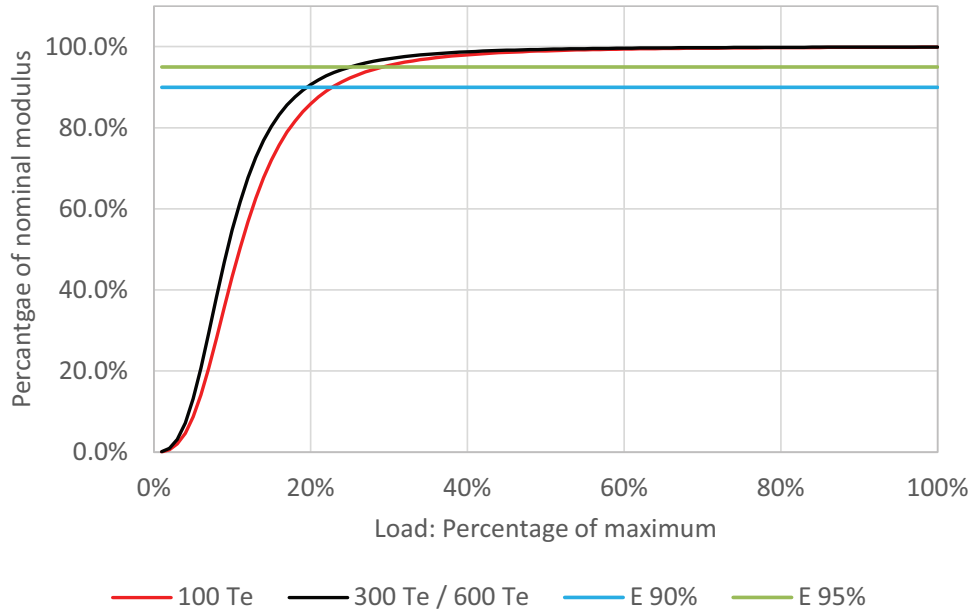

Figure 36: Effective Young's modulus as a function of the prestress level: The effective modulus is shown as a percentage of the nominal modulus.

9.2 Column Model

As long as the load in the guy lines is equal to or larger than 25% of its maximum, the effective modulus is at least equal to 90% of the nominal modulus for the strand jack systems. Beyond this prestress level the stiffness increases very slowly, but it drops rapidly below 25%. It is assumed that the amount of prestressing that is applied, ensures that this criterion is met under all load actions on the gantry.

Therefore, calculations are carried out with a constant effective modulus of 1.8×10^8 kN/m^2. This is conservative in terms of the buckling resistance and the stiffness of the column. It might however underestimate the part of a horizontal load that is taken by the guy lines, since the stiffness might be underestimated a little bit.

Both the MSG and New York Wheel sections are considered. The DS sections are not treated in this section, since analyzing these sections does not add much, considering the similarities between its stiffness and the stiffnesses of the MSG and New York Wheel sections (Figure 12). Since the stiffness of the MSG sections is very similar around the y-axis and z-axis, only the flexural stiffness around the z-axis is considered for this section type.

Table 12: Flexural stiffness [kNm^2] of the different sections: Bending around the y-axis and z-axis of Figure 34 (a).

	MSG	**DS**	**NYW**
y-axis	3.14E+07	1.15E+08	5.97E+08
z-axis	3.07E+07	2.81E+07	1.49E+08

Two guy lines are considered to support each column of the gantry at the top, which means that the column can be modeled as in Figure 35, with the linear elastic spring k_s in Equation 36.

$$k_s = 2 \times \frac{E_{eff} \times n \times A}{L_s} = 2 \times \frac{E_{eff} \times n \times A}{H/sin(\alpha)} \tag{36}$$

Where n is the number of strands in a single strand jack system, A equals the surface of one strand and L_s is the length of the strands. This length depends on the height of the gantry H and the strand angle α. For the MSG sections the 100 Te and 300 Te strand jack systems are considered. The 100 Te system is not sufficient for the New York Wheel sections, since a realistic percentage of horizontal load can result in exceedance of the maximum strand load, for a heavy payload. Therefore, the 300 Te and 600 Te system are used for these. For the rotational spring k_r the stiffnesses are obtained from the soil stiffness calculations in Section 4.1.1. Table 13 shows the resulting values.

Table 13: Rotational stiffness for column on soil: Foundation stiffness [kNm/rad].

	MSG sections			**New York Wheel sections**		
	(1) Loose sand	**(2) Dense sand**	**(3) Dense sand & gravel**	**(1) Loose sand**	**(2) Dense sand**	**(3) Dense sand & gravel**
y-axis	-	-	-	2.33E+07	8.84E+07	7.22E+07
z-axis	3.34E+05	1.27E+06	2.87E+06	8.41E+06	3.19E+07	2.00E+08

The buckling resistance, first order deflection and load distribution are calculated using linear (stability) calculations in SCIA Engineer.

9.3 Strand Angle

The strand angle α of the guy lines can realistically be anything between 40° and 90°. More shallow angles require so much space that they are not considered. In order to assess the influence of the guy

lines, one strand angle is chosen. Therefore, the influence of this angle is first investigated. In Figure 37 the buckling length of a column made out of New York Wheel mast sections is considered, for buckling around the weak axis. This is done for a column that resembles model (a) of Figure 35, for a 60, 80, 100, 120, 140, 160 and 180 m high column and for the 300 Te and 600 Te strand jack systems. In the graph the buckling factor μ is shown, that relates the buckling length H_{cr} to the height of the column: $H_{cr} = \mu \times H$. Using this length in the well known Euler buckling formula gives the buckling resistance.

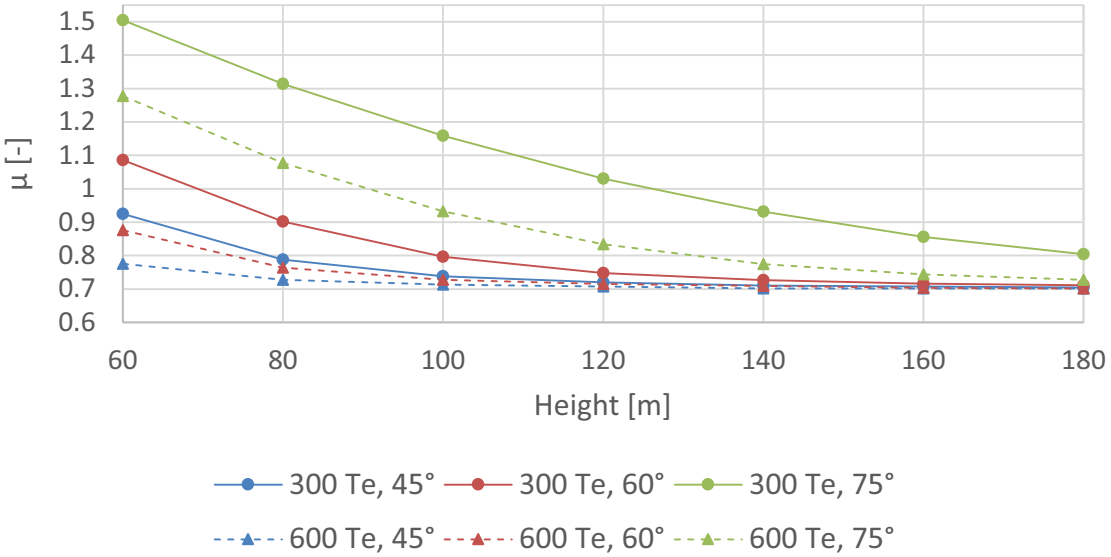

Figure 37: Buckling factor μ for column with guy lines: For model (a) of Figure 35. Results for the 300 Te and 600 Te system, for strand angles of 45°, 60° and 75°, for buckling over the y-axis of the New York Wheel sections.

It is clear that both the type of strand jack system and the strand angle have considerable influence on the buckling length. Also, the guy lines become relatively more stiff compared to the column over height, reducing μ with increasing column height. A guy line under an angle of 75° seems to reduce the buckling length much less than one under a 45° or 60° angle. Still, the reduction is at least 25% and over 50% for greater heights, for the 300 Te system. For the 600 Te system the reduction is much larger. A free standing column has a buckling factor μ equal to 2. The difference between the 45° and 60° angle is much smaller, especially for larger heights. Therefore, a closer look at the angle is taken for one specific height and strand jack system, 140 m and 300 Te. Figure 38 shows the buckling length H_{cr} and first order deflection w as a percentage of the values obtained for a column without guy lines. Also, the percentage of horizontal load taken by the guy lines is shown.

The buckling length and first order deflection do not change too much between 40° and 60°, after which they rapidly increase. The percentage of horizontal load taken by the guy lines decreases faster after this point as well. Therefore, the analysis continues for only one strand angle, equal to 60°. Using a more shallow angle does not bring much buckling resistance and stiffness, but increases the footprint of the gantry a great deal.

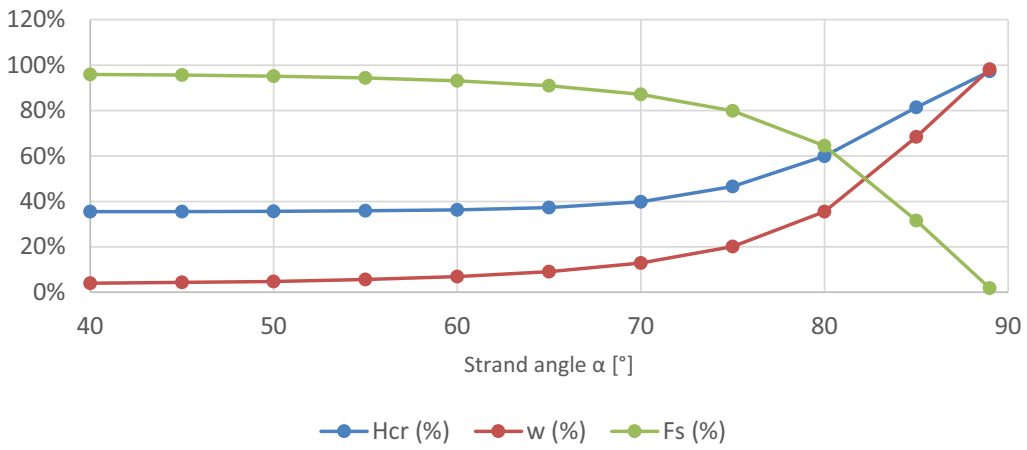

Figure 38: Buckling length, first order deflection and horizontal force in the guy lines: Results for the 300 Te system, for strand angles between 40°, and 89°, for buckling over the y-axis of a 140 m high column made out of New York Wheel sections.

9.4 Results

The buckling length, first order deflections and load distribution have been calculated for a lot of configurations. Models (a) to (d) have been evaluated for both the MSG (z-axis) and New York Wheel (y-axis and z-axis) mast sections, for the foundation stiffnesses in Table 13. For the MSG sections the 100 Te and 300 Te strand jack systems have been applied, for the New York Wheel sections the 300 Te and 600 Te systems. All models have been analyzed without guy lines as well. All these calculations together leave a big pile of results, presented in graphs in Appendix I.

9.4.1 Buckling Length

Figure 39 shows the buckling factors for models (a) and (c), for a free end at the top and for a column that is laterally restraint at the top. The second situation is equivalent to infinitely stiff guy lines. For these two models, the buckling factors for a column with guy lines lie between the two limit cases in the figure.

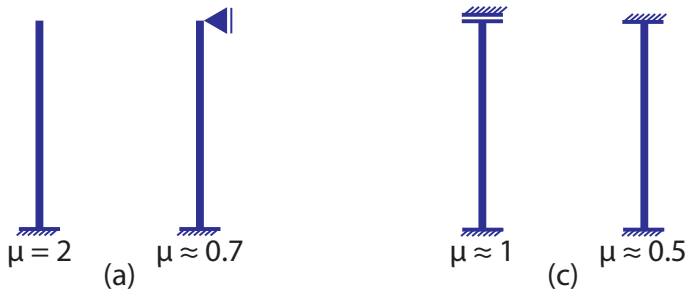

Figure 39: Buckling factors for columns with and without a lateral support at the top, for column models (a) and (c).

The graphs in Appendix I.1 show the buckling factor as a function of the height of the column, for the different mast sections and strand jack systems. The models b1 , b2, b3, d1, d2 and d3 corresponds with

the foundation stiffnesses of Table 13. The results show that a considerable reduction in buckling length is realized from the application of guy lines. For the weak direction of the New York Wheel sections the factor converges towards 0.7 and 0.5, for the (a) and (b) respectively the (c) and (d) models, for increasing height and for both strand jack systems. For a 120 m high column the factors are already around 0.75 and 0.55 for the 300 Te system and even lower for the 600 Te system. Only for a foundation on loose sand, the buckling factor remains significantly larger than 0.7 and 0.5. The guy lines can thus almost be regarded as a perfect lateral restraint. For the strong the direction the situation is quite different. No convergence is visible, but the factor becomes lower and lower for greater heights. For a 120 m high column the factors are around 1.10 and 0.9 for the 300 Te system and around 0.9 and 0.7 for the 600 Te system. Thus, the factors are considerably higher than for the weak direction.

For the MSG sections the situation is again different. The difference between the respective soil types is much larger, due to the limited footprint of the base frame. Also, the factor does not decrease much more above a column height of 100 m. For an infinitely stiff soil, models (a) and (c), the factor converges quickly to 0.7 and 0.5 respectively. The difference between a 100 Te and a 300 Te system is relatively small. However, the 100 Te system might not be strong enough to withstand the horizontal loads on the gantry.

The buckling factors are somewhat lower for the heavier strand jack system, but the difference is not too big and it decreases with increasing height.

9.4.2 First Order Deflection

The first order deflections are shown in the graphs of Appendix I.2, as a percentage of the deflection of the same column without guy lines. A reduction of the deflection results in a decrease in second order effects, increasing the resistance of the gantry. For both section types the decrease is much larger for the columns without a rotational restraint at the top, models (a) and (b), than for models with such a restraint, (c) and (d). For the weak direction of the New York Wheel section the reduction is over 95% for the 300 Te system and even over 95% for the 600 Te system, at considerable heights. The deflection with the 600 Te system is a little more than half of the deflection with the 300 Te system, on average. For the strong direction the situation is again quite different. The influence of the foundation stiffness is much larger and the reduction much smaller. However, for a 120 m high column the reduction can still be as high as 90%, for both strand jack systems. The difference between the systems rapidly decreases with height.

For the MSG sections the soil stiffness has a large influence as well. The reduction in deflection is spectacular for these sections, at least 75% for a 100 m high column. The deflection for the 100 Te systems is double the deflection for the 300 Te system, on average.

9.4.3 Load Distribution

In Appendix I.3 the percentage of horizontal load that is taken by the guy lines, in a linear calculation, is considered. The results show that a large portion of the horizontal load is taken by the strand wires, especially for high columns. Especially for the models (a) and (b) the guy lines take a large portion of

the load. For the weak direction of the New York Wheel sections the share can already be over 90% for a 120 m high column. For the strong direction the percentages are a bit smaller, but still considerable. For the MSG sections the percentage are even higher, at such heights. A 300 Te strand jack system ensure that at least 90% of the horizontal load is taken by the guy lines, if the column is 100 m high or taller.

Where a large portion of the horizontal load is taken by the guy lines, a vertical load on the column is almost entirely carried by the mast sections. This is logical, since the axial stiffness of these sections is much larger than the stiffness of the strands.

9.4.4 Prestress Force

Applying guy lines does not only positively influence the stability and stiffness of the gantry columns. The prestress force in the strand wires results in an extra compressive force in the mast sections. This force has been looked at and for the New York Wheel sections it never exceeds 2% of the buckling resistance. Thus, only a small portion of the buckling resistance is consumed by this extra force. For the MSG sections is does not exceed 5%. Therefore, it is concluded that it is not a problem.

9.5 Conclusion

In conclusion, the application of guy lines results in a significant increase of the buckling resistance, for all systems under consideration. Especially for the weak direction of the New York Wheel sections, where the buckling factor comes close to the limit case in Figure 39. Also, the deflection is reduced greatly, which means that second order effects are much smaller for a column with guy lines than a column without. The guy lines are able to take a large portion of the horizontal load, reducing bending moments in the column, and a vertical load is mostly taken by the mast sections. This is a very efficient load bearing system. For the buckling factor, the deflections and the load in the guy lines the difference between different strand jack systems reduces rapidly with increasing column height.

In Section 9.3 it emerged that a strand angle of 60° is most efficient, in terms of footprint and contribution to stiffness and stability.

10 Conclusion

Within this master thesis, several topics related to lifting gantries have been investigated. These topics are the modelling of the structure, the structural behaviour of the gantry, the input parameters of the model and the standards used for the design. Conclusion are drawn for the research objectives of Section 1.2.

How well do the hand calculation methods under consideration perform, when compared to the benchmark model? Which method is most suitable to go forward with?
Initially, three different hand calculation models were developed to describe the behaviour of a gantry column. Their performance was assessed by comparing the resistance from these models to the resistance found from a numerical model of the column in SCIA Engineer[15]. It was concluded that a model based on the analysis of built-up compression members, from EN 1993-1-1[5], performs best. The results, based on geometrically non-linear calculations, are very close to the results from the finite element method. It was therefore chosen to go forward with this method and to develop a hand calculation model that describes the structural behaviour of the gantry.

How well do the results from the final hand calculation model resemble those from the benchmark model?
The hand calculation model, as described in Section 4.1, calculates the resistance of a portal like gantry (Figure 1) made of two masts and a gantry beam on top. The resistance of several gantry configurations has been calculated with the model and it was concluded the model performs well, two to five percentage difference, and is thus able to describe the structural behaviour of the gantry.

The resistance of the gantry is based on a compression and a tension check of the chords, as well as stability checks in both principal direction of the mast sections, for an ultimate limit state. The model is able to represent a rigid as well as a flexible foundation and a hinged as well as a rigid connection between the columns and the gantry beam(s). The gantry is subject to a vertical load from the self-weight of the mast sections, a vertical load from the weight of the payload and a horizontal point load at the top of the gantry that accounts for operational loads and wind loads on both the structure and the payload. The horizontal load is expressed as a percentage of the weight of the payload.

How large is the influence of the amount of horizontal loading on the allowable payload?
The resistance has been calculated for different percentages of horizontal load between 0% and 6%, for multiple configurations. It was concluded that this percentage is of large influence for the resistance. The difference can easily be between 10-to-30% for the NYW mast sections, between 2% and 4% horizontal load. Also, the influence is larger for a gantry with a rigid beam-column connection than for a hinged connection. The resistance of a gantry with a rigid connection at the top as considerably larger than for a hinged connection, for an asymmetric mast section like the NYW mast sections. For a symmetric mast section, for example the MSG section, this is not the case.

How large is the influence of the global imperfection on the allowable payload?
A sway imperfection has been introduced in the model and the resistance has been calculated for an imperfection equal to 1/250, 1/500 and 1/1000 of the gantry height. The results show that the influence of the imperfection is much smaller than that of the horizontal load, but still significant. The difference between a 1/250 imperfection and no imperfection is 6-to-10% for the NYW sections.

How large is the influence of the foundation stiffness on the allowable payload?
In most cases the structure is placed on top of a large foundation slab. However, in some cases the gantry is placed on a much more flexible subsurface. The influence of the foundation has been investigated for both MSG and NYW mast sections, using the method of Pais and Kausel (1998 [18]). It was concluded that the soil stiffness can have a significant influence on the resistance, especially for a hinged beam-column connection. Also, the effect is much bigger for the MSG sections than for the NYW sections, since the base frame of these sections is much smaller. This leaves a much smaller rotational stiffness at the bottom of the gantry columns. A foundation on dense sand leads to a resistance decrease around 5% for the NYW sections and around 35% for the MSG sections.

How large is the difference in allowable payload between the NYW, MSG and DS sections?
The resistance has been compared for the three mast section types under consideration, the MSG, DS and NYW mast sections, for a rigid foundation. It turns out that for both a hinged and a rigid beam-column connection the NYW sections can bear the highest payload, by far. The resistance of the DS and MSG sections differ much less for a hinged connection than for a rigid connection. The DS sections can always carry a larger payload. The resistance to tensile forces, mostly governed by the strength of the connections, is much lower for the MSG sections than for the DS sections. Also, a rigid connection significantly improves the asymmetrical DS sections. For relevant gantry heights the MSG sections can bear a payload that is roughly 50% of the payload that the DS sections can carry, for a hinged top connection. For a rigid connection it is around 30%. The DS sections can carry 15-to-25% of the load the NYW sections can carry, for a hinged connection. For a rigid connection it is 25-to-35%.

How does the type of beam-column connection influence the allowable payload?
For NYW mast sections on a rigid foundation the resistance of a gantry with a rigid beam-column connection is 1.5 to 4 times higher than for a hinged connection, for reasonable heights. The difference in resistance increases with increasing height and decreases with increasing percentage of horizontal load.

Can the model take into account the application of guy lines? What is the contribution of these guy lines to the stability and stiffness of the gantry?
The behaviour of guy lines is highly non-linear. Therefore, it was found challenging to incorporate them in the hand calculation model accurately. However, a preliminary study has been carried out to assess the influence of the application of guy lines on the stability and first order deflections of the gantry columns.

It was found that the buckling length can be reduced by around 50%, almost to the point where a column with a fixed end at the top is resembled. Also, the first order deflection can be reduced significantly, as over 75% of the horizontal load is taken by the guy lines. This means that the second order effects are drastically reduced. The reduction also has a positive effect on the first order bending moments in the column. A guy line that is installed under a 60° angle with the foundation turns out to be effective in both supporting the column and minimizing the gantry footprint.

How do the different standards deal with the loads on the structure?
It was concluded from the calculations that the European buildings standard EN 1993-1-1 [5] best describes the structural behaviour of the gantry, but the European crane standard EN 13001-1 [9] seems best suited to take into account the load on the structure.

What global imperfection is prescribed by the standards and what is a realistic imperfection for the gantry columns?
The global imperfection Mammoet wants to calculate with equals one thousandth of the height of the gantry, since they believe their gantries can be erected with such high precision. The standards under consideration prescribe a larger imperfection, typically 1/500. The fabrication and erection tolerances are however much tighter for the mast sections than provided by the standards. Also, the analysis in Section 7 shows that a smaller imperfection (1/1000) can be justified, except for very tall gantries and gantries in storm conditions.

What are realistic horizontal loads, related to the load that is lifted by the gantry, and what are the major contributors to the horizontal load on the structure?
The horizontal load on the gantry varies between 2.5% and 4% of the weight of the payload, depending on the direction, the weight of the payload and whether or not skidding of the load is involved. Skidding results in a larger horizontal load in the skid direction. A large portion (40-to-75%) of the horizontal load comes from wind loads, of which the load on the object to be lifted is the biggest contributor. Also, the reverse wind speed capacity, available in case of sudden worsening of the weather, is reasonable for both directions and for both skidding and tailing. Finally, the results indicate that that very tall gantries may not be able to bear the emergency out-of-service wind. Therefore, special attention should be paid to this load situation, for those high gantries.

11 Recommendations

The findings in this thesis lead to several recommendations for the design of a tall and slender gantry, like the gantry shown in Figure 1. Also, the results lead to recommendations for further research.

The use of New York Wheel mast sections results in a considerably larger resistance, compared to the MSG and DS mast sections. Therefore, the NYW sections should certainly be considered for heavily loaded gantries. The NYW and DS mast sections have an asymmetrical shape, and thereby stiffness. This means that a gantry made out of these section is more sensitive to loads in one direction than in the other. For symmetrical loading it is therefore recommended to investigate the possibility of realizing a rigid beam-column connection.

The potential for guy lines is clear from the analysis in Section 9. It is therefore recommended to do further research on the incorporation of guy lines into the hand calculation model.

The European crane standard seems best suited to describe the loads on the gantry, since it best takes into account the operational aspects of lifting. It is therefore recommended to use this standard to determine the loads and load factors for the design of the gantry.

The horizontal loads on the gantry are very important for the resistance of the structure. A major contributor to the horizontal load is the wind on the payload, that depends heavily on the shape of this payload. Research on its exact shape is therefore recommended. Also, the wind load was calculated conservatively to be constant over the complete surface of the payload. This calculation should be enhanced in a more detailed design.

A discrepancy exists between the imperfection that is found from an analysis of the mast sections and the imperfection that is prescribed by the standards. Therefore, it is recommended to built a track record of the imperfection of the gantries before lifting, to support the finding in Section 7 that a smaller imperfection than prescribed by the standards is justified.

References

[1] *NEN-EN 1090-2: Execution of steel structures and aluminium structures - Part 2: Technical requirements for steel structures.* CEN, 2011.

[2] *NEN-EN 1990: Basis of Structural Design.* CEN, 2011.

[3] *NEN-EN 1991: Eurocode 1 - Actions on Structures.* CEN, 2011.

[4] *NEN-EN 1991: Eurocode 1: Actions on structures - Part 1-4: General actions - Wind actions.* CEN, 2005.

[5] *NEN-EN 1993-1-1 - Eurocode 3: Design of Steel Structures, General Rules and Rules for Buildings.* CEN, 2006.

[6] *NEN-EN 1993-3-1 - Eurocode 3: Design of Steel Structures, Towers, Masts and Chimneys - Towers and Masts.* CEN, 2006.

[7] *NEN-EN 1993-1-11: Design of Structures With Tension Components.* CEN, 2007.

[8] *NEN-EN 13000: Cranes - Mobile Cranes.* CEN, 2010.

[9] *NEN-EN 13001-1: Cranes - General Design - Part 1: General Principles and Requirements.* CEN, 2015.

[10] *NEN-EN 13001-2: Cranes - General Design - Part 2: Load Actions.* CEN, 2014.

[11] *NEN-EN 13001-3: Cranes - General Design - Part 3-1: Limit States and proof competence of steel structure.* CEN, 2012.

[12] *ANSI/AISC 360-10: Specification for Structural Steel Buildings.* AISC, 2010.

[13] *ASCE/SEI 7-10: Minimum Design Loads for Buildings and Other Structures.* ASCE, 2010.

[14] *AISC 303-10: Code of Standard Practice for Steel Buildings and Bridges.* AISC, 2010.

[15] Nemetschek AG. *SCIA Engineer, Version 15.0*, 2015. URL `http://www.scia.net/`.

[16] *Basis of Design: PTC-140/200 DS.* Mammoet, 2012.

[17] N. Subramanian. *Design of Steel Structures.* Oxford University Press, Oxford, United Kingdom, 2011.

[18] A. Pais and E. Kausel. Approximate formulas for dynamic stiffnesses of rigid foundations. *Soil dynamics and earthquake engineering*, 7, No. 4:213–227, 1988.

[19] *Soil-Structure Interaction for Building Structures (NIST GCR 12-917-21).* NEHRP Consultants Joint Venture, 2012.

[20] C. Hartsuijker and J.W. Welleman. *Constructiemechanica 3, Module: Stabiliteit van het evenwicht, Deel 1: Theorie.* TU Delft, Delft, Netherlands, 2007.

[21] P. Timoshenko and James M. Gere. *Theory of Elastic Stability.* Mc Graw Hill, Singapore, 1963.

[22] KNMI: Koninklijk Nederlands Meteorologisch Instituut. `http://www.knmi.nl/`.

[23] M.L. Rodenburg. Additional lifting days for single blade installation. Master's thesis, TU Delft, Delft University of Technology, 2015.

[24] Abhijeet Limbhore. Investigation of unguyed gantry systems: Study of alternatives to improve the load carrying capacity of an unguyed gantry system. Master's thesis, TU Delft, Delft University of Technology.

[25] C. S. Durst. Wind Speed Over Short Periods of Time. *Meteorological Magazine*, 89:181–187, 1960.

Appendices

A Equipment

In this appendix some information on the equipment is to be found. Appendix A.1 shows some properties of the MSG base frame. Appendices A.2, A.3 and A.4 give information on the 100 Te, 300 Te and 600 Te strand jack systems.

A.1 MSG Base Frame

MAMMOET

MSG GANTRY SYSTEM

BASE FRAMES
DIMENSIONS AND SPECIFICATIONS

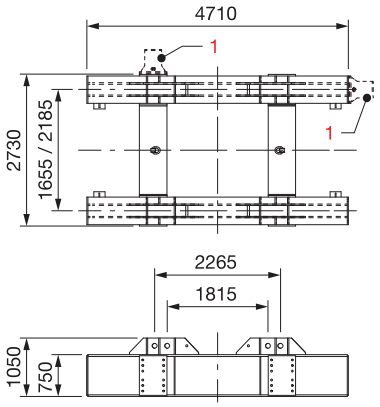

Base frame, type 1

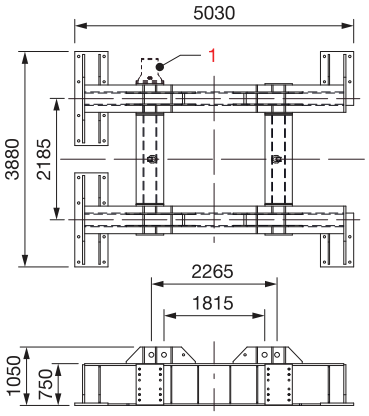

Base frame, type 3

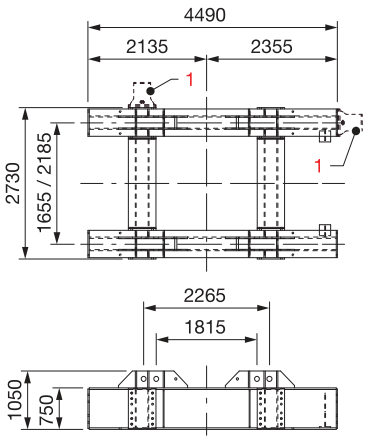

Base frame, type 2

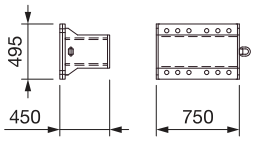

Side bracket

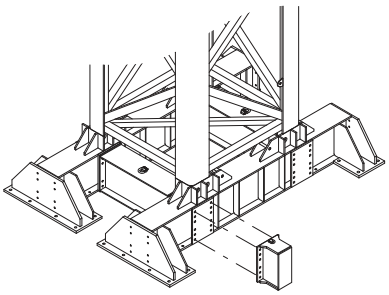

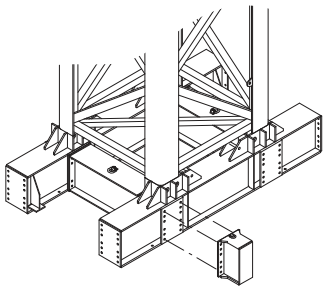

WEIGHT	
Base frame type 1	
With width 1655	6945 kg
With width 2185	7285 kg
Base frame type 2	
With width 1655	7067 kg
With width 2185	7285 kg
Base frame type 3	9660 kg
Side bracket	224 kg

[1] Locations of the side bracket

Dimensions are in millimeters, t = metric tons.
The content in this document is mentioned for reference use only. Values may differ from current data. Always contact Mammoet for current project calculations.

MAMMOET THE BIGGEST THING WE MOVE IS TIME

Version 1, 2015-11-06, SAP No. 4000105969

A.2 100 Te Strand Jack System

MAMMOET

SSL100
STRAND JACK
DIMENSIONS AND SPECIFICATIONS

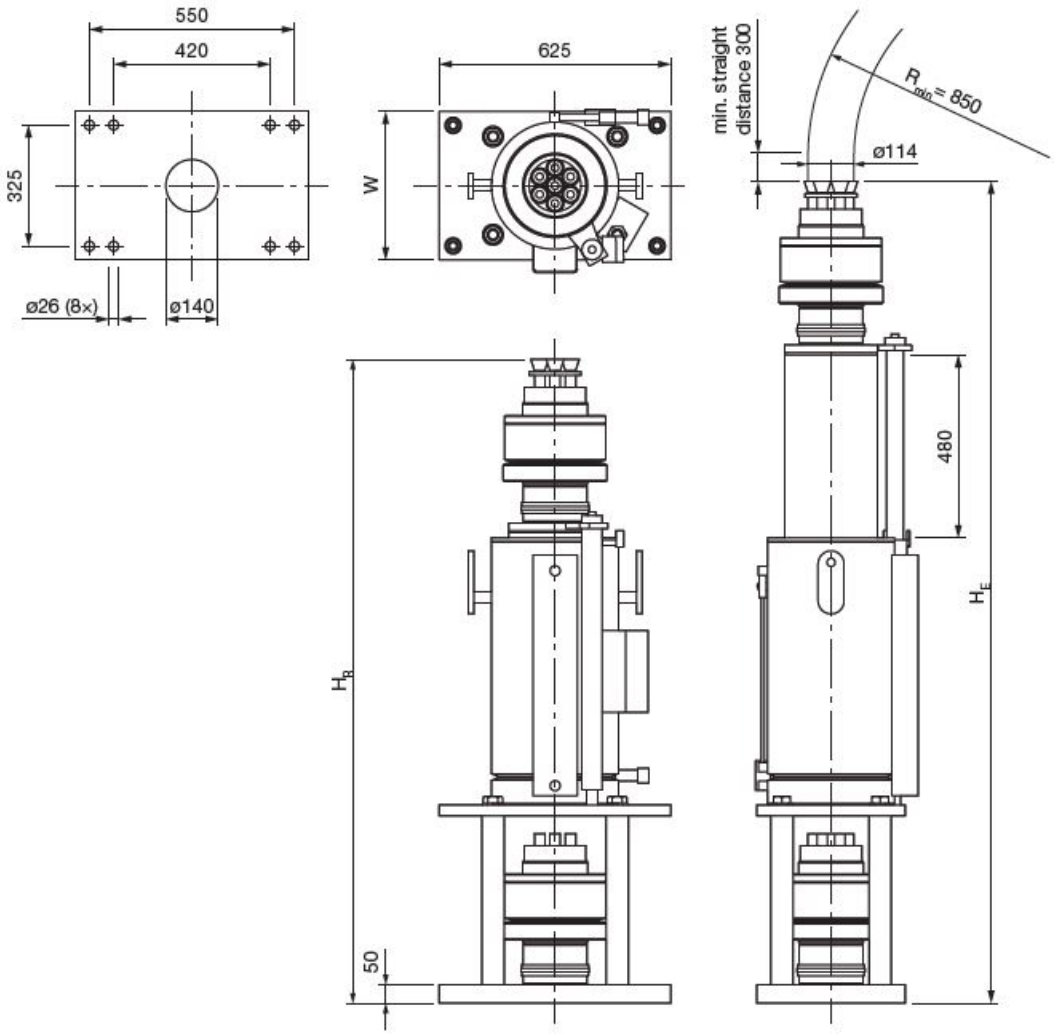

SPECIFICATIONS

	Type 1	Type 2
Capacity	100 t	100 t
Working pressure of the cylinder	200 bar	210 bar
Stroke	480 mm	480 mm
Strand type	Dyform	Dyform
Strand diameter	18 mm	18 mm
Max. no. of strands	7	7
Max. diameter of the strand bundle	114 mm	114 mm
Width (W)	400 mm	408 mm
Length	625 mm	625 mm
Height		
Retracted (H_R)	1737 mm	1926 mm
Extended (H_E)	2217 mm	2406 mm
Weight	950 kg	850 kg

Strand jack SSL100 type 1 is shown.
Dimensions are in millimeters, t = metric tons.
The content in this document is mentioned for reference use only. Values may differ from current data. Always contact Mammoet for current project calculations.

A.3 300 Te Strand Jack System

MAMMOET

SSL280
STRAND JACK
DIMENSIONS AND SPECIFICATIONS

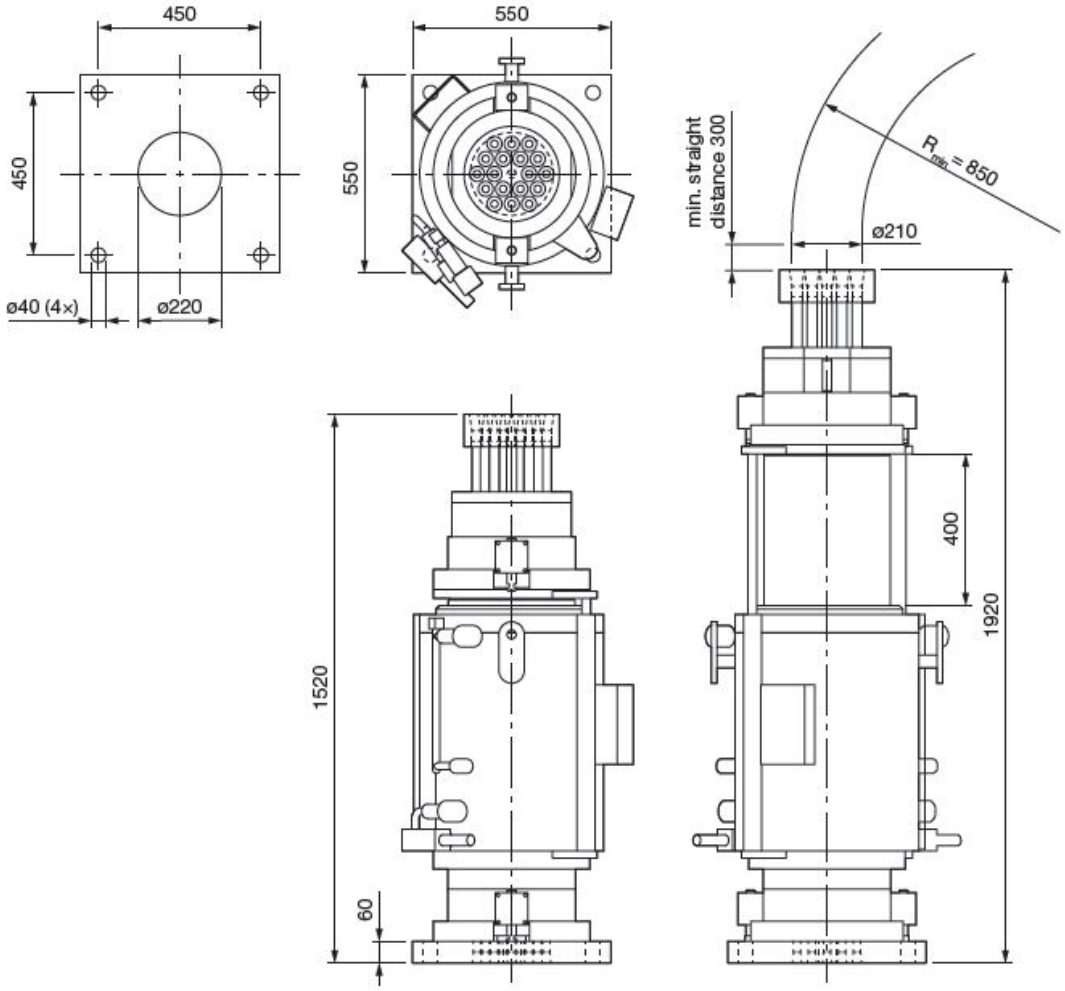

SPECIFICATIONS	
Capacity	300 t
Working pressure of the cylinder	400 bar
Stroke	400 mm
Strand type	Dyform
Strand diameter	18 mm
Max. no. of strands	18
Max. diameter of the strand bundle	210 mm
Width	550 mm
Length	550 mm
Height	
Retracted	1520 mm
Extended	1920 mm
Weight	2000 kg

Dimensions are in millimeters, t = metric tons.
The content in this document is mentioned for reference use only. Values may differ from current data. Always contact Mammoet for current project calculations.

A.4 600 Te Strand Jack System

MAMMOET

SSL550
STRAND JACK
DIMENSIONS AND SPECIFICATIONS

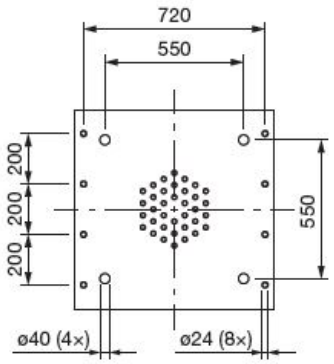

Type 1

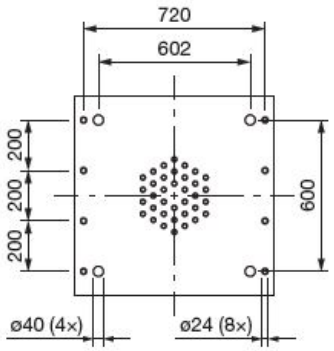

Type 4

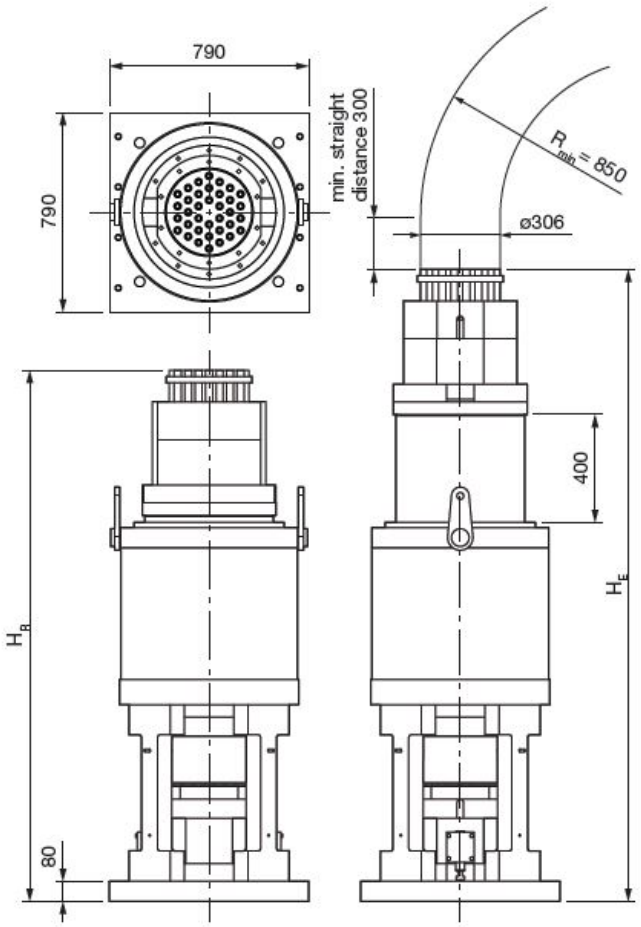

SPECIFICATIONS

	Type 1	Type 4
Capacity	600 t	600 t
Working pressure of the cylinder	400 bar	360 bar
Stroke	400 mm	400 mm
Strand type	Dyform	Dyform
Strand diameter	18 mm	18 mm
Max. no. of strands	36	36
Max. diameter of the strand bundle	306 mm	306 mm
Width	790 mm	790 mm
Length	790 mm	790 mm
Height		
Retracted (H_R)	2105 mm	2170 mm
Extended (H_E)	2505 mm	2570 mm
Weight	3317 kg	3347 kg

B Structural Stiffness

For the gantry to be modeled, the stiffness of the columns is needed. Therefore, the stiffnesses of the mast sections need to be determined. This is done in compliance with EN 1993-1-1 [5], section 6.4.2.1. Both the flexural and the shear stiffness are determined using this method and their influence on deformations is considered. Also, the deformations from this method are compared to the deformations found from tests in SCIA Engineer, both using first order calculations. For very slender structures the shear stiffness plays a minor role, whereas for more bulky structures it can become an important factor. As the New York mast sections under development by Mammoet are more bulky than the MSG and DS sections, the shear stiffness might become of more importance when these sections are applied. The slenderness of the structure depends on the dimensions of the cross-section in relation to the dimensions of the structure itself. Therefore, it is important to look not only at the properties of the mast sections, but also at their influence as the height of the structure varies.

In order to find and analyze the properties, a cantilever column with a height varying from one to twenty sections is considered (Figure 40). The theoretical deformation w_t of such a column, for the combined effect of flexural w_b and shear deformation w_s, is given in Equation 37.

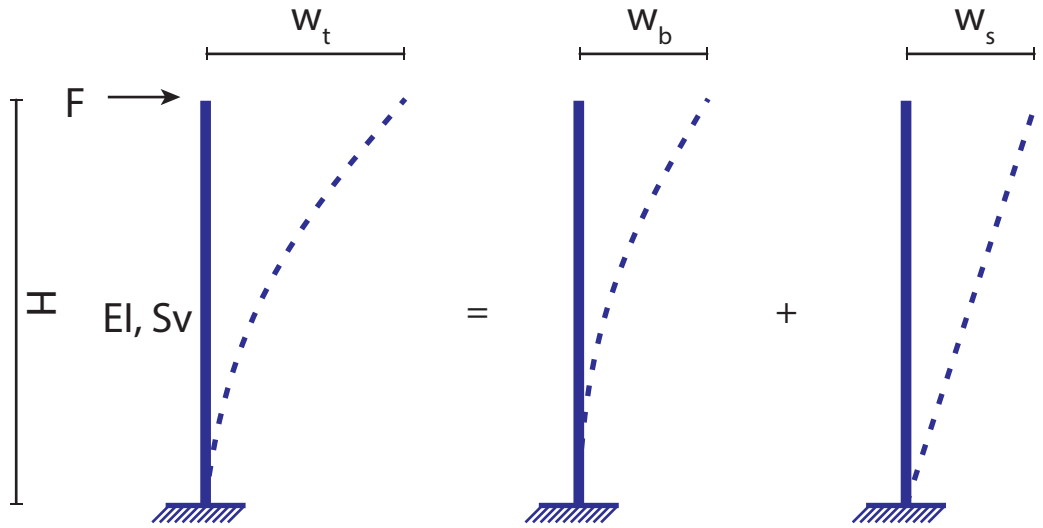

Figure 40: Flexural and shear deformations of a cantilever column.

$$w_t = w_b + w_s = \frac{FH^3}{3EI} + \frac{FH}{S_v} \tag{37}$$

The flexural stiffness of the three mast section types is based on the moment of inertia of the section chords. The chord layouts are shown in Figure 41. The flexural stiffness is calculated as the sum of the four steiner terms of the chords. The shear stiffness comes from the diagonals and is calculated in accordance with the equations in figure 6.9 of EN 1993-1-1 [5]. The resulting stiffnesses around the y-axis and z-axis, where the y-axis is always the stronger direction of the section, are given in Table 14. For the reference calculations the mast sections are modelled in SCIA Engineer, all members included.

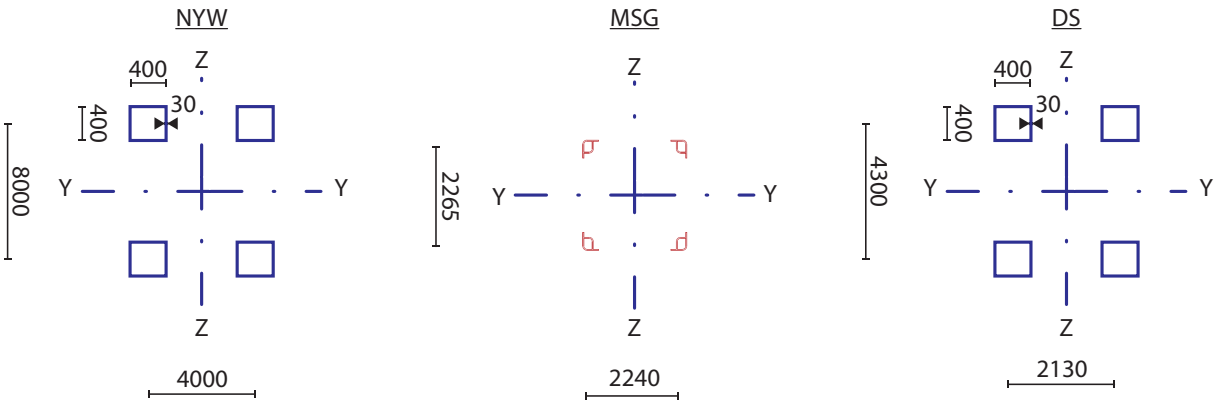

Figure 41: Chord cross-section of the different mast section types.

Table 14: Mast section stiffnesses: Flexural stiffness EI [kNm^2] and shear stiffness Sv [kN].

	MSG sections		**DS sections**		**NYW sections**	
	EI [kNm^2]	**Sv [kN]**	**EI [kNm^2]**	**Sv [kN]**	**EI [kNm^2]**	**Sv [kN]**
y-axis	3.14E+07	5.76E+05	1.15E+08	1.16E+06	5.97E+08	1.96E+06
z-axis	3.07E+07	5.75E+05	2.81E+07	5.82E+05	1.49E+08	1.54E+06

B.1 Results

Figure 42 shows the ratio of flexural over shear deformation for the different section types, for a column of one to twenty sections. It is clearly visible that the flexural deformation becomes dominant as the height increases and the column thus becomes more slender. The relevant range of application for the MSG sections runs approximately from 50 to 100 meters. In this range the flexural deformation is at least fifteen times the shear deformation. The DS and NYW sections can be used for even higher gantries, roughly from 80 till 150 meters, and show the same pattern. The MSG section is very much symmetrical, whereas the DS and NYW section clearly have a strong and a weak direction. This is also visible in the results, where the ratio increases more rapidly for the weaker, less bulky, direction.

In Figure 43, 44 and 45 the theoretical deformations are compared to those found using the finite element (FEM) calculations in SCIA Engineer, where the 95% line is indicated as well. The ratio of theoretical flexural deformation to finite element deformations, as well as the ratio of the total theoretical deformations to the finite element deformations, is shown. From Figure 43 it is visible that the flexural deformation converges to the finite element deformation for increasing height, but for small heights the difference is quite large. However, at a height of 51.3 meter (nine sections) the ratio is already larger than 0.92 for both directions, for the MSG sections. The combined deformation due to flexural and shear effects converges even faster and its ratio is 0.98 at the same height.

For the DS sections the convergence is quicker for the weaker direction, where the shear stiffness is less. It thus seems that this stiffness is overestimated, underestimating the shear deformations. The ratio of total deformation to FEM deformation is already 0.98 for the y-axis and even 0.99 for the z-axis, for a height of 79.8 meter (7 sections). Thus the combined effect of flexural and shear stiffness closely resembles the FEM calculations. The bending over FEM ratio are 0.94 and 0.97 respectively, for this

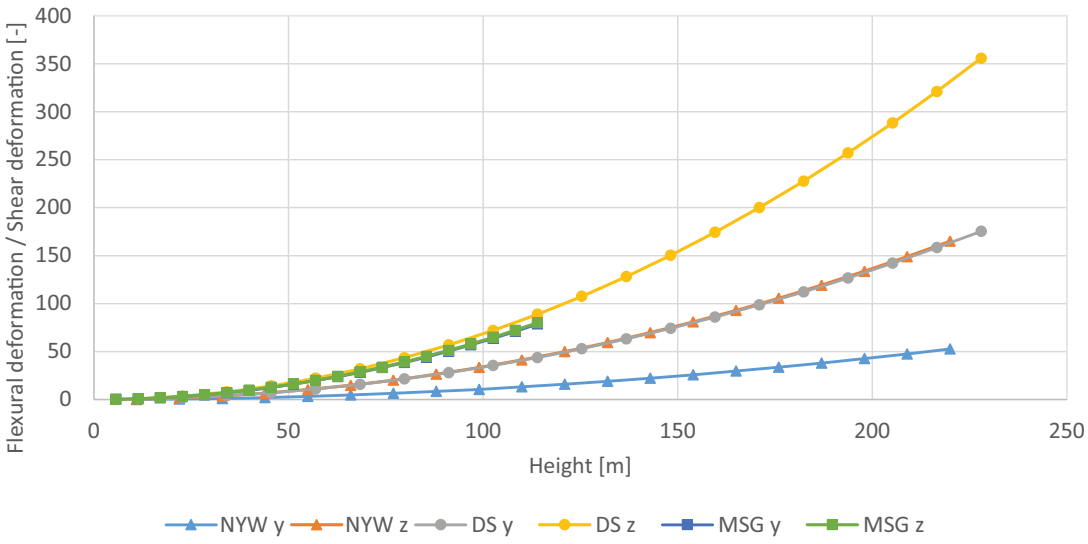

Figure 42: Flexural versus shear deformation, for all section types and related to the height of the column.

height. The bending deformations are thus already very close to the FEM deformations for this section, in the relevant height range.

The New York Wheel section is the most bulky one (in the y-direction), which results in relatively large differences in the ratios for bending and total deformations. The results for the z-direction are similar to those for the DS section. The deformations around the y-axis however show that theoretical bending results in deformations that are 11% smaller for a height of 99 meters (9 sections).

It is concluded that it is sufficient to only consider the bending stiffness. For a preliminary design the difference can be disregarded if the gantry is high enough.

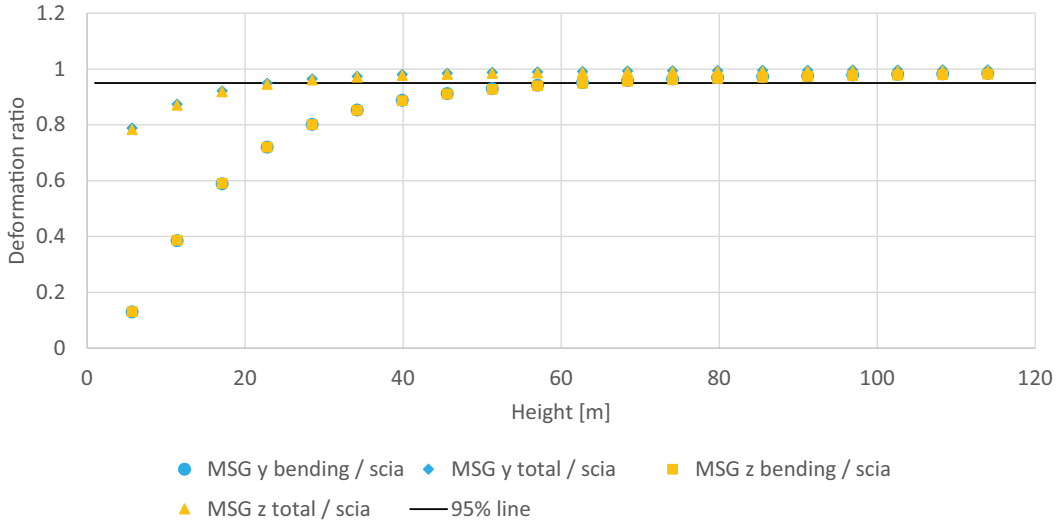

Figure 43: Theoretical shear and total deformation versus finite element deformation, for MSG sections.

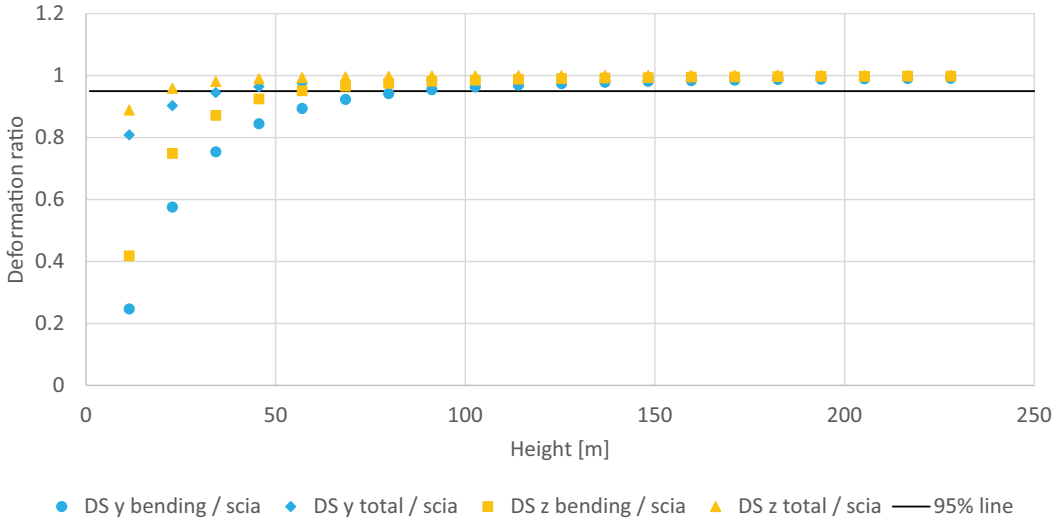

Figure 44: Theoretical shear and total deformation versus finite element deformation, for DS sections.

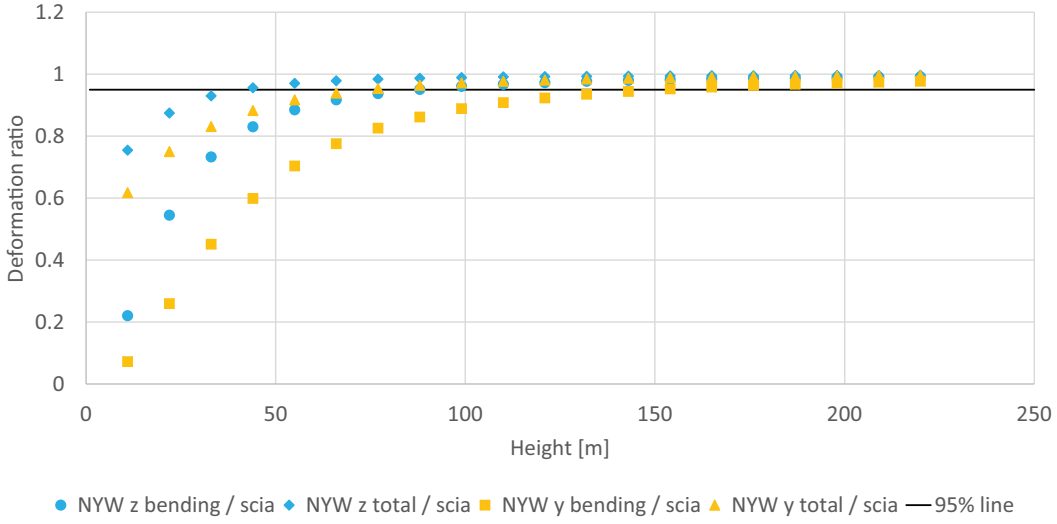

Figure 45: Theoretical shear and total deformation versus finite element deformation, for NYW sections.

C Model Selection

The Graphs in Appendix C.1 show the ratio of first order to second order resistance, for method 2, for a single free standing column.

C.1 Second Order Versus First Order Calculations

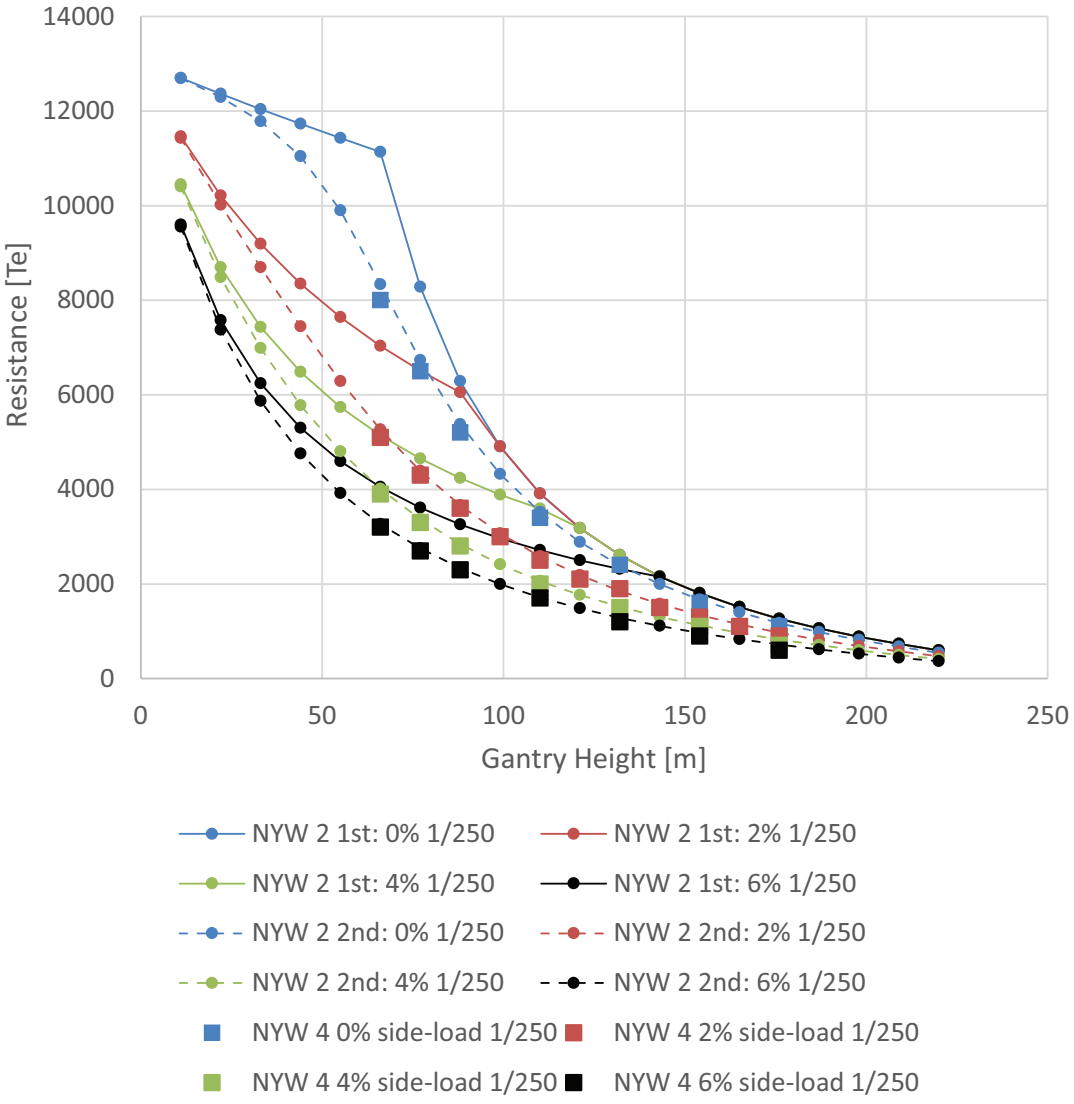

Figure 46: Resistance versus Height for method 2, second order versus first order, and for method 4, for 1/250 imperfection and all horizontal load percentages.

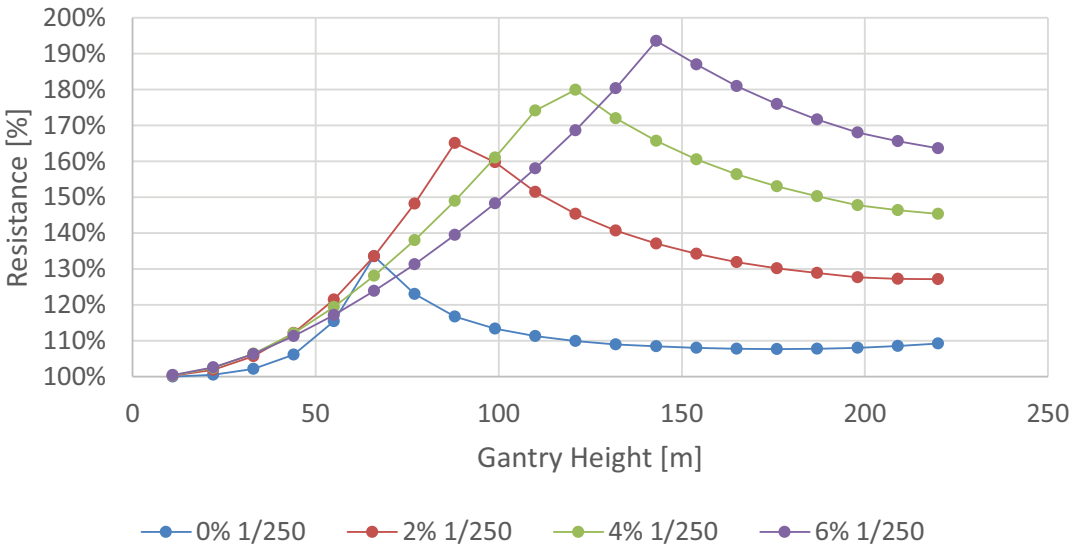

Figure 47: Resistance versus Height for method 2, the first order resistance as a percentage of the second order resistance, second order versus first order: For 1/250 imperfection and all horizontal load percentages.

D Derivation of Buckling Loads, Moments and Deflections

The buckling loads, deflections and bending moments of the gantry columns depend on their boundary conditions. In this appendix, these properties are derived for the column configurations under consideration. Figure 48, on the next page, shows a summary of the findings in this sections, for the column models under consideration. In Appendix D.1, the Euler-Bernoulli beam theorem is used to derive the first order bending moments and deflections, while the buckling loads are derived in Appendices D.2 and D.3. Also, the theory behind the multiplication factor for second order deflections and moments is described in Appendix D.5.

1

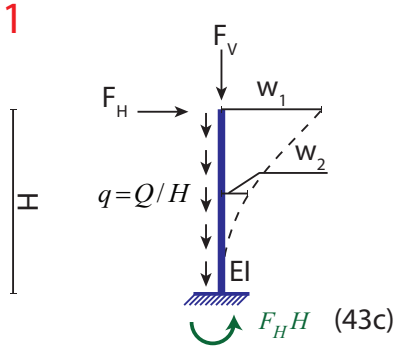

(69) $F_{cr} = \frac{\pi^2 EI}{4H^2}$

(57) $Q_{cr} = \frac{7.83EI}{H^2}$

(43a) $w_1 = \frac{F_H H^3}{3EI}$

(43b) $w_2 = \frac{5F_H H^3}{48EI}$

2

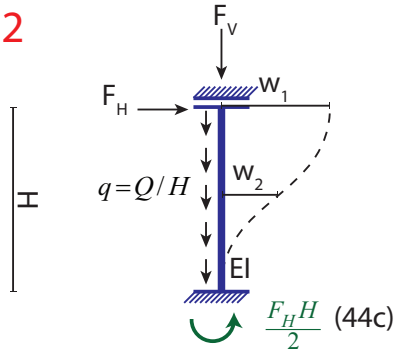

(71) $F_{cr} = \frac{\pi^2 EI}{H^2}$

(61) $Q_{cr} = \frac{1.92EI}{H^2}$

(44a) $w_1 = \frac{F_H H^3}{12EI}$

(44b) $w_2 = \frac{F_H H^3}{24EI}$

3

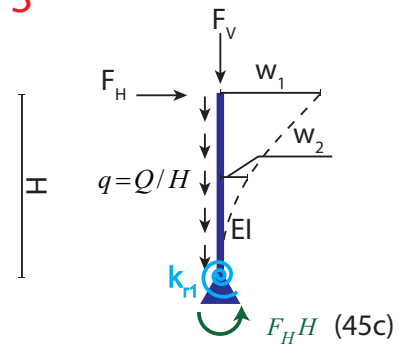

(74b) $F_{cr} = \frac{k_{r1} H}{4k_{r1} H + 10EI} \frac{\pi^2 EI}{H^2}$

(63) $Q_{cr} = \frac{2k_{r1} 7.83\,EI}{H\,7.83\,EI + 2k_{r1} H^2}$

(45a) $w_1 = \frac{F_H H^3}{3EI} + \frac{F_H H^2}{k_{r1}}$

(45b) $w_2 = \frac{5F_H H^3}{48EI} + \frac{F_H H^2}{2k_{r1}}$

4

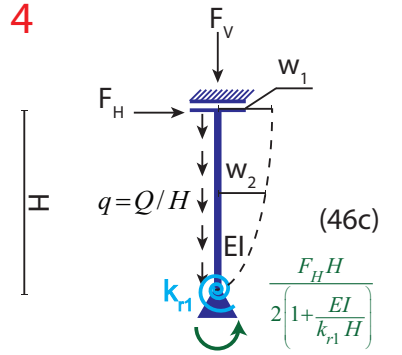

(82) $F_{cr} = \left(\frac{\eta_1 + 4}{2\eta_1}\right)^2 \frac{\pi^2 EI}{H^2}$ *with* $\eta_1 = 4 + \frac{10\,EI}{k_{k1} H}$

(64) $Q_{cr} = 1.6 \times F_{cr}$

(45a) $w_1 = -\frac{F_H H^3}{6\,EI} + \frac{1}{4}\frac{k_{r1} F_H H^4 / EI + 2F_H H^3}{k_{r1} H + EI}$

(45b) $w_2 = -\frac{F_H H^3}{48EI} + \frac{1}{16}\frac{k_{r1} F_H H^4 / EI + 4F_H H^3}{k_{r1} H + EI}$

Figure 48: Column properties, for different boundary conditions: Buckling load for point load F_{cr} and distributed load Q_{cr} and first order deflections w_1 and w_2. The numbers between parentheses indicate the equation in which these equations are derived.

D.1 First Order Bending Moments and Deflections

First, the differential equation for bending (Equation 38) is solved for the general column model in Figure 49 (a). A horizontal load F acts on the column at the top and the spring constants k_{r1} and k_{r2} are unknown. Next, the resulting relations are evaluated for specific boundary conditions, i.e. spring properties.

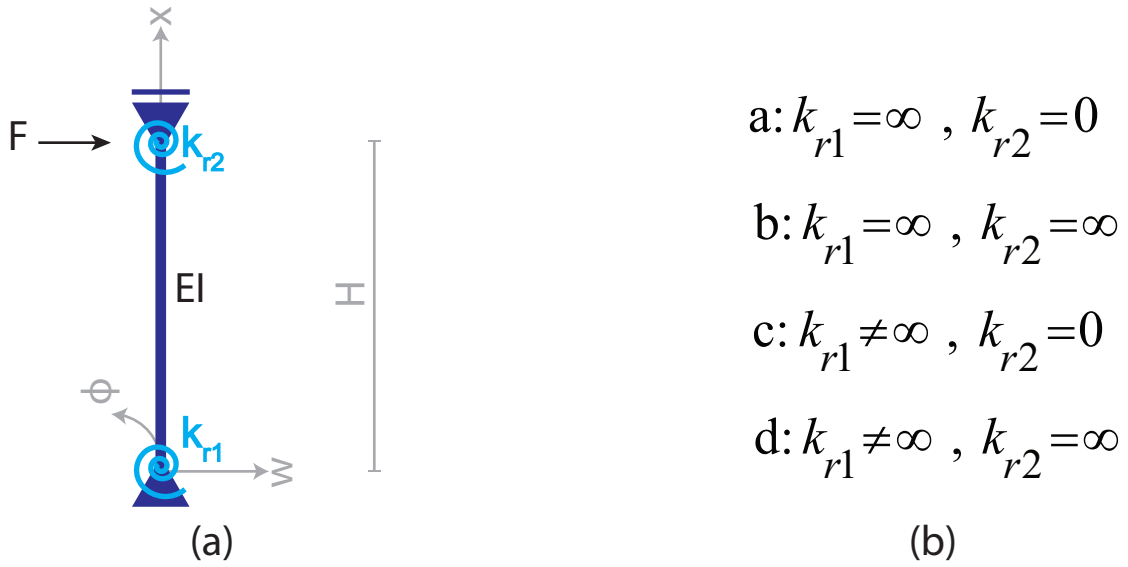

Figure 49: Column model used to calculate bending moments and deflections: Column model with springs for first order moments and deflections (a) and possible rotational spring constants for the different column configurations (b).

$$EIw'''' = q \tag{38}$$

The differential equation comes from the famous Euler-Bernoulli beam theory and describes load-bearing and deformation characteristics of a beam, in accordance with the simplified theory of elasticity. The general solution for the deflection w of the beam, in the absence of a distributed load q, is shown in Equation 39 (a). The constants C_1 to C_4 depend on the boundary conditions. The rotation of the beam ϕ, considered positive if counterclockwise the bending moment M and the shear force V in the beam are related to the deflection of the beam through Equations 39b, c and d. All depend on the location along the beam axis, denoted by x.

$$w = C_1x^3 + C_2x^2 + C_3x + C_4 \tag{39a}$$

$$\phi = -w' = -3C_1x^2 - 2C_2x - C_3 \tag{39b}$$

$$M = EI\kappa = EI\phi' = EI(-6C_1x - 2C_2) \tag{39c}$$

$$V = M' = -6C_1EI \tag{39d}$$

The unknown constants are solved using the boundary conditions. The column is laterally supported at the bottom ($x = 0$), meaning that the deflection is zero (Equation 40a). The second boundary condition relates the moment at the bottom of the column to the rotation, via the rotational spring. The end of the column is shown in Figure 50 (a), the boundary condition in Equation 40b. The third condition relates the moment at the top of the column to the rotation, via the rotational spring. The end of the column is shown in Figure 50 (b), the boundary condition in Equation 40c. The fourth and last boundary condition introduces the horizontal load F. It relates this load to the shear force at the top of the column ($x = H$), as indicated in Figure 50 (c). The resulting relation is given in Equation 40d.

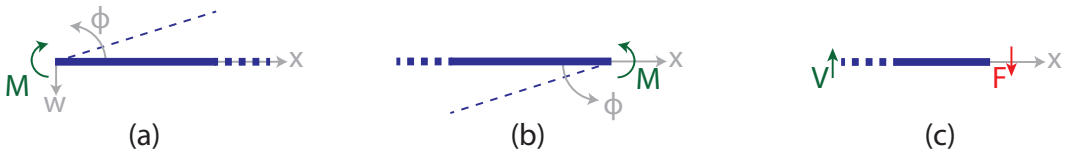

Figure 50: Boundary conditions for the gantry column model: (a) relates the bending moment at the bottom to the rotation, (b) relates the bending moment at the top to the rotation, (c) introduces the horizontal load F at the top. The shear force and bending moment are drawn in positive directions.

$$x = 0 : w = 0 \rightarrow C_1 0^3 + C_2 0^2 + C_3 0 + C_4 = 0 \tag{40a}$$

$$x = 0 : M = k_{r1}\phi \rightarrow EI(-6C_1 0 - 2C_2) = k_{r1}(-3C_1 0^2 - 2C_2 0 - C_3) \tag{40b}$$

$$x = H : M = -k_{r2}\phi \rightarrow EI(-6C_1 H - 2C_2) = -k_{r2}(-3C_1 H^2 - 2C_2 H - C_3) \tag{40c}$$

$$x = H : V = F \rightarrow -6C_1 EI = F \tag{40d}$$

From these four conditions, the constants C_1 to C_4 can be solved (Equation 41).

$$C_1 = \frac{-F}{6EI} \quad , \quad C_2 = \frac{1}{4}\frac{k_{r1}FH(2EI + k_{r2}H}{EI(k_{r1}EI + k_{r1}k_{r2}H + k_{r2}EI)} \quad , \quad C_3 = \frac{2EI}{k_{r1}}C_2 \quad , \quad C_4 = 0 \tag{41a}$$

Filling in the constants in Equation 39 leaves the necessary relations. Equation 42a and b give the first order deflections at the top of and halfway the column respectively, related to the influence of the vertical load at the top of the gantry and the resultant of the self-weight of the column. The latter acts on the column at half its height. The relation in Equation 42c gives the first order bending moment at the bottom of the column.

$$x = H \rightarrow w = -\frac{FH^3}{6EI} + \frac{1}{4}\frac{k_{r1}FH(2EI + k_{r2}H)}{EI(k_{r1}EI + k_{r1}k_{r2}H + k_{r2}EI)}H^2 + \frac{1}{2}\frac{FH(2EI + k_{r2}H)}{(k_{r1}EI + k_{r1}k_{r2}H + k_{r2}EI)}H \tag{42a}$$

$$x = \frac{H}{2} \rightarrow w = -\frac{FH^3}{48EI} + \frac{1}{16}\frac{k_{r1}FH(2EI + k_{r2}H)}{EI(k_{r1}EI + k_{r1}k_{r2}H + k_{r2}EI)}H^2 + \frac{1}{4}\frac{FH(2EI + k_{r2}H)}{(k_{r1}EI + k_{r1}k_{r2}H + k_{r2}EI)}H \tag{42b}$$

$$x = 0 \rightarrow M = -\frac{1}{2}\frac{k_{r1}FH(2EI + k_{r2}H)}{k_{r1}EI + k_{r1}k_{r2}H + k_{r2}EI} \tag{42c}$$

Depending on the gantry model that is studied, the mechanical scheme of a column differs, which means that the boundary conditions are different. Below, the results in Equation 42 are evaluated for the different models.

Model a

For this model, $k_{r1} = \infty$ and $k_{r2} = 0$. The resulting relations are given in Equation 43.

$$x = H \rightarrow w = \frac{FH^3}{3EI} \tag{43a}$$

$$x = \frac{H}{2} \rightarrow w = \frac{5FH^3}{48EI} \tag{43b}$$

$$x = 0 \rightarrow M = -FH \tag{43c}$$

Model b

For this model, $k_{r1} = \infty$ and $k_{r2} = \infty$. The resulting relations are given in Equation 44.

$$x = H \rightarrow w = \frac{FH^3}{12EI} \tag{44a}$$

$$x = \frac{H}{2} \rightarrow w = \frac{FH^3}{24EI} \tag{44b}$$

$$x = 0 \rightarrow M = -\frac{FH}{2} \tag{44c}$$

Model c

For this model, $k_{r1} \neq \infty$ and $k_{r2} = 0$. The resulting relations are given in Equation 45.

$$x = H \rightarrow w = \frac{FH^3}{3EI} + \frac{FH^2}{k_{r1}} \tag{45a}$$

$$x = \frac{H}{2} \rightarrow w = \frac{5H^3}{48EI} + \frac{FH^2}{2k_{r1}} \tag{45b}$$

$$x = 0 \rightarrow M = -FH \tag{45c}$$

Model d

For this model, $k_{r1} \neq \infty$ and $k_{r2} = \infty$. The resulting relations are given in Equation 46.

$$x = H \rightarrow w = -\frac{FH^3}{6EI} + \frac{1}{4}\frac{k_{r1}FH^4/EI + 2F_H H^3}{k_{r1}H + EI} \tag{46a}$$

$$x = \frac{H}{2} \rightarrow w = -\frac{FH^3}{48EI} + \frac{1}{16}\frac{k_{r1}FH^4/EI + 4F_H H^3}{k_{r1}H + EI} \tag{46b}$$

$$x = 0 \rightarrow M = -\frac{FH}{2\left(1 + \frac{EI}{k_{r1}H}\right)} \tag{46c}$$

D.2 Buckling Load For A Distributed Load

The buckling load is considered for a point load and a distributed load separately. The load is determined for the models in Figure 51, using two different methods. Depending on the model at hand, the approximation method of Rayleigh or the well known fourth order differential equation is used. The buckling load for a distributed load is derived first, to be followed by the load for a point load.

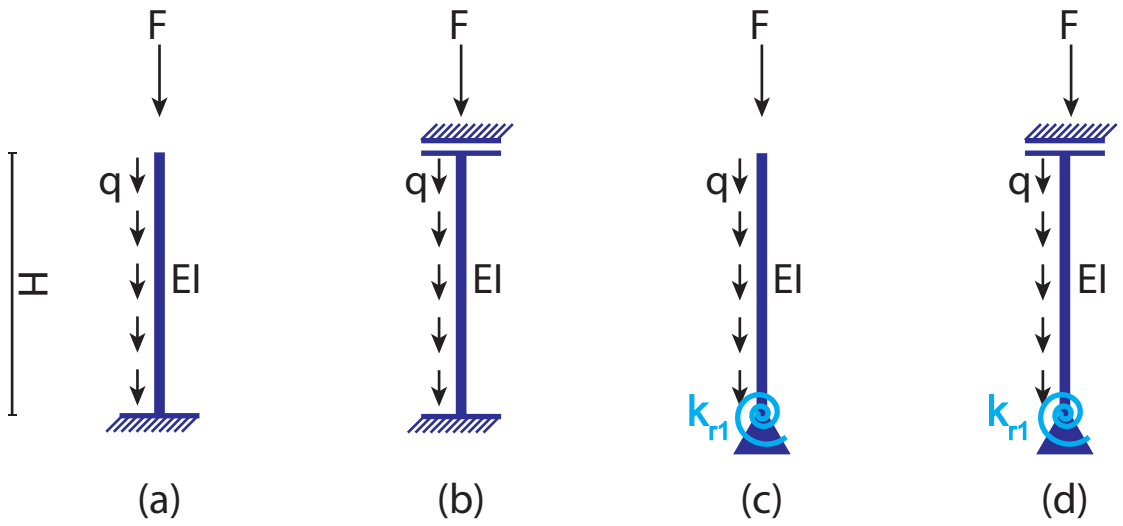

Figure 51: Columns models for buckling load: (a) to (d) represent the four models for which the buckling load is determined, both for the point load F and the distributed load q.

Model a

This model is analyzed using the method of Rayleigh, that is based on an energy consideration. This method considers the work done by the load and the energy necessary for the deformation of the column, when it buckles. The deformation energy for a rod of length H, loaded in extension and bending and with linear elastic behaviour of its material, is given in Equation 47.

$$E_d = \int_0^H E_d^* dx = \int_0^H \frac{1}{2} EA\varepsilon^2 dx + \int_0^H \frac{1}{2} EI\kappa^2 dx \tag{47}$$

Where ε is the extension and κ the curvature of the rod. Just before buckling the rod is completely straight, which means that the curvature of the rod is zero. The difference between the situation just before and after buckling is thus equal to the bending term (Equation 48).

$$\Delta E_d = \int_0^H \frac{1}{2} EI\kappa^2 dx = \int_0^H \frac{1}{2} EI \left(\frac{d^2 w}{dx^2} \right)^2 dx \tag{48}$$

The work done by a single point load F is equal to the load times the displacement u along the axis of the rod ($A = F \times u$). The displacement u is derived from the deflection of the rod and can ultimately be described by Equation 49. For a detailed derivation of this relation, reference is made to Hartsuijker and Welleman (2007)[20].

$$u = \int_0^H \frac{1}{2}\left(\frac{dw}{dx}\right)^2 dx \tag{49}$$

In order to find the critical buckling force, the work done by the load is set equal to the energy for deformation ($A = \Delta E_v$). From this equality, the buckling force is derived (Equation 50). This formula can be used for a single point load that is applied at the end of the column.

$$F = \frac{\int_0^H \frac{1}{2} EI\left(\frac{d^2w}{dx^2}\right)^2 dx}{\int_0^H \frac{1}{2}\left(\frac{dw}{dx}\right)^2 dx} \tag{50}$$

The effect of a distributed load is approximated by means of n point loads, applied with equal spacing. The more point loads one uses, the more accurate the approximation becomes. The combined work done by these point loads can be calculated in accordance with Equation 51. For the model in Figure 51 (a), the buckling shape in Equation 52 is assumed. This is the exact buckling shape for a column loaded by a single point load at the top, with the same boundary conditions. The quality of the approximation relies on the buckling shape that is assumed. If the exact shape is used, the buckling load is exact as well. If not, the Rayleigh method overestimates the buckling load.

$$A = F \times \sum_{i=1}^{n} u\Big(\frac{i}{n}H\Big) \tag{51}$$

$$w = C\Big[1 - cos\Big(\frac{\pi x}{2H}\Big)\Big] \tag{52}$$

From the assumed buckling shape, the first w' and second order derivate w'' can be determined (Equation 53).

$$w' = \frac{C\pi}{2H} sin\Big(\frac{\pi x}{2H}\Big) \tag{53a}$$

$$w'' = \frac{C\pi^2}{4H^2} cos\Big(\frac{\pi x}{2H}\Big) \tag{53b}$$

The second derivative can be used in Equation 49, which results in Equation 54.

$$u(x) = \int_0^x \frac{1}{2}\left(\frac{dw}{dx}\right)^2 dx = \frac{C^2\pi^2}{8H^2}\int_0^x sin^2\Big(\frac{\pi x}{2H}\Big)dx = \frac{C^2\pi^2}{16H^2}\int_0^x \Big[1 - cos\Big(\frac{\pi x}{H}\Big)\Big]dx \tag{54a}$$

$$u(x) = \frac{C^2\pi}{16H^2}\Big[\pi x - H sin\Big(\frac{\pi x}{H}\Big)\Big] \tag{54b}$$

Where the trigonometric identity $sin^2(x) = 1/2 - 1/2\ cos(2x)$ is used. The total work done is then found with Equation 55.

$$A = F \times \sum_{i=1}^{n} u\left(\frac{i}{n}H\right) = F \times \frac{C^2\pi}{16H^2} \times \sum_{i=1}^{n} \left[\pi\frac{i}{n}H - Hsin\left(\frac{\pi i}{n}\right)\right] \tag{55}$$

The bending energy can be derived using the second order derivative (Equation 56).

$$\Delta E_d = \int_0^H \frac{1}{2}EI\left(\frac{d^2w}{dx^2}\right)^2 dx = \frac{C^2\pi^4 EI}{32H^4}\int_0^H cos^2\left(\frac{\pi x}{2H}\right)dx = \frac{C^2\pi^4 EI}{64H^4}\int_0^H \left[1 + cos\left(\frac{\pi x}{H}\right)\right]dx \tag{56a}$$

$$\Delta E_d = \frac{C^2\pi^4 EI}{64H^4}\left[H + \frac{H}{\pi}sin(\pi) - 0 - \frac{H}{\pi}sin(0)\right] = \frac{C^2\pi^4 EI}{64H^3} \tag{56b}$$

Where the trigonometric identity $cos^2(x) = 1/2 + 1/2\ cos(2x)$ is used. For the number of point loads n equal to ten thousand, the buckling load Q_{cr} can be found using Equation 57. Figure 52 shows the approximate buckling load for n from one to one thousand, as well as the load for n equal to ten thousand. The buckling load converges to a value close to the one found for ten thousand point loads. In the limit case of just one point load at the top, the factor becomes $2.47 \approx \pi^2/4$, which will turn out to be quite relevant.

$$Q_{cr} = q_{cr} \times H = n \times F = \frac{8.30EI}{H^2} \tag{57}$$

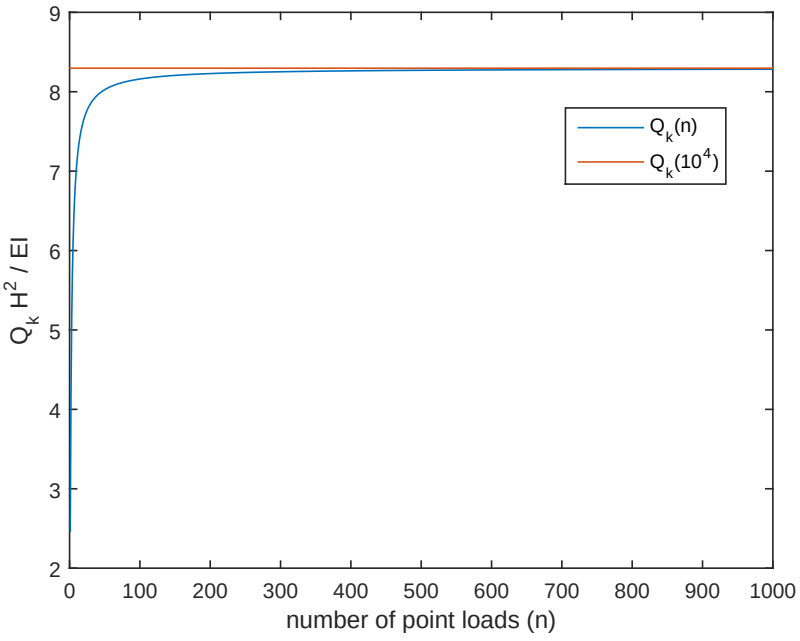

Figure 52: Approximate buckling load for a distributed load, for an increasing amount of discrete loads and for the model in Figure 51 (a).

Model b

The method of Rayleigh is also applied to model b, where the buckling shape is assumed to follow Equation 58. This is again the exact shape for a single point load at the top.

$$w = C\Big[1 - cos\Big(\frac{\pi x}{H}\Big)\Big] \tag{58}$$

The work done by the point loads can then be described by Equation 59, while the bending deformation equals that of Equation 60.

$$A = F \times \frac{C^2\pi^2}{4H^2} \times \sum_{i=1}^{n}\Big[\frac{i}{n}H + \frac{H}{2}sin\Big(\frac{2\pi i}{n}\Big)\Big] \tag{59}$$

$$\Delta E_d = \frac{C^2\pi^4 EI}{4H^3} \tag{60}$$

For n equal to ten thousand this gives the buckling load of Equation 61

$$Q_{cr} = q_{cr} \times H = n \times F = \frac{19.74EI}{H^2} \approx \frac{2\pi^2 EI}{H^2} \tag{61}$$

Figure 53 shows that again the buckling converges for an increasing amount of point loads. The value for ten thousand point loads is very closure to the limit value. For a single point load, the factor equals $9.87 \approx \pi^2$.

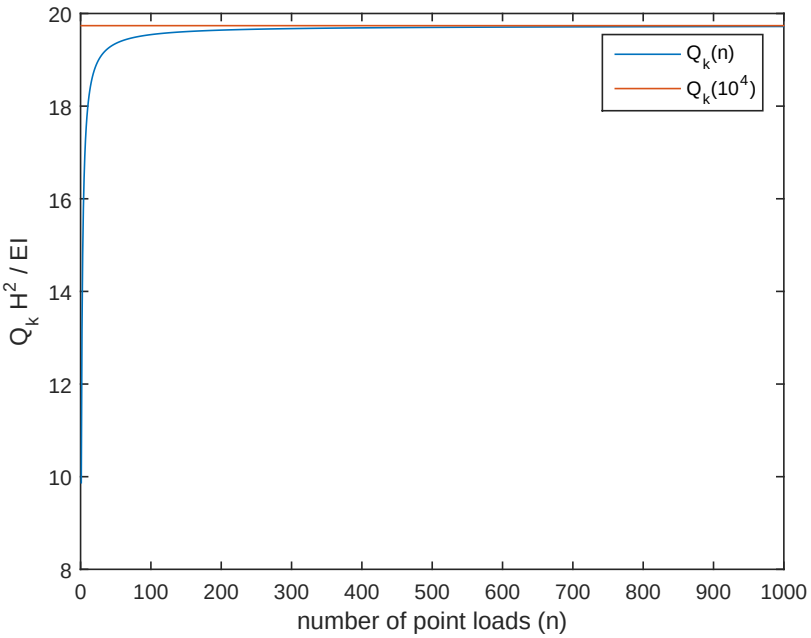

Figure 53: Approximate buckling load for a distributed load, for an increasing amount of discrete loads and for the model in Figure 51 (b).

Model c

In this model the foundation of the column is not infinitely stiff, in contrast to models a and b. An approximate buckling load is derived, combining the influence of the foundation stiffness and the stiffness of the rod itself. On the left side of Figure 54 model a is shown, along with its buckling load. In the middle, an infinitely stiff rod on a flexible foundation is shown. The buckling load for this model can be found by evaluating the equilibrium in the deformed state, with a deflection w at the top. The moment balance in the deformed state, along with the resulting buckling load, is given in Equation 62.

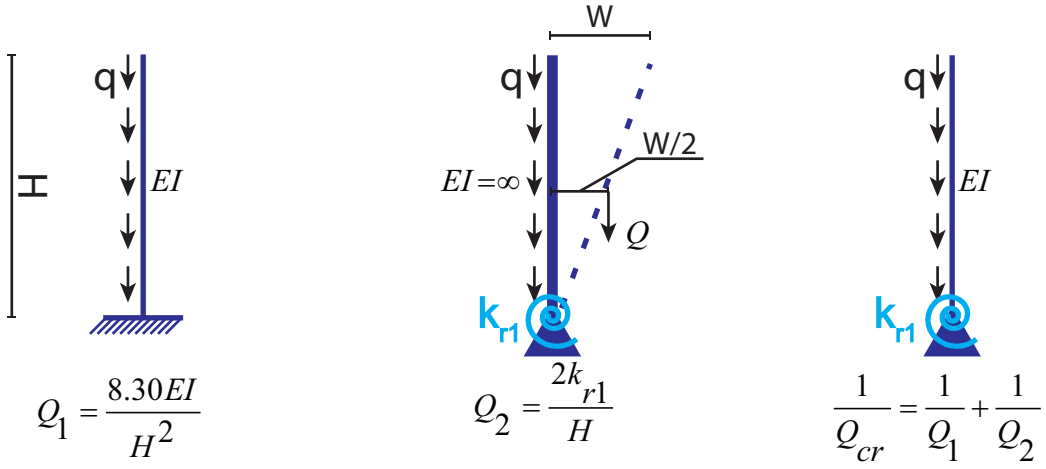

Figure 54: Column models for buckling load analysis of model c, for a distributed load: Flexible rod on rigid foundation (left), rigid rod on flexible foundation (middle) and combined effect (right).

$$Q \times w/2 = k_{r1} \times w/H \rightarrow Q_2 = 2 \times k_{r1}/H \tag{62}$$

The approximate buckling load is calculated using the formula on the right side of Figure 54, because the stiffness of the rod and the foundation form a parallel system. This leaves the buckling load in Equation 63.

$$Q_{cr} = \left(\frac{1}{Q_1} + \frac{1}{Q_2}\right)^{-1} = \left(\frac{H^2}{8.30EI} + \frac{H}{2k_{r1}}\right)^{-1} = \left(\frac{H^2}{\pi^2 EI}\frac{H2k_{r1} + 0.84\pi^2 EI}{1.68k_{r1}H}\right)^{-1} = \frac{\pi^2 EI}{H^2}\frac{1.68k_{r1}H}{H2k_{r1} + 0.84\pi^2 EI} \tag{63}$$

Model d

It is very hard to determine the buckling load of this model with good enough accuracy. An approximate method, as was used for model c, does not yield useful results in this case. Also, the method of Rayleigh is not applicable, since the buckling shape is completely unknown. For model a and b it is known that the buckling shape is close to that of a point load on the same column and the buckling shape for a point load is known in these cases. For this model, that is not true.

For multiple values of $\frac{EI}{k_{r1}H}$, a factor that defines the amount of influence of the rotational and bending stiffness, the buckling load for a distributed load is compared to the load for a point load. For realistic values of this ratio, values that occur for the soil stiffnesses under consideration, it turns out that the buckling load for the distributed load is 1.4 to 1.8 times bigger than for a point load. Therefore, the

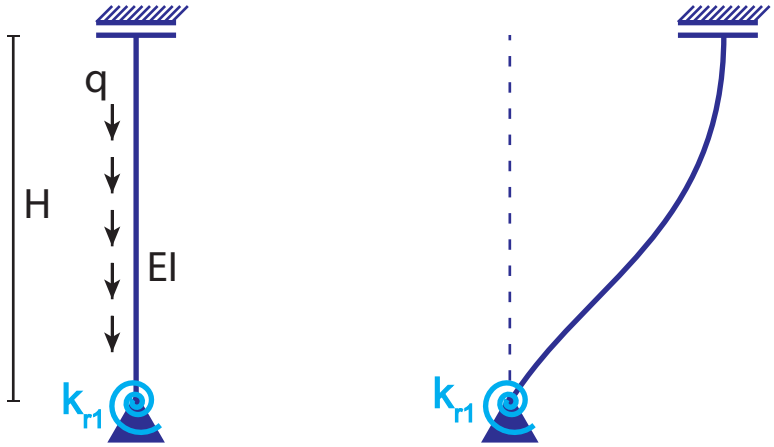

Figure 55: Column models for buckling load analysis of model d, for a distributed load.

buckling load for a distributed load is considered 1.6 times the buckling load for a point load (Equation 64). The comparison was carried out using linear stability calculations in SCIA Engineer.

$$Q_{cr} = 1.6 \times F_{cr} \tag{64}$$

D.3 Buckling Load For A Point Load

For the point load, use is made of the well known fourth order differential equation for buckling.

Model a

The fourth order differential equation is derived from the equilibrium of a small element of the deformed rod (Figure 56) and is given in Equation 65.

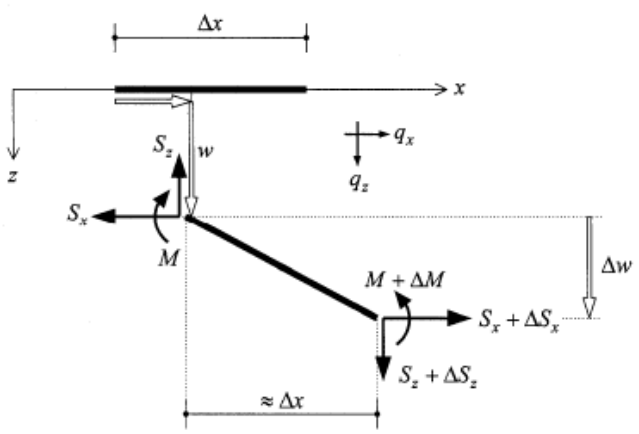

Figure 56: Portion of buckling member, in the deformed state (Hartsuijker and Welleman (2007) [20]).

$$w'''' + \alpha^2 w'' = 0, \quad \text{with} \quad \alpha^2 = \frac{F}{EI} \tag{65}$$

Via the kinematic, constitutive and equilibrium relations, the relations in Equation 66 can be found.

$$w = Acos(\alpha x) + Bsin(\alpha x) + Cx + D \tag{66a}$$

$$\phi = -w' = A\alpha sin(\alpha x) - B\alpha cos(\alpha x) - C \tag{66b}$$

$$M = EI\kappa = -EIw'' = EI(A\alpha^2 cos(\alpha x) + B\alpha^2 sin(\alpha x)) \tag{66c}$$

$$S_z = M' - Fw' = -FC \tag{66d}$$

where S_z is the vertical section force. This force does not equal the shear force, since the section is rotated. For the model in Figure 51 (a), The boundary conditions are shown and applied in Equation 67.

$$x = 0\ ,\ w = 0 \rightarrow Acos(0) + Bsin(0) + C0 + D = 0 \rightarrow A + D = 0 \tag{67a}$$

$$x = 0\ ,\ \phi = 0 \rightarrow A\alpha sin(0) - B\alpha cos(0) - C = 0 \rightarrow B\alpha + C = 0 \tag{67b}$$

$$x = H\ ,\ M = 0 \rightarrow EI(A\alpha^2 cos(\alpha H) + B\alpha^2 sin(\alpha H)) = 0 \rightarrow B = \frac{-A}{tan(\alpha H)} \tag{67c}$$

$$x = H\ ,\ S_z = 0 \rightarrow -FC = 0, \tag{67d}$$

From these equations, the buckling load can be found. Equation 67d shows that $C = 0$, which means that $B = 0$ as well (Equation 67b). Equation 67c can only be true if $tan(\alpha H) = \infty$. This means that $\alpha H = n\pi/2$, where $n = 1, 2, 3, ...$ Since α also equals $\sqrt{(F/EI)}$, the forces that comply with this requirement can be found from Equation 68.

$$F = \frac{n^2\pi^2 EI}{4H^2} \tag{68}$$

The buckling load is found for the lowest value of F ($n = 1$), which leaves Equation 69.

$$F_{cr} = \frac{\pi^2 EI}{4H^2} \tag{69}$$

The work and energy method of Rayleigh yields a buckling load that is equal to Equation 69. Both methods thus give the same result.

Model b

The boundary conditions of this model are given in Equation 70.

$$x = 0\ ,\ w = 0 \rightarrow Acos(0) + Bsin(0) + C0 + D = 0 \rightarrow A + D = 0 \tag{70a}$$

$$x = 0\ ,\ \phi = 0 \rightarrow A\alpha sin(0) - B\alpha cos(0) - C = 0 \rightarrow B\alpha + C = 0 \tag{70b}$$

$$x = H\ ,\ \phi = 0 \rightarrow A\alpha sin(\alpha H) - B\alpha cos(\alpha H) - C = 0 \tag{70c}$$

$$x = H\ ,\ S_z = 0 \rightarrow -FC = 0 \tag{70d}$$

From Equation 70d it is clear that $C = 0$. This means that $B = 0$ as well (Equation 70b). Equation 70c then leaves $B = A\ tan(\alpha H) = 0$. A non-trivial solutions, where $A \neq 0$, is found four $tan(\alpha H) = 0$. This is the case for $\alpha H = \sqrt{(F/EI)} = n\pi$, for $n = 1, 2, 3, ...$ The buckling load is then given in Equation 71 and is equal to the one found using the work and energy method of Rayleigh.

$$F_{cr} = \frac{\pi^2 EI}{H^2} \tag{71}$$

Model c

The third model of Figure 51, model c, contains a rotational spring. This means that again the boundary conditions are a bit different (Equation 72).

$$x = 0\ ,\ w = 0 \rightarrow Acos(0) + Bsin(0) + C0 + D = 0 \rightarrow A + D = 0 \tag{72a}$$

$$x = 0\ ,\ M = k_{r1}\phi \rightarrow -EI(-A\alpha^2 cos(0) - B\alpha^2 sin(0)) = -k_{r1}(-A\alpha sin(0) + B\alpha cos(0) + C) \tag{72b}$$

$$x = H\ ,\ M = 0 \rightarrow EI(A\alpha^2 cos(\alpha H) + B\alpha^2 sin(\alpha H)) = 0 \rightarrow B = \frac{-A}{tan(\alpha H)} \tag{72c}$$

$$x = H\ ,\ S_z = 0 \rightarrow -FC = 0 \tag{72d}$$

From these relations, the transcendent relation in Equation 73 can be derived.

$$\alpha H \, tan(\alpha H) = \frac{k_{r1} H}{EI} \tag{73}$$

It is not possible to derive an analytical solution for this equation. Therefore, another approach is followed. The buckling load is approximated by the combined effect of an infinitely stiff rod with a spring at the bottom and a flexible rod that is clamped at the bottom (Figure 57).

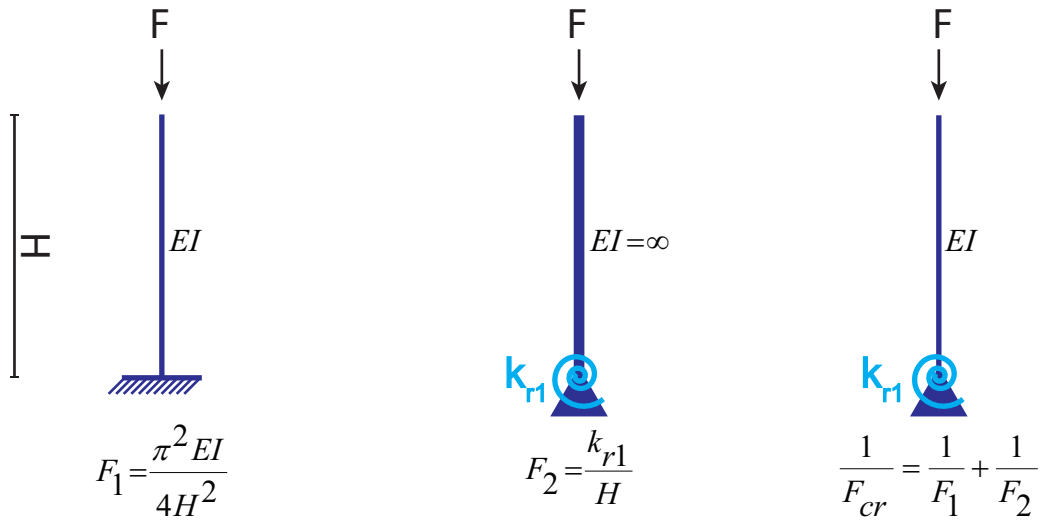

Figure 57: Column models for buckling load analysis of model c, for a point load.

The buckling load F_1 is the load from model a, while the load F_2 can be found from the equilibrium in the deformed state ($k_{r1}\phi = F\phi H \rightarrow F = k_{r1}/H$). Where ϕ is the rotation in the spring k_{r1}. Hartsuijker and Welleman (2007)[20] show that this approximation does very well (Figure 58). They find that the error is 4% at he most. In this figure the parameter $\rho = k_{r1}H/EI$ is used.

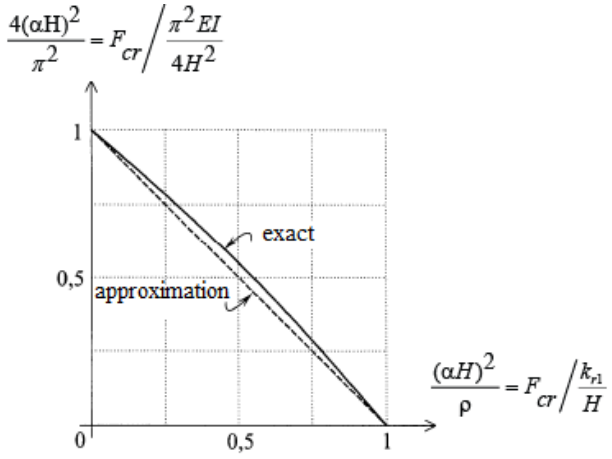

Figure 58: Exact buckling load versus approximation, for a cantilever column with a rotational spring: From the graph it is clear that this load can be approximated with a linear relation very well.

The buckling load for the flexible column with spring in Figure 57 can be rewritten in a form that resembles the Euler buckling formula (Equation 74).

$$\frac{1}{F_{cr}} = \frac{4H^2}{\pi^2 EI} + \frac{H}{k_{r1}} = \frac{H^2}{\pi^2 EI}\frac{4k_{r1}H + \pi^2 EI}{k_{r1}H} \tag{74a}$$

$$\rightarrow F_{cr} = \frac{\pi^2 EI}{H^2}\frac{k_{r1}H}{4k_{r1}H + \pi^2 EI} = \frac{\pi^2 EI}{H^2}\frac{k_{r1}H/EI}{4k_{r1}H/EI + \pi^2} = \frac{\pi^2 EI}{H^2}\frac{\rho}{4\rho + \pi^2} \approx \frac{\pi^2 EI}{H^2}\frac{\rho}{4\rho + 10} \tag{74b}$$

Model d

An approximate buckling load is derived for model d, using the result from model c. A column without lateral support at the top, but with a rotational spring at both ends (k_{r1} and k_{r2}) is analyzed. It is shown in Figure 59.

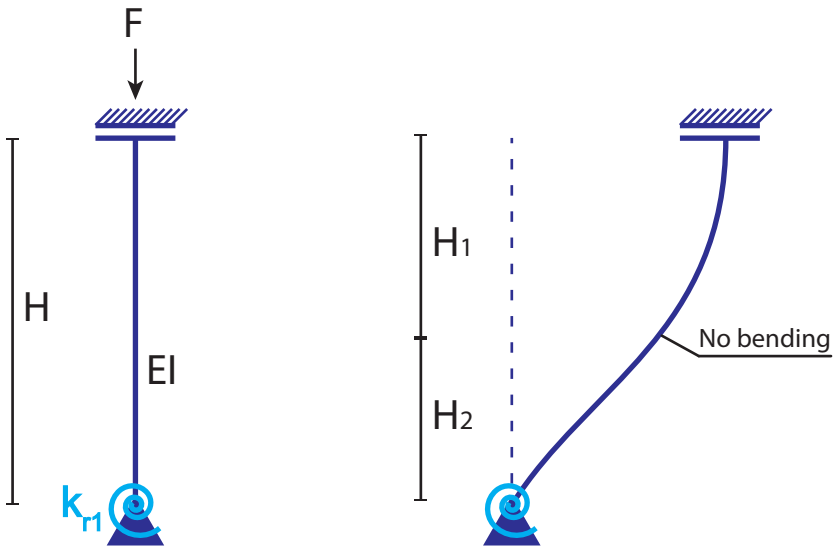

Figure 59: Column model with rotational springs, for buckling load derivation: Undeformed shape (Left) and deformed shape (Right).

This rod is divided into two parts, with lengths H_1 and H_2, in the point where the bending moment is zero. Both rods represent model c and they have the same buckling load and length (Equation 75).

$$H_{cr}^2 = H_1^2\left(4 + \frac{10EI}{k_{r1}H_1}\right) = H_2^2\left(4 + \frac{10EI}{k_{r2}H_2}\right) \tag{75}$$

For future computations, the identities in Equation 76 are introduced.

$$\rho_1 = \frac{k_{r1}H}{EI}\ ,\ \eta_1 = 4 + \frac{10}{\rho_1} = 4 + \frac{10EI}{k_{r1}H} \quad \text{and} \quad \rho_2 = \frac{k_{r2}H}{EI}\ ,\ \eta_2 = 4 + \frac{10}{\rho_2} = 4 + \frac{10EI}{k_{r2}H} \tag{76}$$

The identity that defines η_1 can be rewritten into Equation 77. The same thing can be done for η_2.

$$(\eta_1 - 4)H = \frac{10EI}{k_{r1}} \tag{77}$$

If this is combined with Equation 75, the relation in Equation 78 is obtained.

$$H_{cr}^2 = H_1(4H_1 + \eta_1 H - 4H) = H_2(4H_2 + \eta_2 H - 4H) \tag{78}$$

Using $H_2 = H - H_1$, the derivations in Equation 79 can be executed.

$$H_1(4H_1 + \eta_1 H - 4H) = (H - H_1)(4H - 4H_1 + \eta_2 H - 4H) \tag{79a}$$

$$H_1(4H_1 + \eta_1 H - 4H) = (H - H_1)(\eta_2 H - 4H_1) \tag{79b}$$

$$4H_1^2 + \eta_1 H H_1 - 4H H_1 = \eta_2 H^2 - 4H H_1 - \eta_2 H H_1 + 4H_1^2 \tag{79c}$$

$$H_1(\eta_1 + \eta_2)H = \eta_2 H^2 \tag{79d}$$

$$H_1 = \frac{\eta_2}{\eta_1 + \eta_2} H \tag{79e}$$

$$H_2 = \frac{\eta_1}{\eta_1 + \eta_2} H \tag{79f}$$

The relations in Equation 79e and f can be combined with Equation 75 to find the buckling length H_{cr}. The resulting buckling load is given in Equation 80.

$$Q_{cr} = \frac{(\eta_1 + \eta_2)^2}{\eta_1 \eta_2 (\eta_1 + \eta_2 - 4)} \frac{\pi^2 EI}{H^2} \tag{80}$$

In absence of the rotational stiffness at the top ($k_{r2} = 0$), model c emerges from model d. For this case $\rho_2 = 0$, which means that $\eta_2 = \infty$. If both the denominator and the enumerator of Equation 80 are divided by η_2^2, the buckling load in Equation 81 is found. This is indeed equal to what was found for model c. In the same manner, the load for the models a and b can be found.

$$Q_{cr} = \frac{1}{\eta_1} \frac{\pi^2 EI}{H^2} = \frac{\rho_1}{4\rho_1 + 10} \frac{\pi^2 EI}{H^2} \tag{81}$$

In model d the rotational stiffness at the top (k_{r2}) is infinitely large. This means that $\rho_2 = \infty$ and $\eta_2 = 4$. The buckling load is then equal to Equation 82.

$$Q_{cr} = \frac{(\eta_1 + 4)^2}{4\eta_1^2} \frac{\pi^2 EI}{H^2} \tag{82}$$

D.4 Buckling Load, Formulas Evaluated

The buckling loads derived in Section D.2 and D.3 have been compared to the loads found using linear stability calculations in SCIA Engineer. This comparison was carried out for multiple column lengths and rotational stiffnesses. All formulas give loads that are within 5% of the values found from the finite element calculations in SCIA Engineer and are therefore considered to be accurate.

D.5 Second Order Moment And Multiplication Factor

The second order moments are calculated using the first order deflections (from horizontal loads and imperfections), the vertical load on the gantry and the multiplication factor $n/n-1$. In this section, the theory behind the use of this factor is explained. First, the rigid column in Figure 60 (a) is considered. The multiplication factor for second order deflections and bending moments is derived. Secondly, this factor is used for a flexible column, to approximate the second order deflections and bending moments.

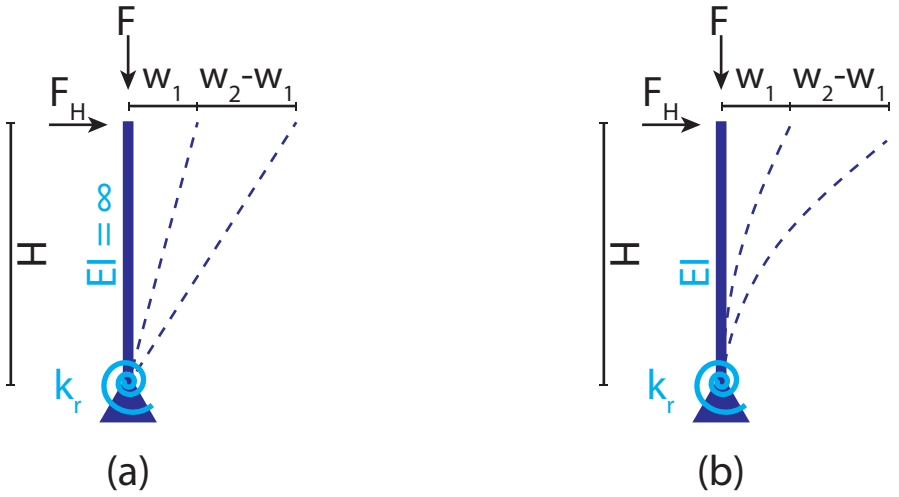

Figure 60: Second order deflection for a column: For a rigid column (a) and a flexible column (b).

The moment equilibrium in the deformed state is given in Equation 83. The buckling load can be found by elimination of the horizontal force F_H. Solving the remaining equation leaves $F_{cr} = k_r/H$. The first order deflection w_1 is found if the second order moment, from the vertical force F and the deflection w_2, is removed from the equation. This leaves the deflection in Equation 84.

$$F_H H + Fw - k_r \frac{w}{H} = 0 \tag{83}$$

$$w_1 = \frac{F_H H^2}{k_r} \tag{84}$$

Solving Equation 83 for w_2 gives the deflection in Equation 85.

$$w_2 = \frac{F_H H}{\frac{k_r}{H} - F} = w_1 \frac{F_H H \frac{k_r}{F_H H^2}}{F_{cr} - F} = w_1 \frac{F_{cr}}{F_{cr} - F} = w_1 \frac{n}{n-1}, \tag{85}$$

where $n = F_{cr}/F$. This shows that the second order deflection equals the first order deflection times the multiplication factor. The second order bending moment can be found from the relation in Equation 85, using that the moment in the spring equals $M = k_r \varphi = k_r w/H$. The first order moment M_1 is simply $F_H H$, from which the second order moment follows in Equation 86.

$$M_2 = k_r \frac{w_2}{H} = k_r \frac{w_1}{H} \frac{n}{n-1} = k_r \frac{F_H H^2}{k_r H} \frac{n}{n-1} = F_H H \frac{n}{n-1} = M_1 \frac{n}{n-1} \tag{86}$$

Thus, the second order moment can also be calculated using the multiplication factor. The same method can be used if the first order deflection is caused by an imperfection instead of a horizontal load.

For the flexible column in Figure 60 (b) the multiplication factor is not exact. It can however be used as an approximation. The second order behaviour of the columnn is described by Equation 87 and the general solution is given in Equation 88. The boundary conditions for the column are given in Equation 89.

$$w'''' + \alpha^2 w'' = 0 \quad with \quad \alpha^2 = \frac{F}{EI} \tag{87}$$

$$w = C_1 + C_2 x + C_3 sin(\alpha x) + C_4 cos(\alpha x) \tag{88}$$

$$x = 0 \rightarrow w = 0 \tag{89a}$$

$$x = 0 \rightarrow M = -k_r w' \tag{89b}$$

$$x = H \rightarrow M = 0 \tag{89c}$$

$$x = H \rightarrow S_z = F_H \tag{89d}$$

The solution for the column in Figure 60 (b), for the deflection w_2 at the top of the column ($x = H$) is given in Equation 90. The first order deflection is given by Equation 91.

$$w_2 = \left(\frac{\rho \, tan(\alpha H)}{(\alpha H)^3 (\rho - \alpha H tan(\alpha H))} - \frac{1}{(\alpha H)^2} \right) \frac{F_H H^3}{EI} \tag{90}$$

$$w_1 = \frac{F_H H^3}{3EI} + \frac{F_H H^3}{k_r} = \left(\frac{3+\rho}{3\rho} \right) \frac{F_H H^3}{EI}, \tag{91}$$

with $\rho = k_r H / EI$. This is the exact solution. The second order deflection, that can not be calculated so easily for other column configurations, can also be approximated by means of the solution that was derived for the rigid column (Equation 85). The second order moment can be approximated with Equation 92. Hartsuijker and Welleman (2007) [20] show that for this column w_2 can be approximated with a maximum error of around 7%, if F is equal to or less than 70% of the buckling load and the value of ρ lies between 0.1 and 10. This range is realistic for the soil types under consideration. For the bending moment the maximum error is then around 10%.

$$M_2 = M_1 + F w_2 = M_1 + F \frac{n}{n-1} w_1 \tag{92}$$

E SCIA Model

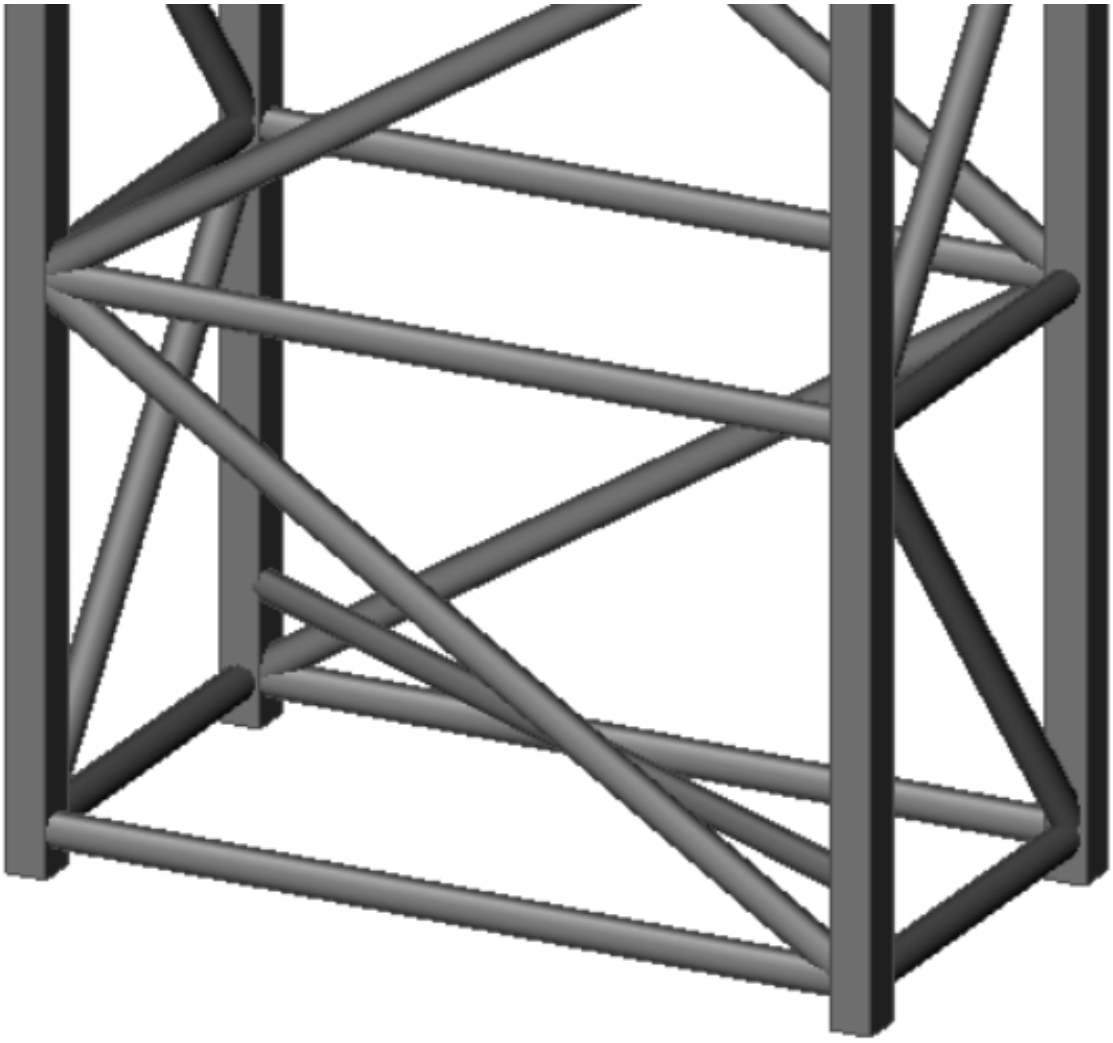

Figure 61: New York Wheel mast section in SCIA Engineer.

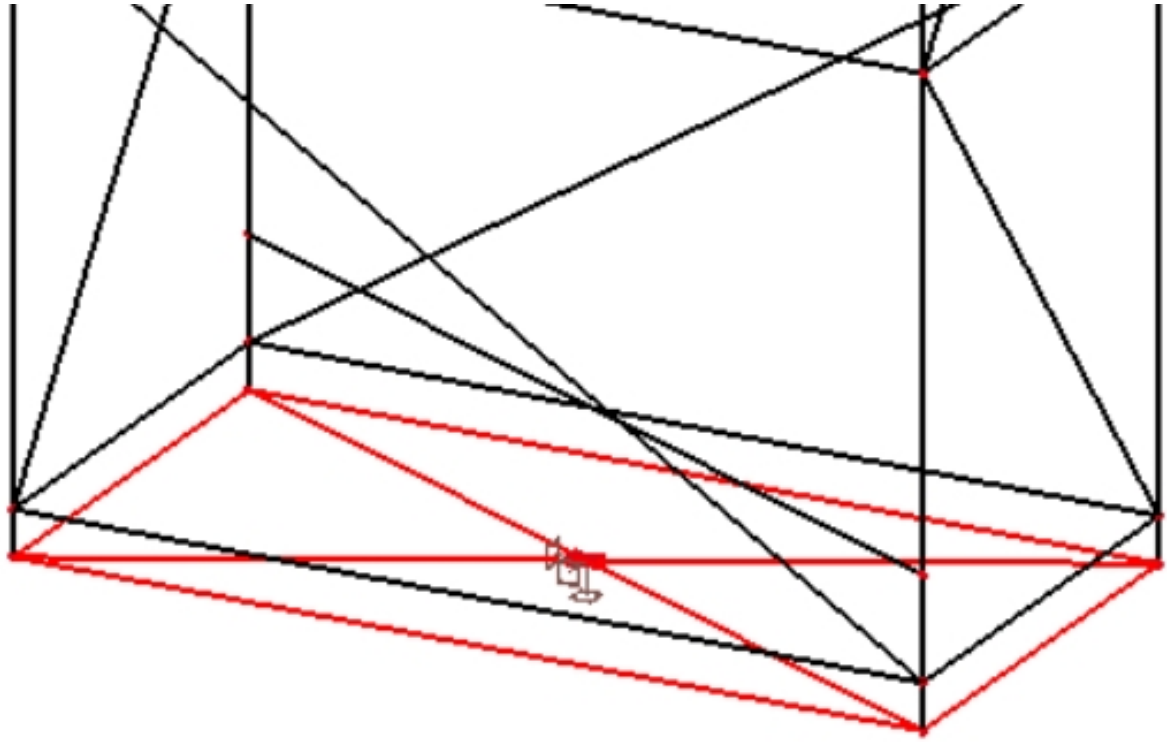

Figure 62: Modelling of base frame in SCIA Engineer: The red lines represent very stiff dummy elements, that mimic an infinitely stiff base frame. The mast section is connected to this base frame by means of hinges. The base is connected to the world by means of a (infinitely stiff) rotational spring.

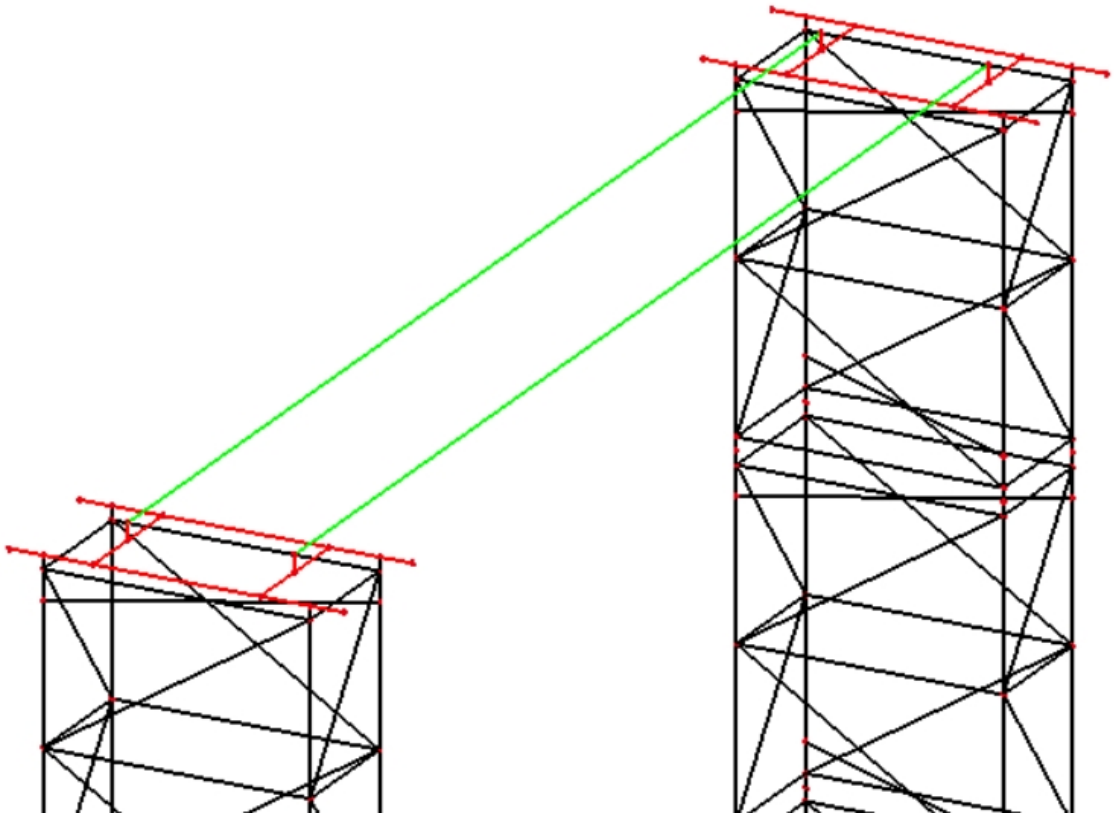

Figure 63: Rigid connection between gantry beams and mast sections in SCIA Engineer: The green lines represent the gantry beams and the red lines very stiff dummy elements.

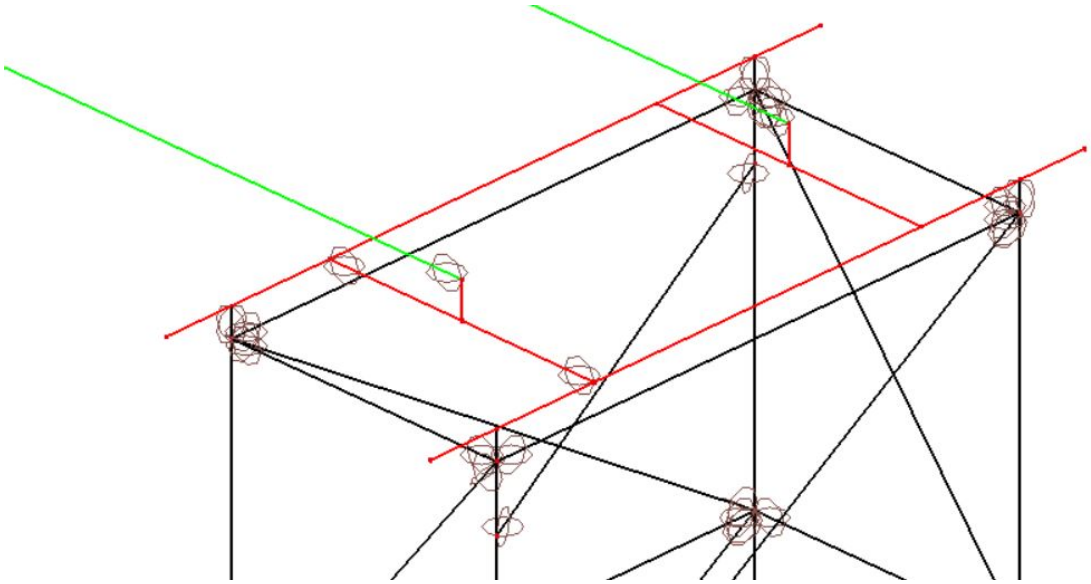

Figure 64: Hinged connection between gantry beams and mast sections in SCIA Engineer: The green lines represent the gantry beams and the red lines very stiff dummy elements. The hinges are also indicated.

F Results

This appendix contains graphs associated with the results discussed in Section 5. The structure of this appendix equals that of the results section.

F.1 Load Percentage

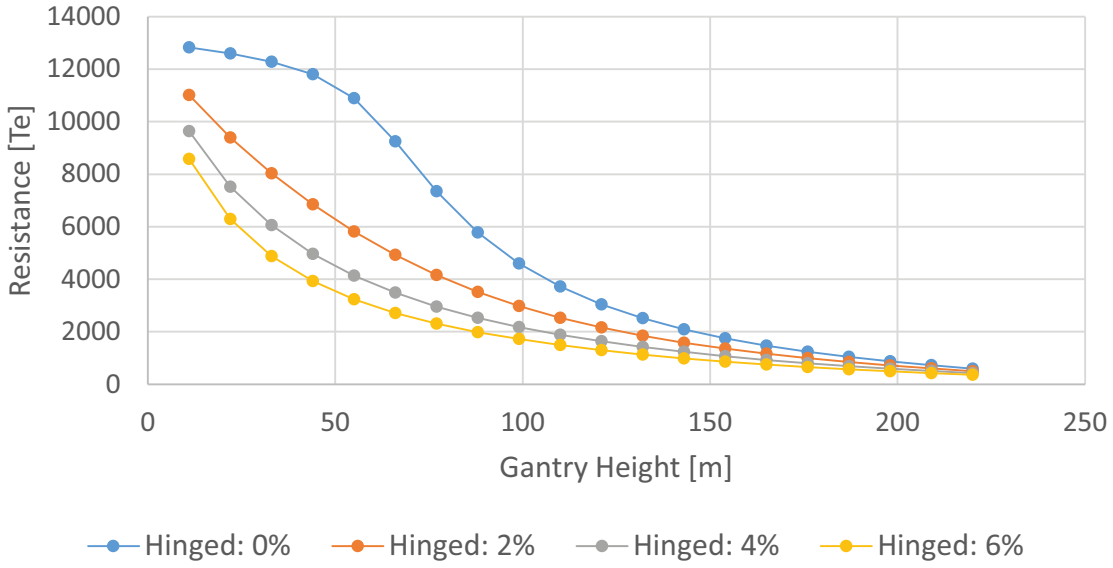

Figure 65: Resistance of New York Wheel mast section gantry: For a rigid foundation and a hinged connection at the top, for different amounts of horizontal load and a 1/500 imperfection.

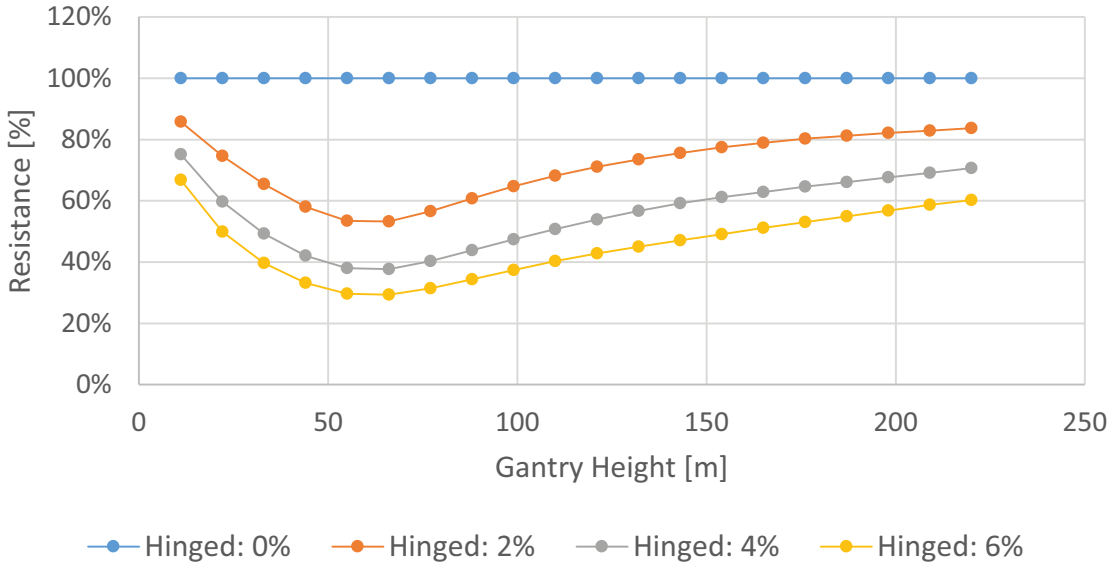

Figure 66: Relative resistance of New York Wheel mast section gantry: For a rigid foundation and a hinged connection at the top, for different amounts of horizontal load and a 1/500 imperfection. Relative to a 0% horizontal load.

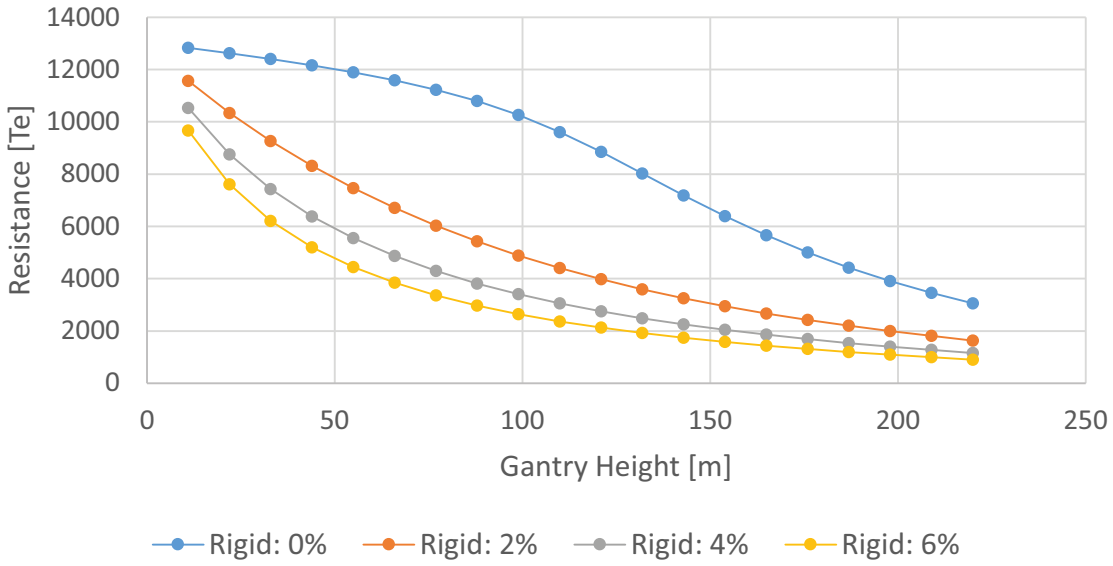

Figure 67: Resistance of New York Wheel mast section gantry: For a rigid foundation and a rigid connection at the top, for different amounts of horizontal load and a 1/500 imperfection.

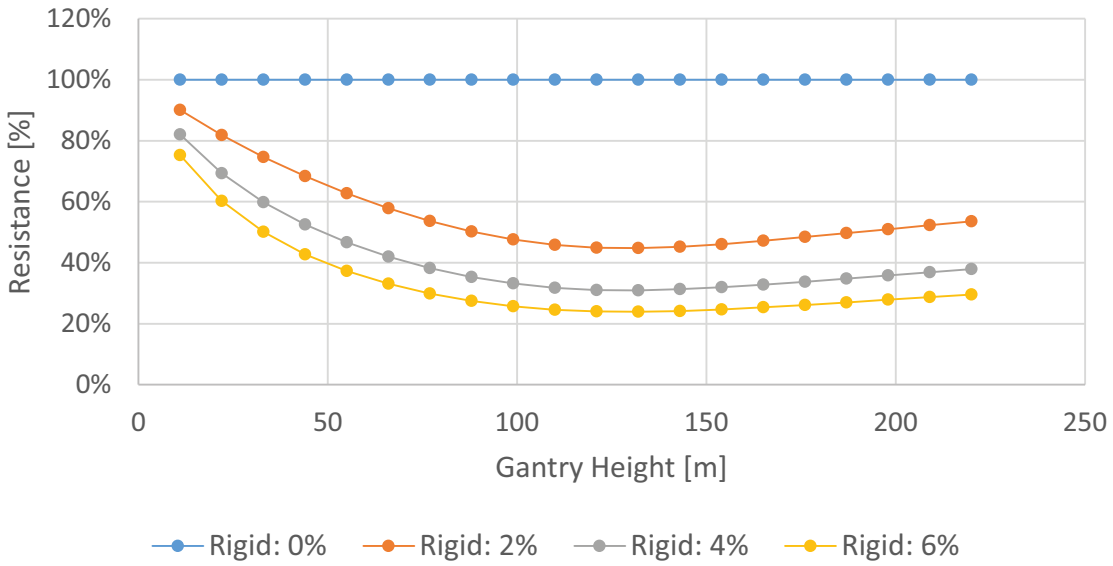

Figure 68: Relative resistance of New York Wheel mast section gantry: For a rigid foundation and a rigid connection at the top, for different amounts of horizontal load and a 1/500 imperfection. Relative to a 0% horizontal load.

F.2 Critical Angle of Horizontal Load

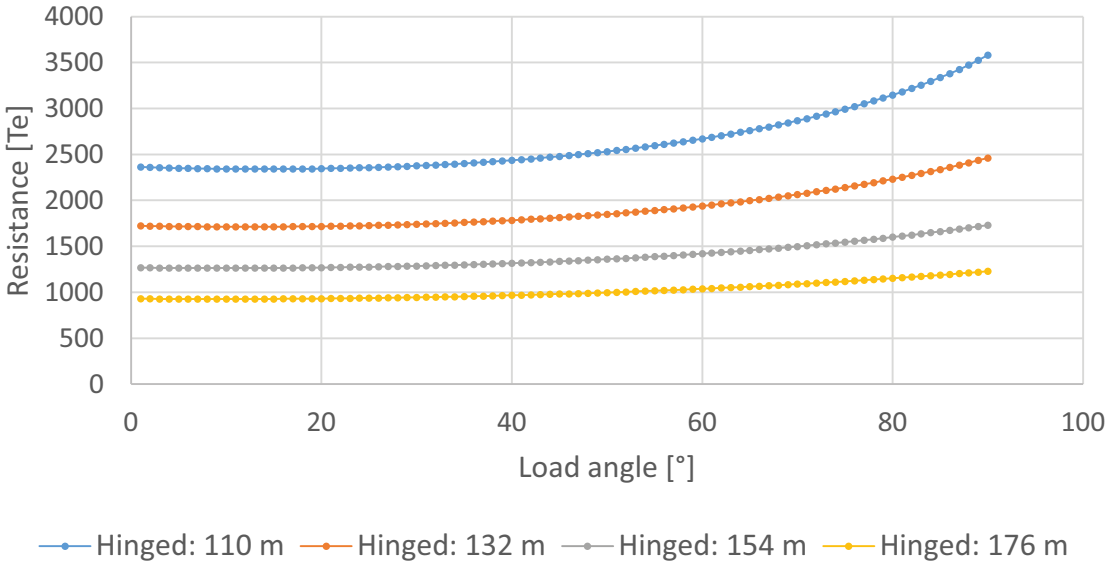

Figure 69: Resistance of New York Wheel mast section gantry depending on the load angle: For four different heights, a rigid foundation, a hinged top connection, 3% horizontal load and a 1/500 imperfection.

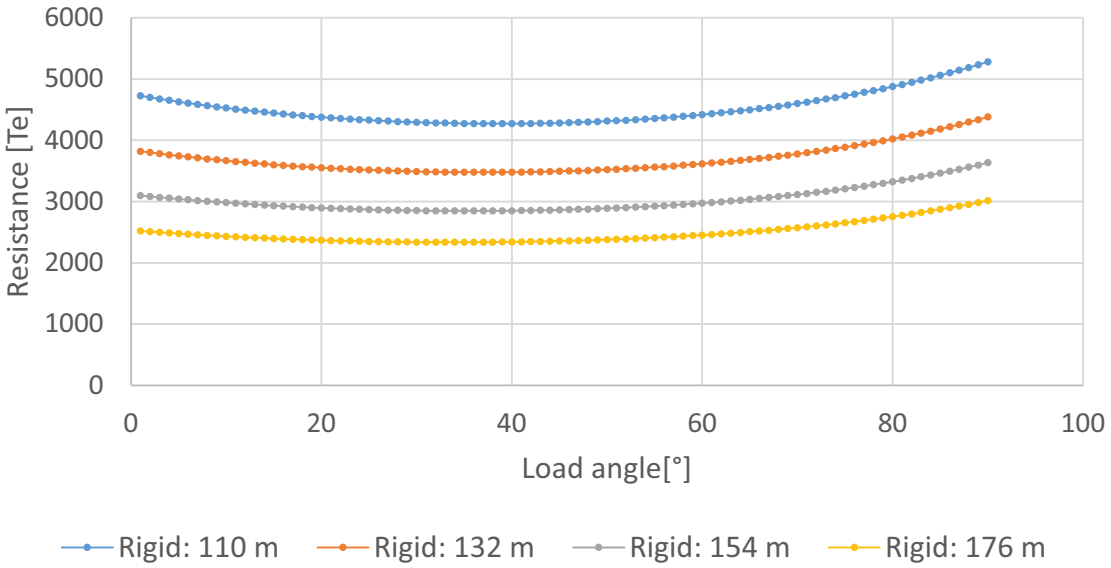

Figure 70: Resistance of New York Wheel mast section gantry depending on the load angle: For four different heights, a rigid foundation, a rigid top connection, 3% horizontal load and a 1/500 imperfection.

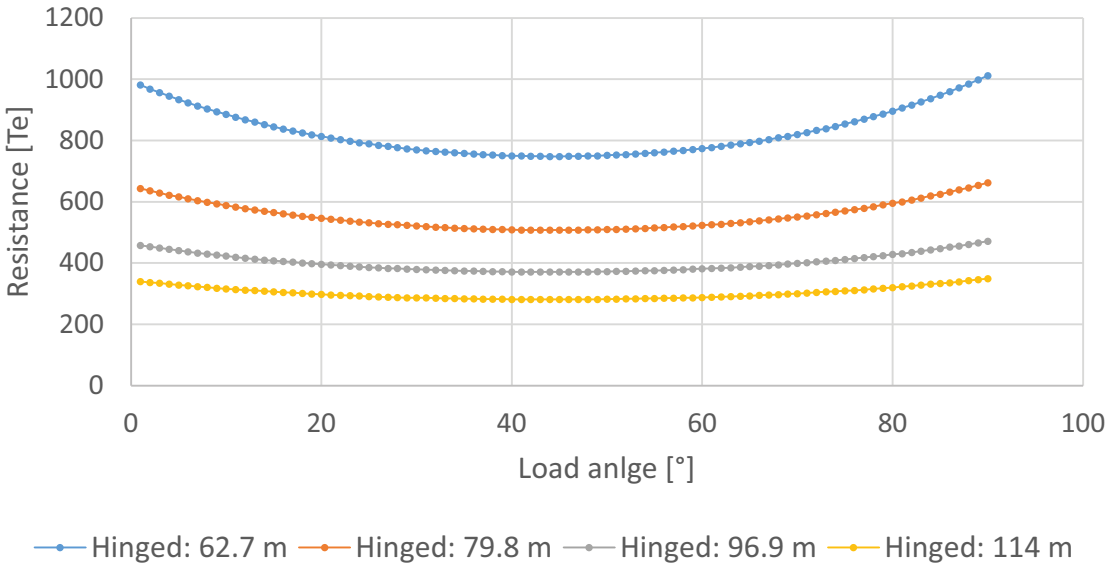

Figure 71: Resistance of MSG mast section gantry depending on the load angle: For four different heights, a rigid foundation, a hinged top connection, 3% horizontal load and a 1/500 imperfection.

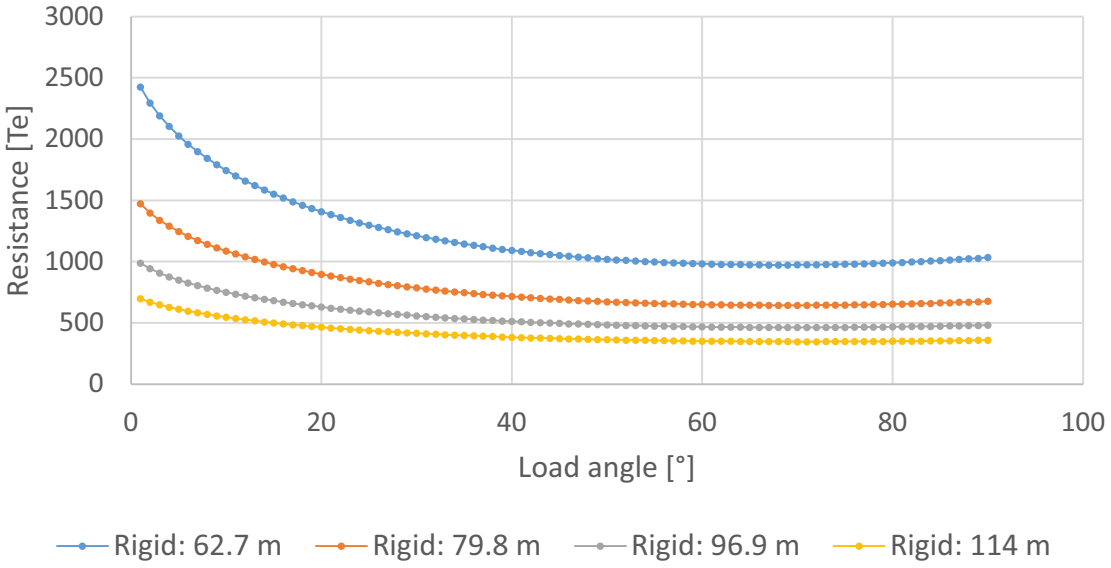

Figure 72: Resistance of MSG mast section gantry depending on the load angle: For four different heights, a rigid foundation, a rigid top connection, 3% horizontal load and a 1/500 imperfection.

F.3 Imperfection

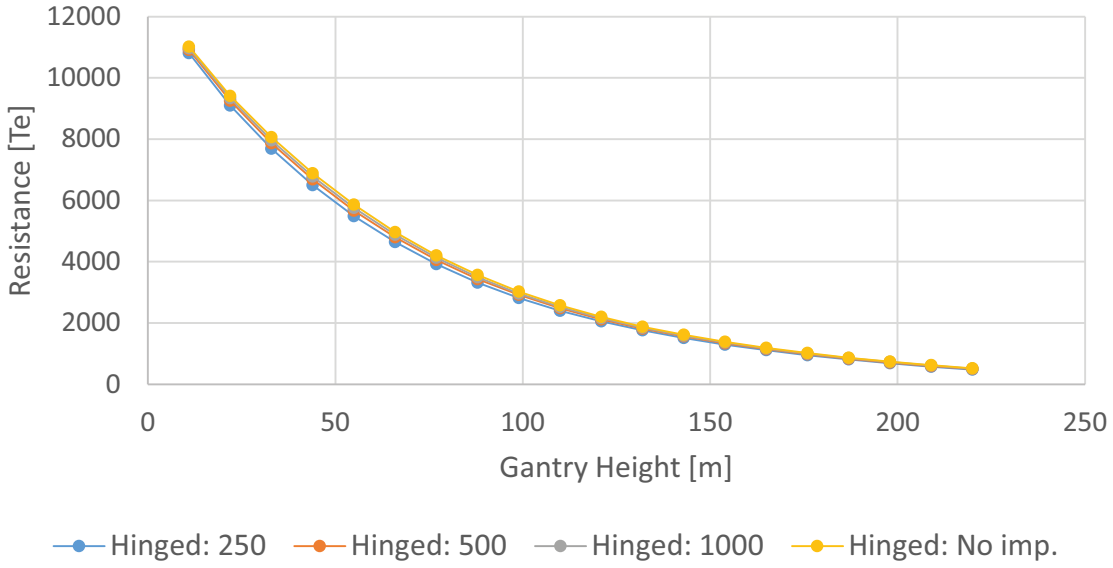

Figure 73: Resistance of New York Wheel mast section gantry depending on the imperfection: For four different imperfections, a rigid foundation, a hinged top connection and 3% horizontal load at a 45° angle.

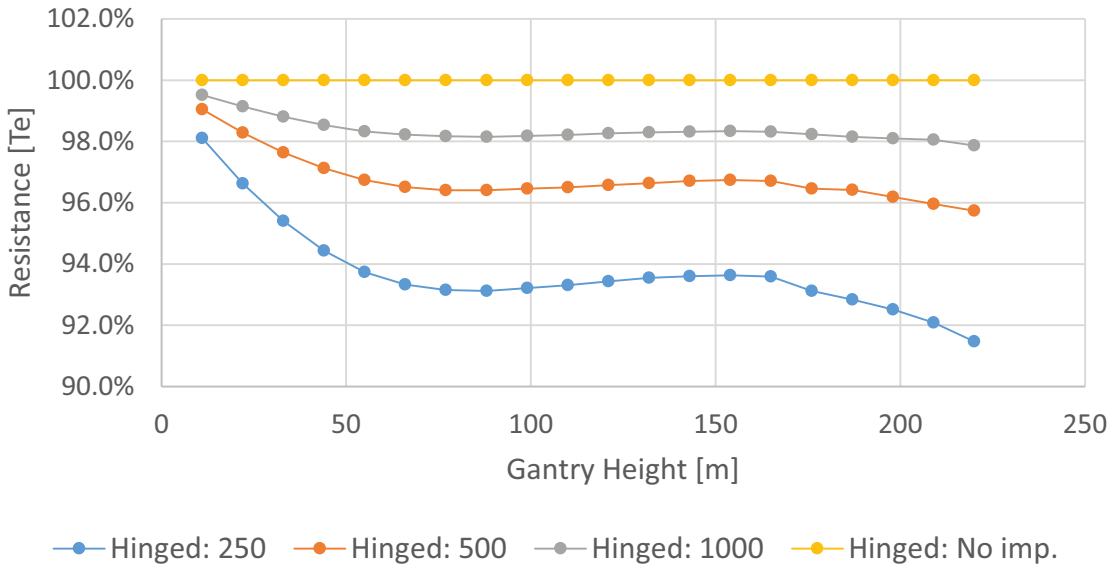

Figure 74: Relative resistance of New York Wheel mast section gantry depending on the imperfection: For four different imperfections, a rigid foundation, a hinged top connection and 3% horizontal load at a 45° angle. Relative to a gantry with no imperfection.

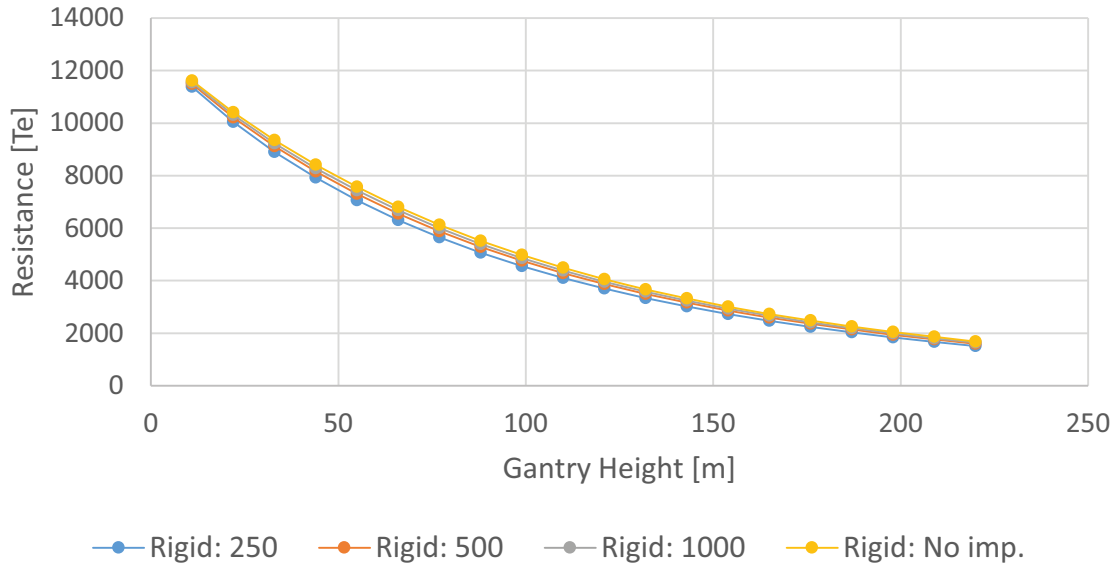

Figure 75: Resistance of New York Wheel mast section gantry depending on the imperfection: For four different imperfections, a rigid foundation, a rigid top connection and 3% horizontal load at a 45° angle.

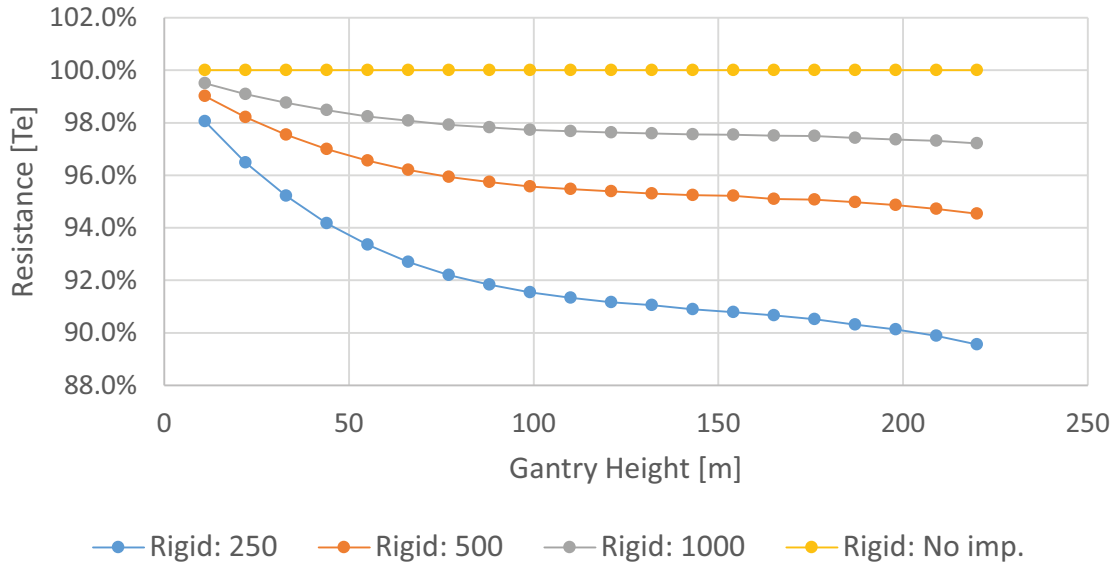

Figure 76: Relative resistance of New York Wheel mast section gantry depending on the imperfection: For four different imperfections, a rigid foundation, a rigid top connection and 3% horizontal load at a 45° angle. Relative to a gantry with no imperfection.

F.4 Soil Stiffness

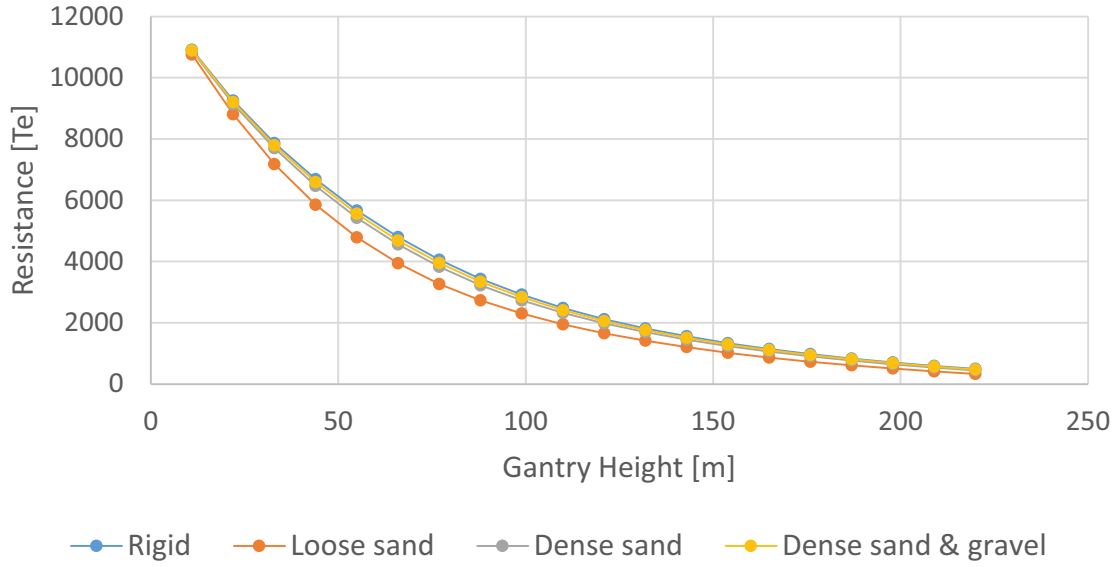

Figure 77: Resistance of New York Wheel mast section gantry depending on the foundation stiffness: For a hinged top connection, 3% horizontal load at a 45° angle and a 1/500 imperfection.

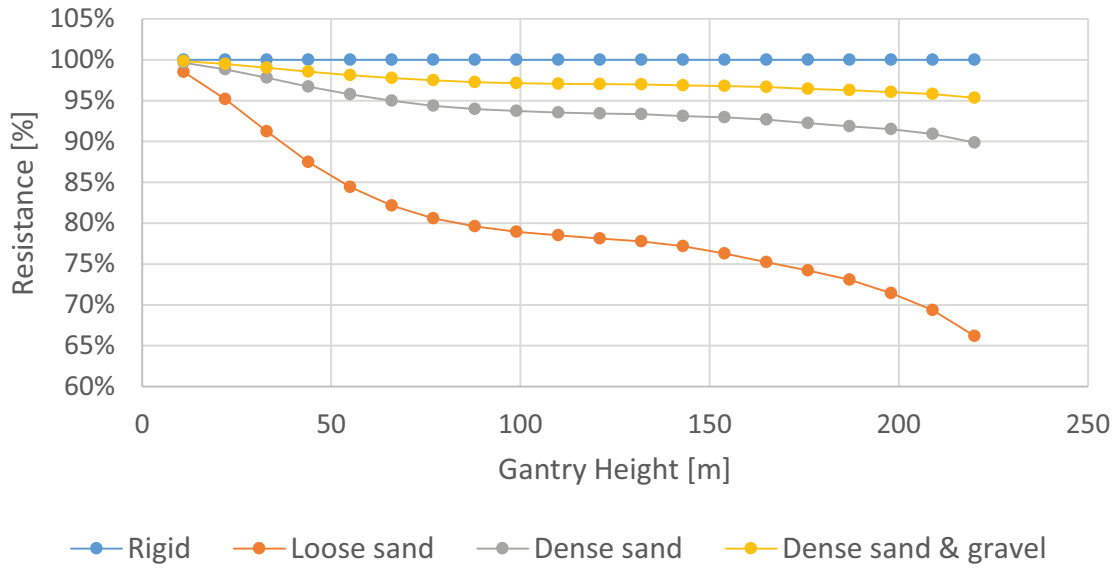

Figure 78: Relative resistance of New York Wheel mast section gantry depending on the foundation stiffness: For a hinged top connection, 3% horizontal load at a 45° angle and a 1/500 imperfection. Relative to a rigid foundation.

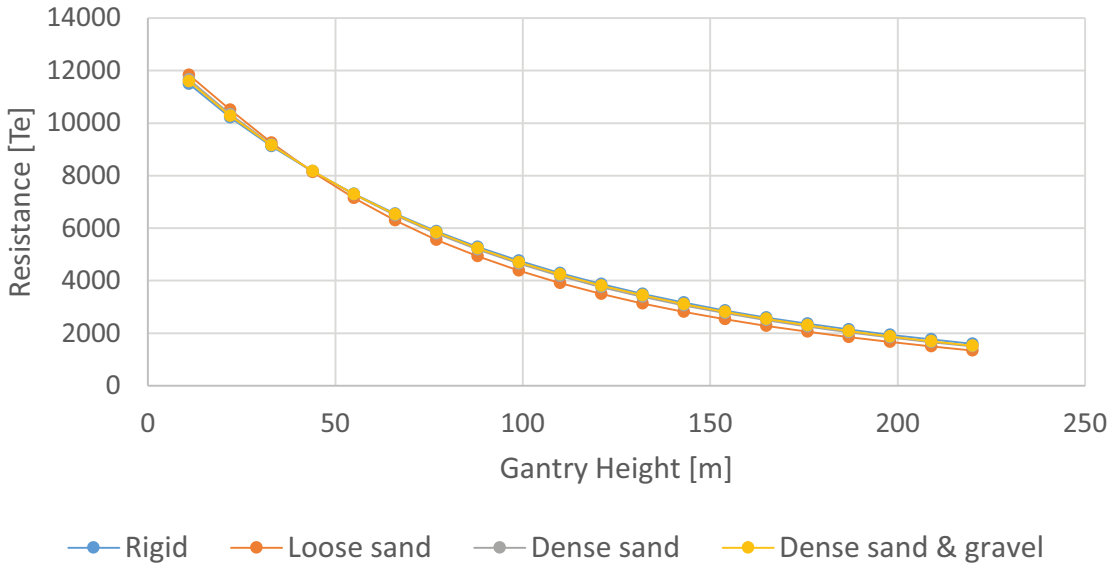

Figure 79: Resistance of New York Wheel mast section gantry depending on the foundation stiffness: For a rigid top connection, 3% horizontal load at a 45° angle and a 1/500 imperfection.

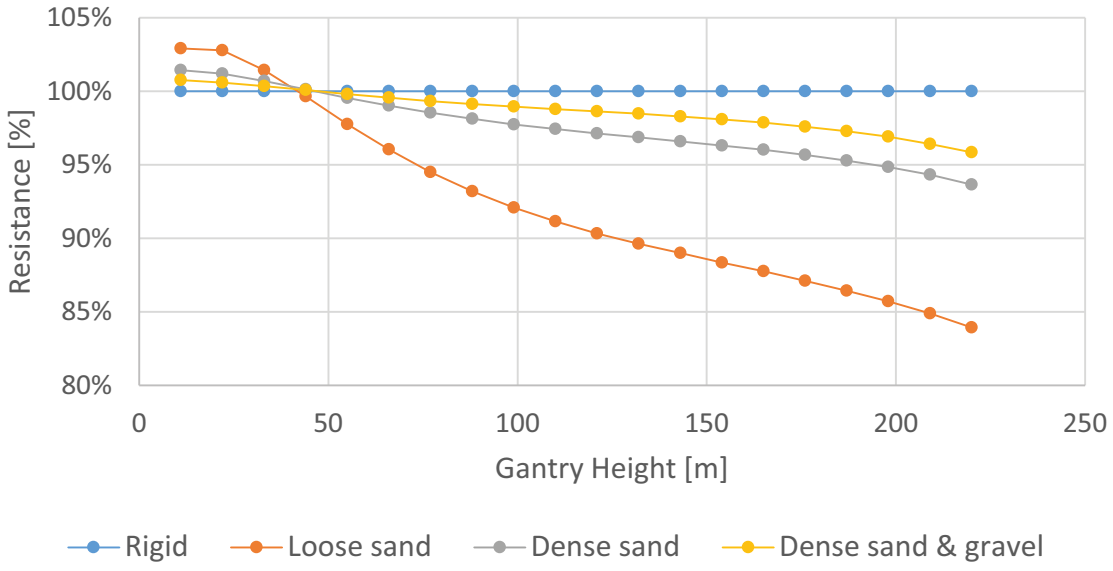

Figure 80: Relative resistance of New York Wheel mast section gantry depending on the foundation stiffness: For a rigid top connection, 3% horizontal load at a 45° angle and a 1/500 imperfection. Relative to a rigid foundation.

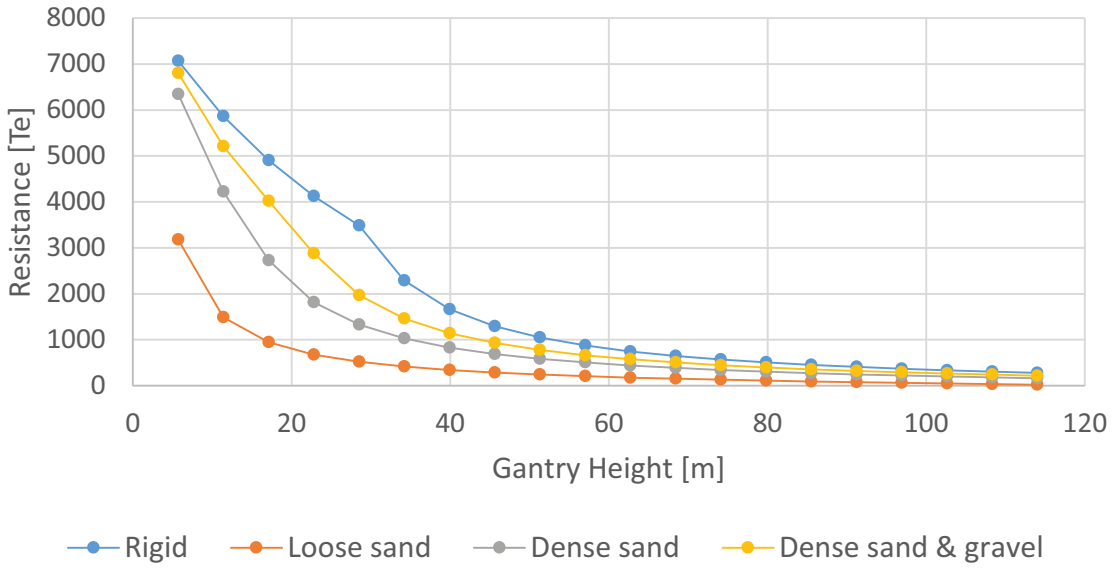

Figure 81: Resistance of MSG mast section gantry depending on the foundation stiffness: For a hinged top connection, 3% horizontal load at a 45° angle and a 1/500 imperfection.

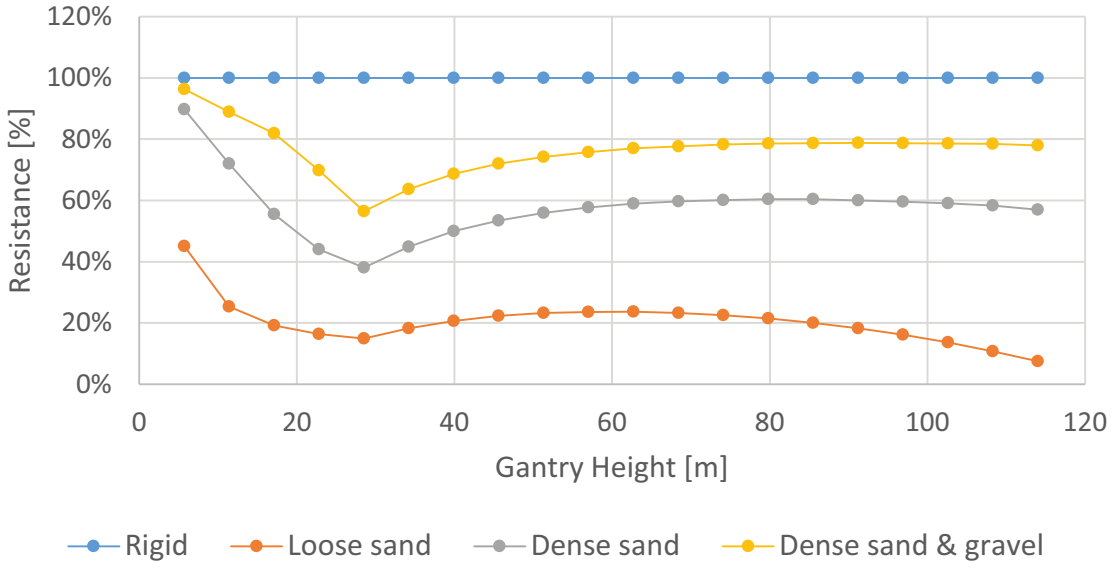

Figure 82: Relative resistance of MSG mast section gantry depending on the foundation stiffness: For a hinged top connection, 3% horizontal load at a 45° angle and a 1/500 imperfection. Relative to a rigid foundation.

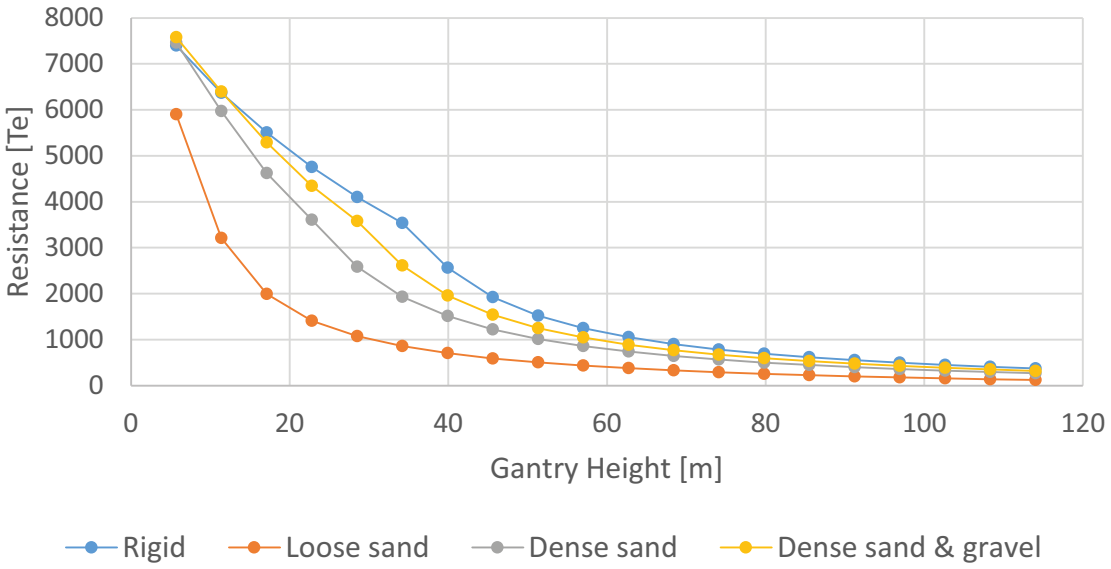

Figure 83: Resistance of MSG mast section gantry depending on the foundation stiffness: For a rigid top connection, 3% horizontal load at a 45° angle and a 1/500 imperfection.

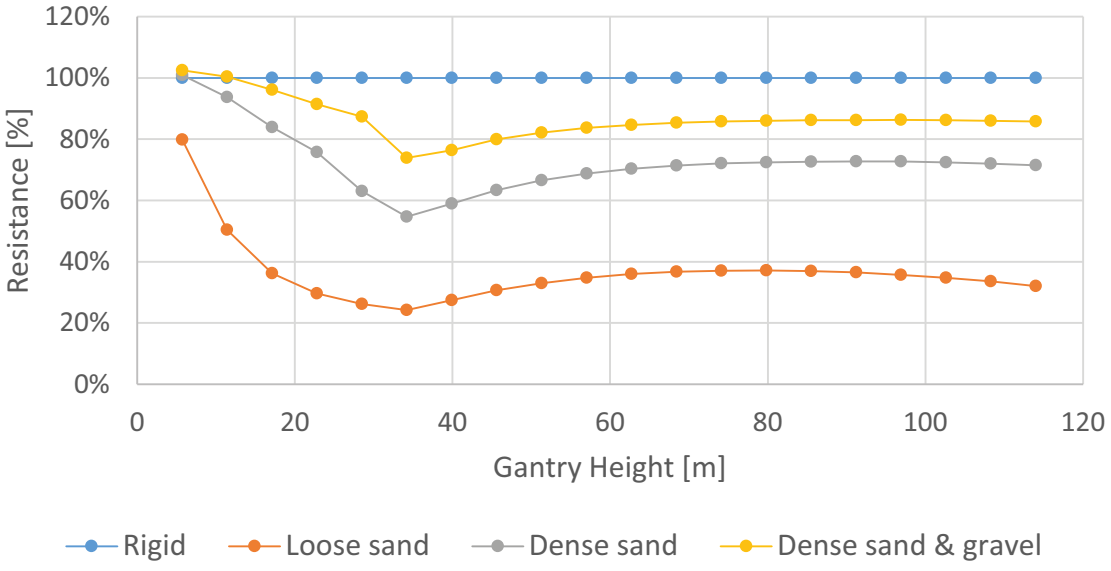

Figure 84: Relative resistance of MSG mast section gantry depending on the foundation stiffness: For a rigid top connection, 3% horizontal load at a 45° angle and a 1/500 imperfection. Relative to a rigid foundation.

G Horizontal Load On The Gantry Structure

Table 15: Horizontal loads on the gantry: For a gantry made out of New York Wheel mast sections. Loads from Cases 1 and 2, loads in the longitudinal direction of the gantry beam. Skidding included.

	Case 1 L1				**Case 1 L2**				**Case 1 L3**			
	Load [Te]				Load [Te]				Load [Te]			
z [m]	400	800	1200	1600	1800	2000	2200	2400	2600	2800	3000	3200
88	5.2%	4.6%	4.4%	4.3%	3.6%	3.6%	3.6%	3.6%	3.2%	3.1%	3.1%	3.1%
110	5.4%	4.7%	4.5%	4.3%	3.7%	3.6%	3.6%	3.6%	3.2%	3.2%	3.2%	3.2%
132	5.7%	4.8%	4.5%	4.4%	3.7%	3.7%	3.7%	3.6%	3.2%	3.2%	3.2%	3.2%
154	5.9%	5.0%	4.6%	4.5%	3.8%	3.7%	3.7%	3.7%	3.3%	3.3%	3.2%	3.2%
176	6.2%	5.1%	4.7%	4.5%	3.8%	3.8%	3.8%	3.7%	3.3%	3.3%	3.3%	3.3%

	Case 2 L1				**Case 2 L2**				**Case 2 L3**			
	Load [Te]				Load [Te]				Load [Te]			
z [m]	400	800	1200	1600	1800	2000	2200	2400	2600	2800	3000	3200
88	1.6	1.8	1.8	1.9	2.2	2.3	2.3	2.3	2.7	2.7	2.8	2.8
110	1.6	1.7	1.8	1.9	2.2	2.2	2.2	2.3	2.7	2.7	2.7	2.7
132	1.5	1.7	1.8	1.8	2.2	2.2	2.2	2.2	2.6	2.6	2.7	2.7
154	1.5	1.7	1.8	1.8	2.1	2.1	2.2	2.2	2.6	2.6	2.6	2.6
176	1.5	1.6	1.7	1.8	2.1	2.1	2.1	2.2	2.5	2.5	2.6	2.6

Table 16: Horizontal loads on the gantry: For a gantry made out of New York Wheel mast sections. Loads from Cases 1 and 2, loads in the transverse direction of the gantry beam. Skidding included.

	Case 1 L1				**Case 1 L2**				**Case 1 L3**			
	Load [Te]				Load [Te]				Load [Te]			
z [m]	400	800	1200	1600	1800	2000	2200	2400	2600	2800	3000	3200
88	4.8%	3.9%	3.6%	3.4%	2.8%	2.7%	2.7%	2.7%	2.3%	2.2%	2.2%	2.2%
110	5.0%	4.0%	3.6%	3.5%	2.8%	2.7%	2.7%	2.7%	2.3%	2.3%	2.2%	2.2%
132	5.1%	4.0%	3.7%	3.5%	2.8%	2.8%	2.7%	2.7%	2.3%	2.3%	2.3%	2.2%
154	5.3%	4.1%	3.7%	3.5%	2.9%	2.8%	2.8%	2.7%	2.3%	2.3%	2.3%	2.3%
176	5.5%	4.2%	3.8%	3.6%	2.9%	2.8%	2.8%	2.8%	2.4%	2.3%	2.3%	2.3%

	Case 2 L1				**Case 2 L2**				**Case 2 L3**			
	Load [Te]				Load [Te]				Load [Te]			
z [m]	400	800	1200	1600	1800	2000	2200	2400	2600	2800	3000	3200
88	**1.3**	**1.3**	1.4	1.4	1.6	1.6	1.6	1.6	1.8	1.8	1.8	1.8
110	**1.3**	**1.3**	1.4	1.4	1.6	1.6	1.6	1.6	1.8	1.8	1.8	1.8
132	**1.2**	**1.3**	1.4	1.4	1.5	1.6	1.6	1.6	1.8	1.8	1.8	1.8
154	**1.2**	**1.3**	1.4	1.4	1.5	1.6	1.6	1.6	1.8	1.8	1.8	1.8
176	**1.2**	**1.3**	1.4	1.4	1.5	1.5	1.6	1.6	1.7	1.8	1.8	1.8

Table 17: Horizontal loads on the gantry: For a gantry made out of New York Wheel mast sections. Loads from Cases 1 and 2, loads in the longitudinal direction of the gantry beam. Tailing included.

	Case 1 L1				**Case 1 L2**				**Case 1 L3**			
	Load [Te]				Load [Te]				Load [Te]			
z [m]	400	800	1200	1600	1800	2000	2200	2400	2600	2800	3000	3200
88	4.2%	3.6%	3.4%	3.3%	2.6%	2.6%	2.6%	2.6%	2.2%	2.1%	2.1%	2.1%
110	4.4%	3.7%	3.5%	3.3%	2.7%	2.6%	2.6%	2.6%	2.2%	2.2%	2.2%	2.2%
132	4.7%	3.8%	3.5%	3.4%	2.7%	2.7%	2.7%	2.6%	2.2%	2.2%	2.2%	2.2%
154	4.9%	4.0%	3.6%	3.5%	2.8%	2.7%	2.7%	2.7%	2.3%	2.3%	2.2%	2.2%
176	5.2%	4.1%	3.7%	3.5%	2.8%	2.8%	2.8%	2.7%	2.3%	2.3%	2.3%	2.3%

	Case 2 L1				**Case 2 L2**				**Case 2 L3**			
	Load [Te]				Load [Te]				Load [Te]			
z [m]	400	800	1200	1600	1800	2000	2200	2400	2600	2800	3000	3200
88	**1.3**	1.4	1.4	1.4	1.6	1.6	1.6	1.6	1.9	1.9	1.9	1.9
110	**1.3**	1.4	1.4	1.4	1.6	1.6	1.6	1.6	1.8	1.8	1.9	1.9
132	**1.3**	1.4	1.4	1.4	1.6	1.6	1.6	1.6	1.8	1.8	1.8	1.8
154	**1.3**	**1.3**	1.4	1.4	1.6	1.6	1.6	1.6	1.8	1.8	1.8	1.8
176	**1.2**	**1.3**	1.4	1.4	1.5	1.6	1.6	1.6	1.8	1.8	1.8	1.8

Table 18: Horizontal loads on the gantry: For a gantry made out of New York Wheel mast sections. Loads from Cases 1 and 2, loads in the transverse direction of the gantry beam. Tailing included.

	Case 1 L1				**Case 1 L2**				**Case 1 L3**			
	Load [Te]				Load [Te]				Load [Te]			
z [m]	400	800	1200	1600	1800	2000	2200	2400	2600	2800	3000	3200
88	4.8%	3.9%	3.6%	3.4%	2.8%	2.7%	2.7%	2.7%	2.3%	2.2%	2.2%	2.2%
110	5.0%	4.0%	3.6%	3.5%	2.8%	2.7%	2.7%	2.7%	2.3%	2.3%	2.2%	2.2%
132	5.1%	4.0%	3.7%	3.5%	2.8%	2.8%	2.7%	2.7%	2.3%	2.3%	2.3%	2.2%
154	5.3%	4.1%	3.7%	3.5%	2.9%	2.8%	2.8%	2.7%	2.3%	2.3%	2.3%	2.3%
176	5.5%	4.2%	3.8%	3.6%	2.9%	2.8%	2.8%	2.8%	2.4%	2.3%	2.3%	2.3%

	Case 2 L1				**Case 2 L2**				**Case 2 L3**			
	Load [Te]				Load [Te]				Load [Te]			
z [m]	400	800	1200	1600	1800	2000	2200	2400	2600	2800	3000	3200
88	**1.3**	**1.3**	1.4	1.4	1.6	1.6	1.6	1.6	1.8	1.8	1.8	1.8
110	**1.3**	**1.3**	1.4	1.4	1.6	1.6	1.6	1.6	1.8	1.8	1.8	1.8
132	**1.2**	**1.3**	1.4	1.4	1.5	1.6	1.6	1.6	1.8	1.8	1.8	1.8
154	**1.2**	**1.3**	1.4	1.4	1.5	1.6	1.6	1.6	1.8	1.8	1.8	1.8
176	**1.2**	**1.3**	1.4	1.4	1.5	1.5	1.6	1.6	1.7	1.8	1.8	1.8

H Imperfection

The nominal dimensions and the positive and negative tolerances of the section measures are given in Table 19.

Table 19: DS section dimensions of interest (Nom. dim. stands for nominal dimension).

Symbol	**Description**	**Nom. dim. [mm]**	**Tolerance + [mm]**	**Tolerance - [mm]**
E1 - E8	Hole diameter at chords end	141	-0.1	-0.4
M1 - M8	Hole diameter top-bottom connection	61	-0.1	-0.4
C1 - C5	Hole diameter at chords edge	61	-0.1	-0.4
W1 - W2	width between chords	1770	2	1
L1 - L4	Chord length	11400	0.2	-0.2
D1 - D2	Center chord to center middle	2150	0.2	-0.2
B1 - B12	Center edge hole to center middle hole	1800	0.2	-0.2

The next two pages show examples of the measured dimensions, along with the nomenclature of Table 19. Figures 85, 86, 87 and 88 show the measurements on the hole diameter and the distance between the chords.

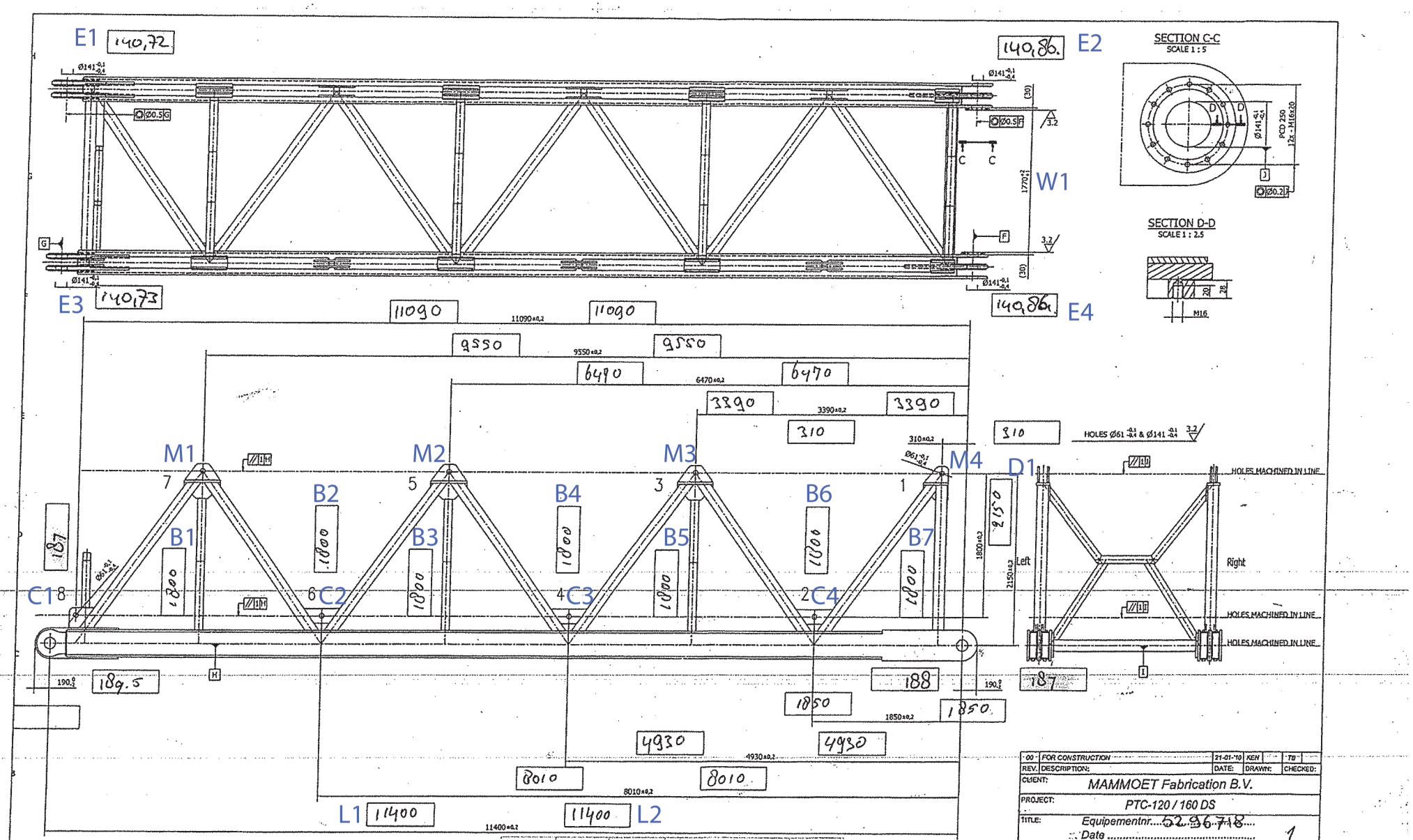

	Gemeten	Gemeten		Gemeten	Gemeten
Ø 61	Left	Right	Ø 61	Left	Right
1	60,75	60,8	5	60,73	60,79
2	60,72	60,75	6	60,73	60,74
3	60,76	60,8	7	60,74	60,8
4	60,74	60,74	8	60,73	60,75

REV.	DESCRIPTION:	DATE:	DRAWN:	CHECKED:
00	FOR CONSTRUCTION	21-01-10	KEN	TB

CLIENT: MAMMOET Fabrication B.V.

PROJECT: PTC-120 / 160 DS

TITLE: Equipementnr....52.96.718....
Date .....
MACHINING Report LOWER PART

1

MAMMOET

SIZE: A1 | SCALE: 1:20 | SHT: 2 / 2 | DRAWING NUMBER (VAULT)

PROJECT No: 0010036889-NL06 | ITEM No: 002000 - 31 - 06 - 01 - 00 | SUB1: | SUB2: | PART: | REV.

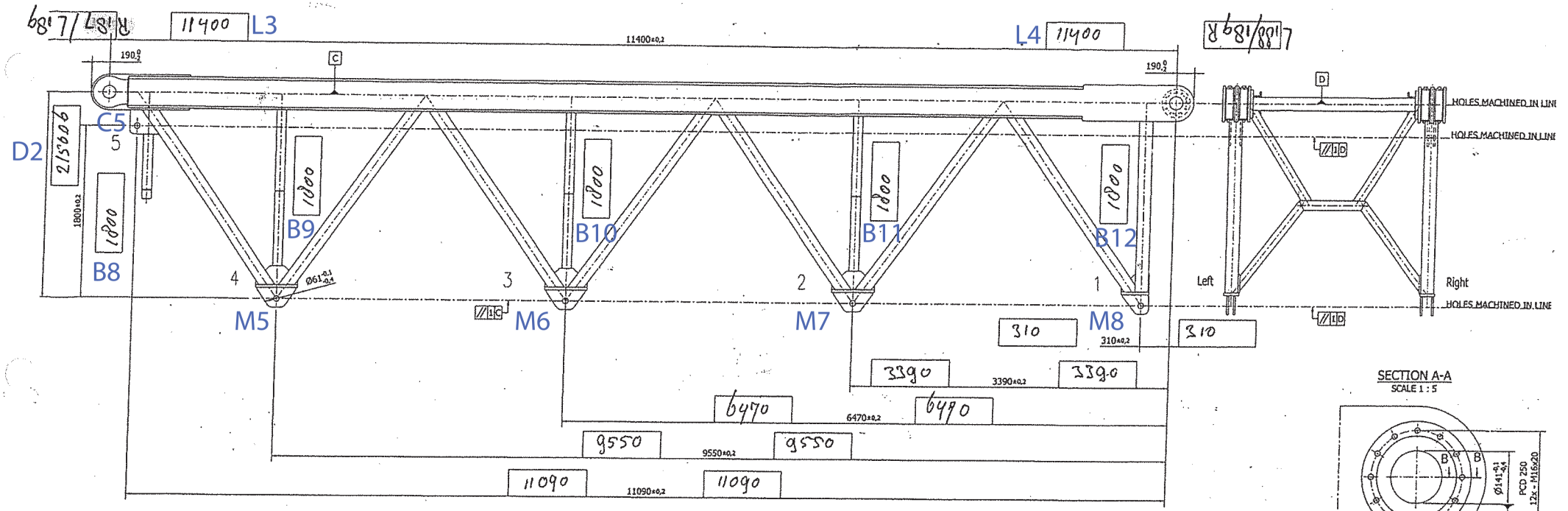

Equipementnr 718/719

E5 140,78

E6 14973

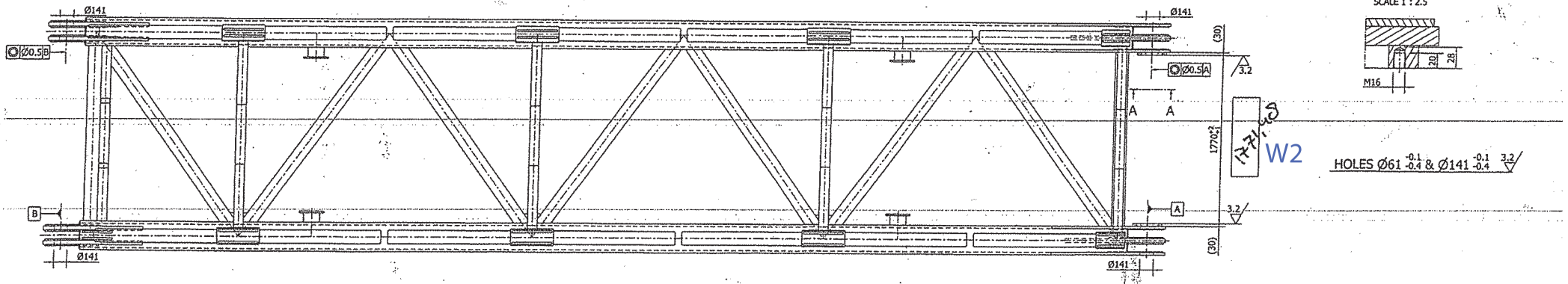

E7 140,79

E8 140,74

	-0,1 Ø 61 -0,4	Left	Right
1		60,715	60,74
2		60,75	60,74
3		60,74	60,72
4		60,74	60,7
5		60,77	60,72

CROSS REFERENCES	
DESCRIPTION	REFERENCE
ASSEMBLY	002000 - 31 - 06 - 00
MACHINING	002000 - 31 - 06 - 01
WELDING	002000 - 31 - 06 - 02
WELDING DETAILS	002000 - 31 - 06 - 03
PARTS - PLATES	002000 - 31 - 06 - 04
PARTS - MACHINED	002000 - 31 - 06 - 05
HANDLING	002000 - 31 - 06 - 08

REV.	DESCRIPTION:	DATE:	DRAWN:	CHECKED

CLIENT: MAMMOET Fabrication B.V.

PROJECT: PTC-120 / 160 DS

TITLE: Equipement nr...6296.719.....
Date .....Name.....
MACHINING Report UPPER PART

1

MAMMOET

Karel Doormanweg 47, 3115 JD Schiedam, Harbour 565
P.O. Box 670, 3100 AR Schiedam, THE NETHERLANDS
Tel. +31(0)10-2042441 / Fax. +31(0)10-2042442
www.mammoet.com

SIZE: A1 | SCALE: 1:20 | SHT: 1 / 2 | DRAWING NUMBER (VAULT)

PROJECT No: | ITEM No: | SUB1: | SUB2: | PART: | RI

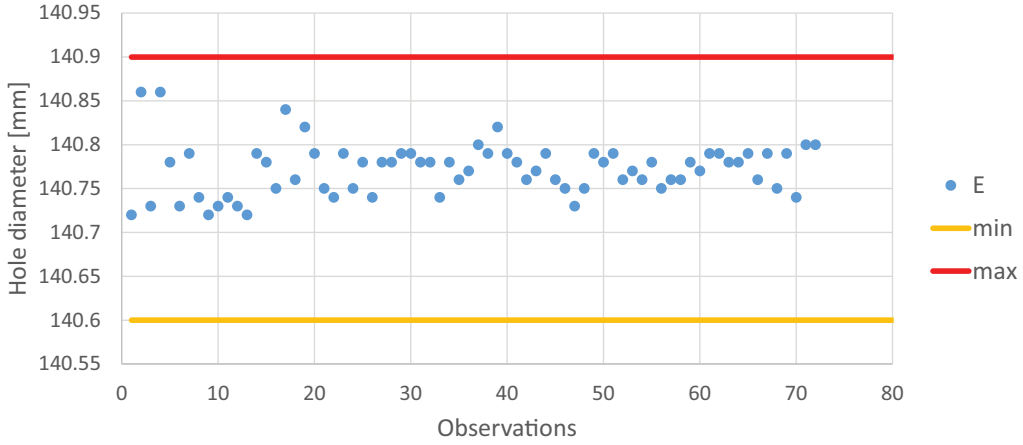

Figure 85: Hole diameter observations for holes at the ends of the chords: With the maximum and minimum value according to the tolerances.

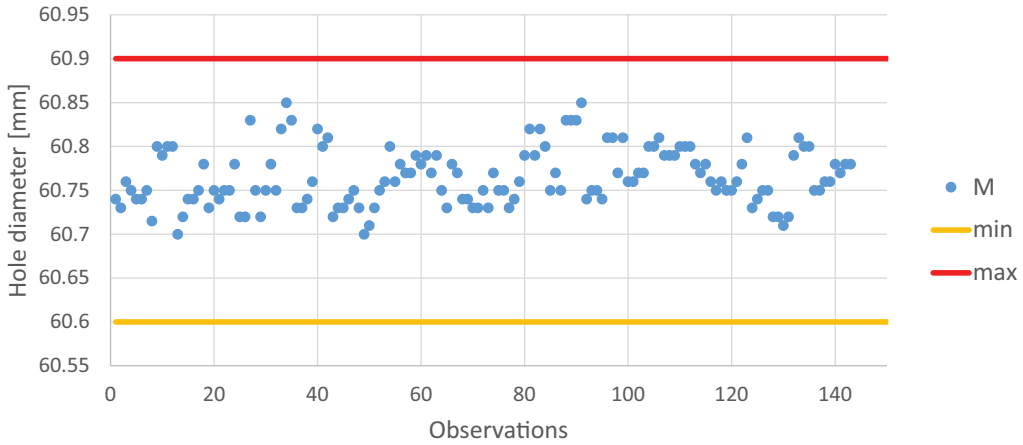

Figure 86: Hole diameter observations for holes at the connection of the top and bottom part of the section: With the maximum and minimum value according to the tolerances.

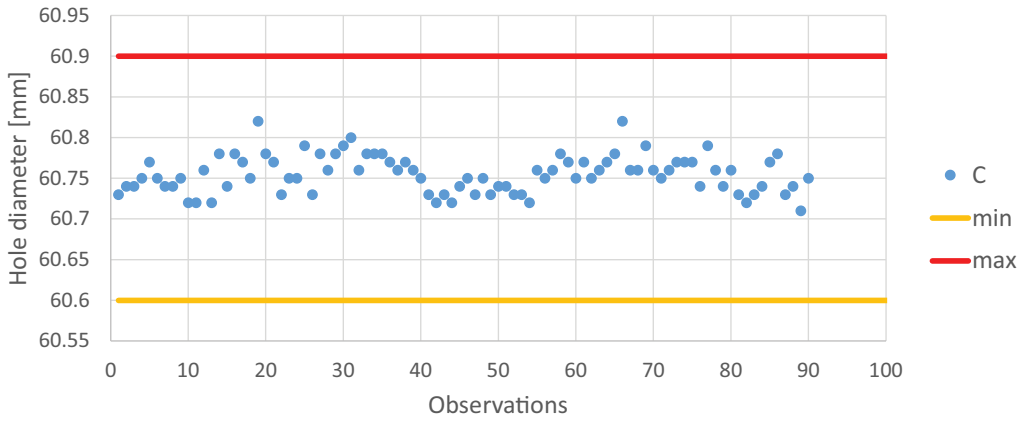

Figure 87: Hole diameter observations for holes at the edge of the chords: With the maximum and minimum value according to the tolerances.

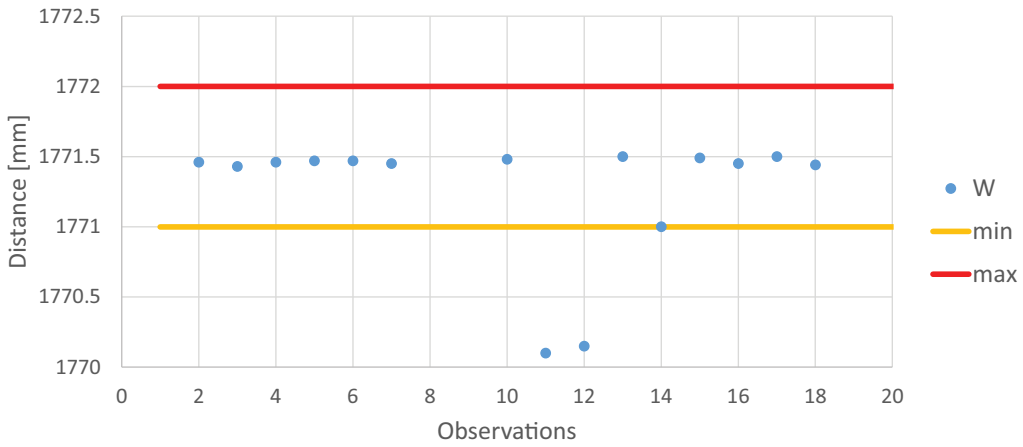

Figure 88: Distance between the chords: With the maximum and minimum value according to the tolerances.

I Guy Lines

Several graphs that result from the analysis into the application of guy lines carried out in Section 9 are given in this Appendix. In Appendix I.1 the buckling factor is shown in graphs, for different configurations. Appendix I.2 and I.3 show the graphs for the first order deflections and the load distribution respectively.

I.1 Buckling Factor

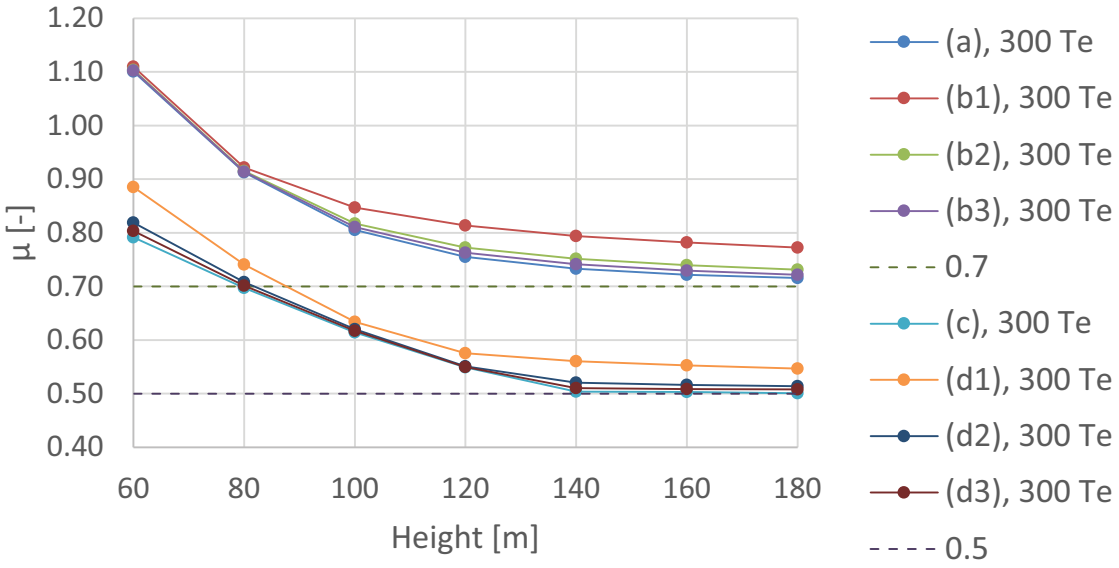

Figure 89: Buckling factor for the weak direction of the NYW sections, for the 300 Te system.

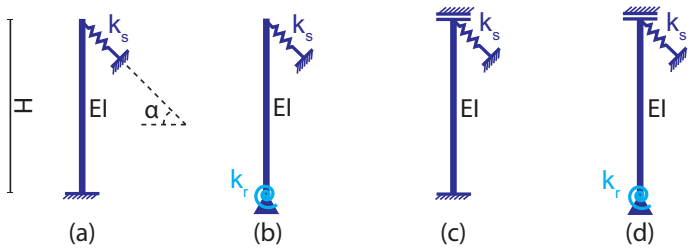

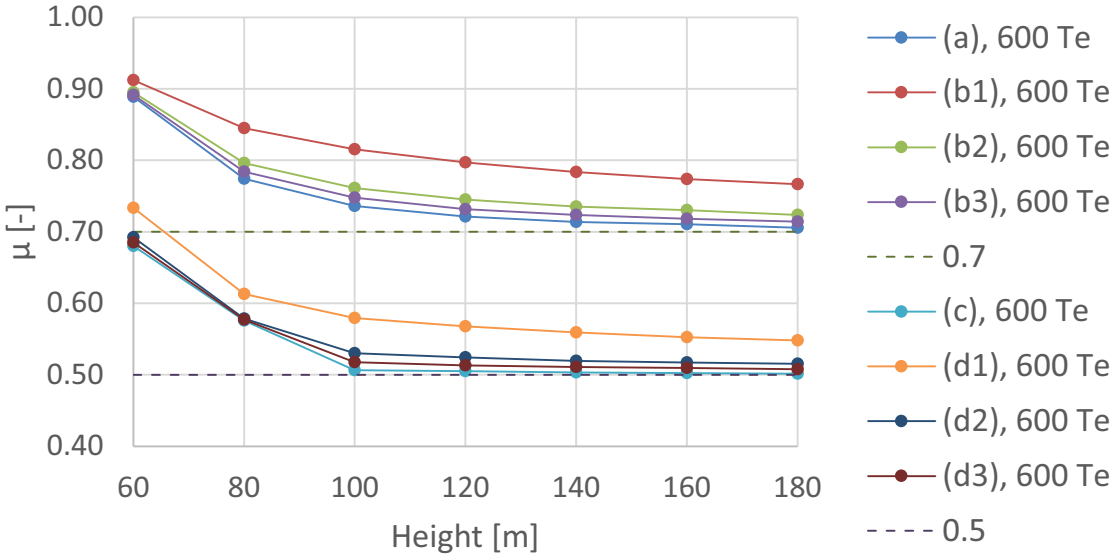

Figure 90: Buckling factor for the weak direction of the NYW sections, for the 600 Te system.

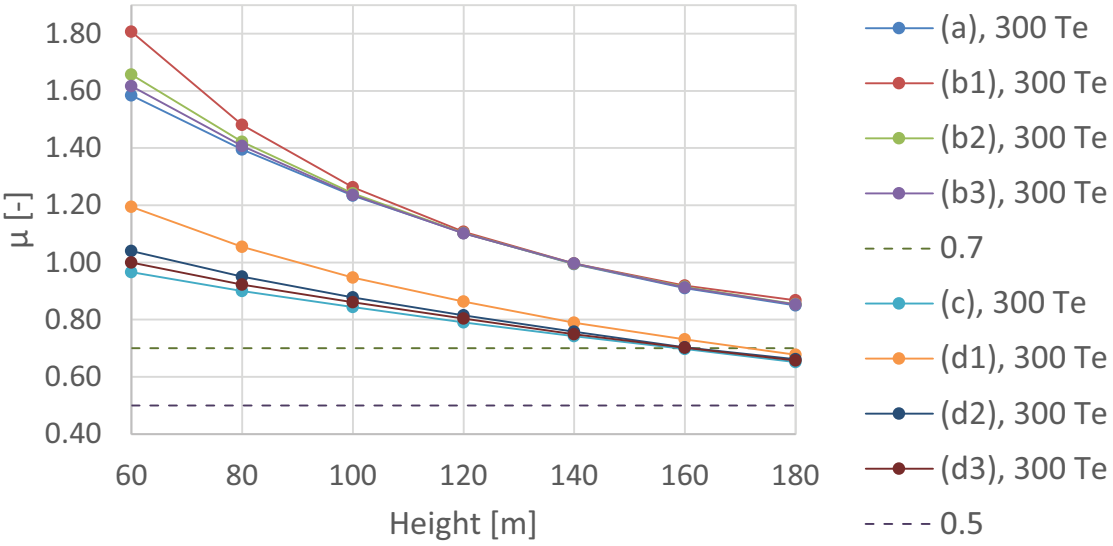

Figure 91: Buckling factor for the strong direction of the NYW sections, for the 300 Te system.

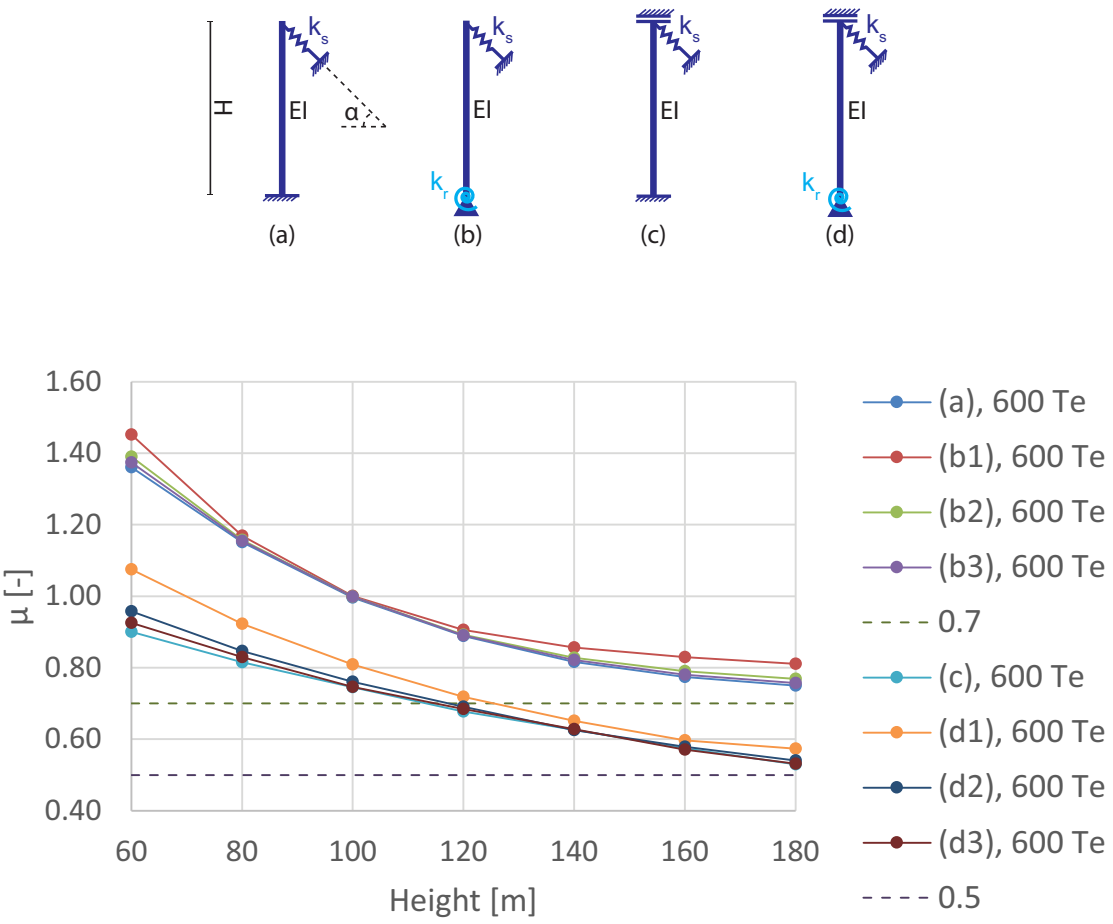

Figure 92: Buckling factor for the strong direction of the NYW sections, for the 600 Te system.

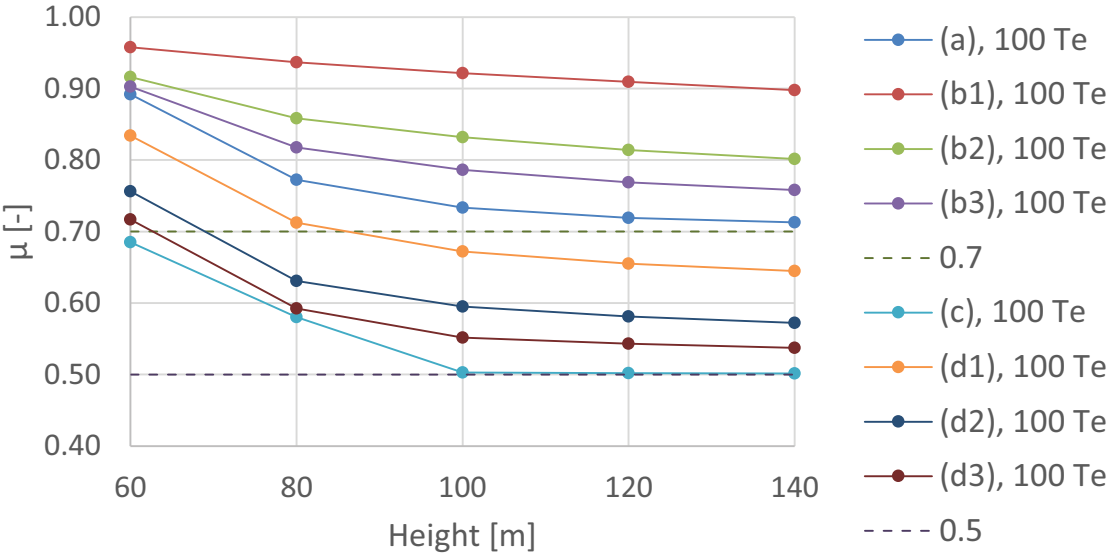

Figure 93: Buckling factor for the MSG sections, for the 100 Te system.

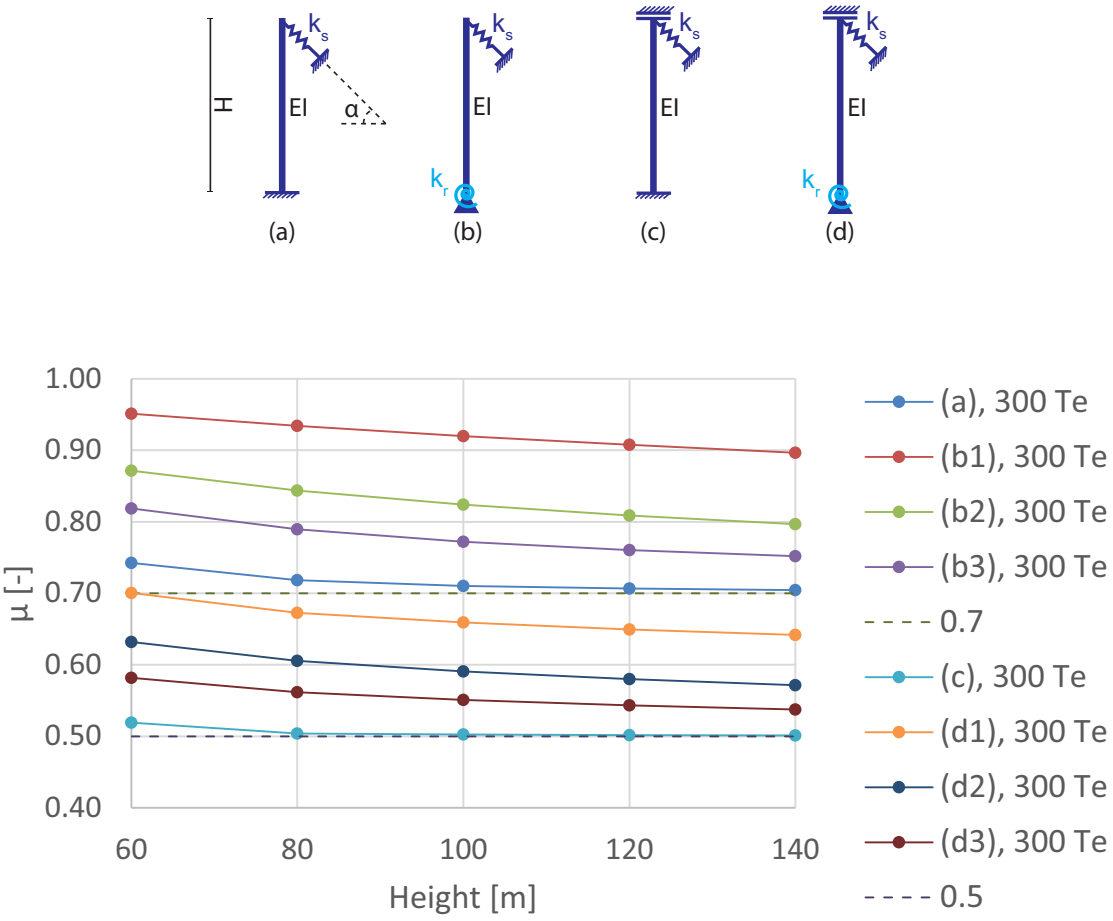

Figure 94: Buckling factor for the MSG sections, for the 300 Te system.

I.2 Deflection

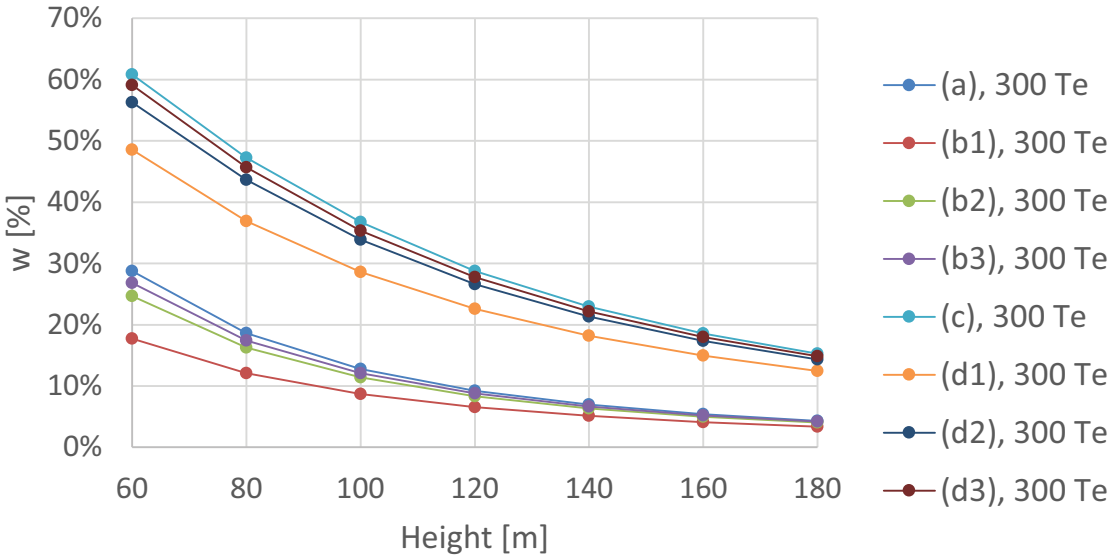

Figure 95: Deflection of column with guy lines, as a percentage of deflection without guy lines: Weak direction of the NYW sections and the 300 Te strand jack system.

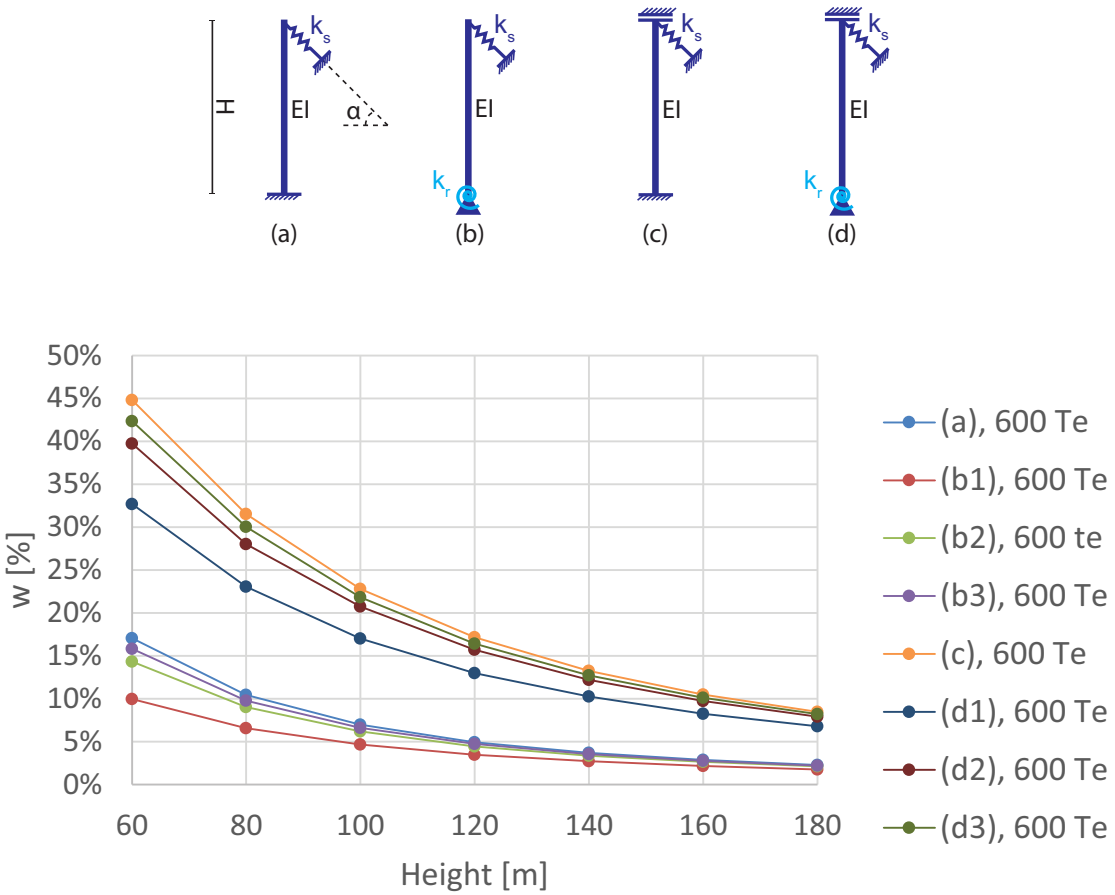

Figure 96: Deflection of column with guy lines, as a percentage of deflection without guy lines: Weak direction of the NYW sections and the 600 Te strand jack system.

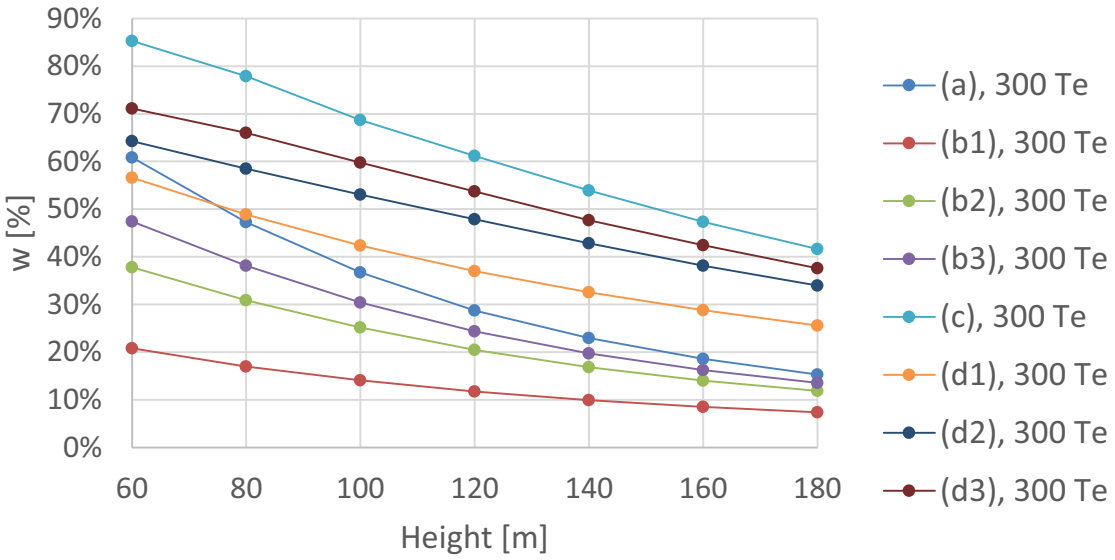

Figure 97: Deflection of column with guy lines, as a percentage of deflection without guy lines: Strong direction of the NYW sections and the 300 Te strand jack system.

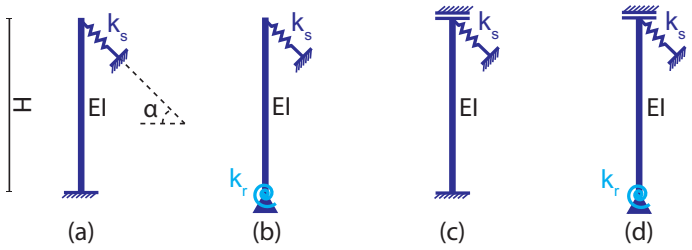

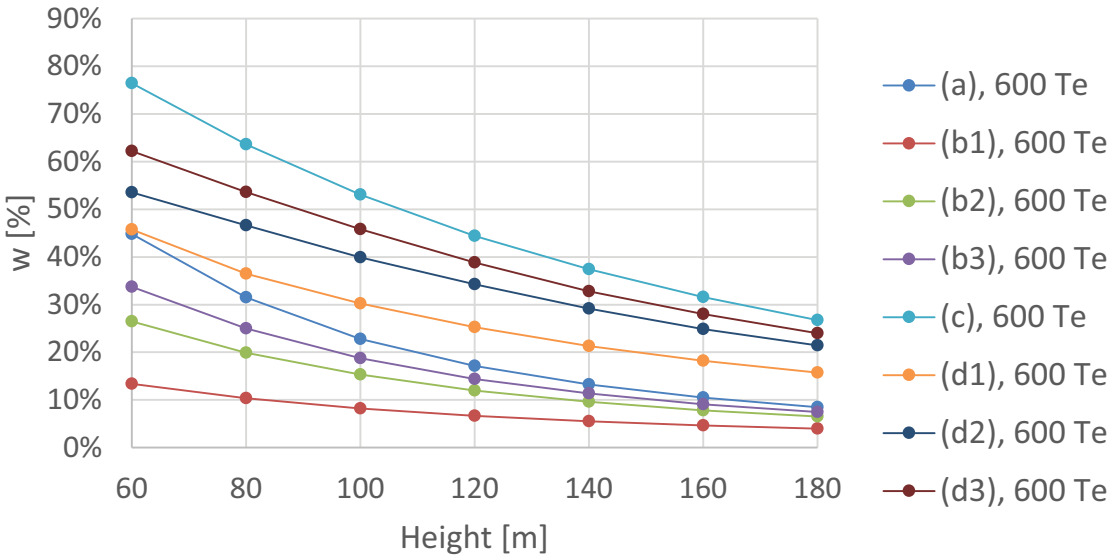

Figure 98: Deflection of column with guy lines, as a percentage of deflection without guy lines: Strong direction of the NYW sections and the 600 Te strand jack system.

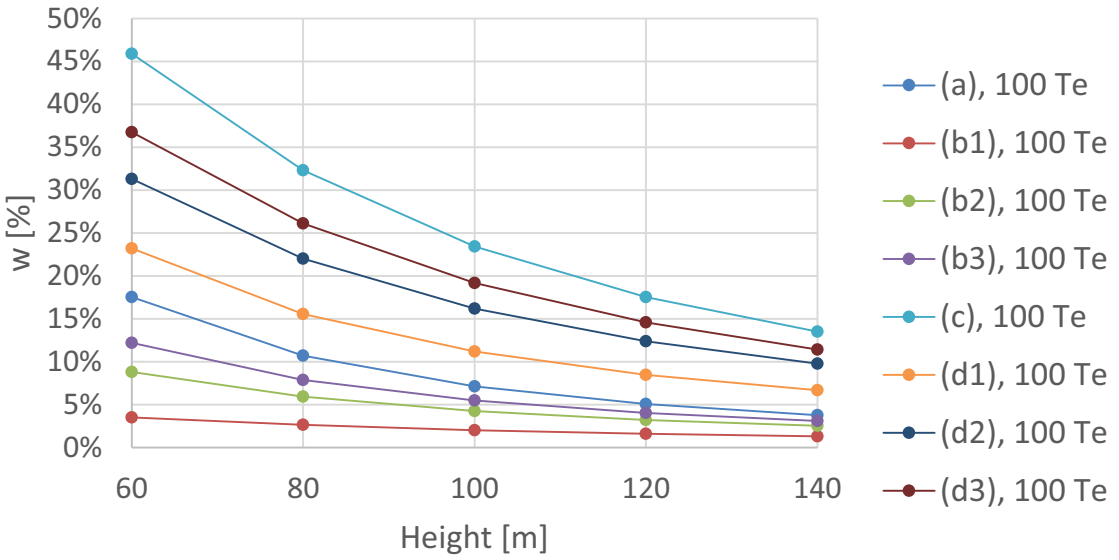

Figure 99: Deflection of column with guy lines, as a percentage of deflection without guy lines: MSG sections and the 100 Te strand jack system.

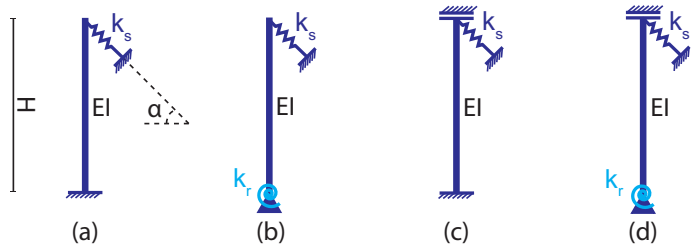

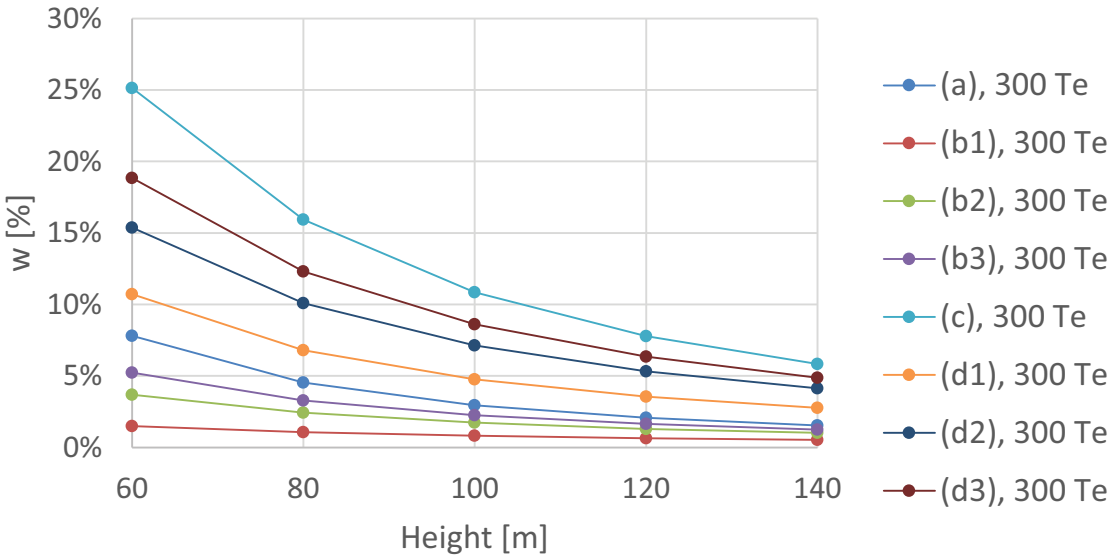

Figure 100: Deflection of column with guy lines, as a percentage of deflection without guy lines: MSG sections and the 300 Te strand jack system.

I.3 Load Distribution

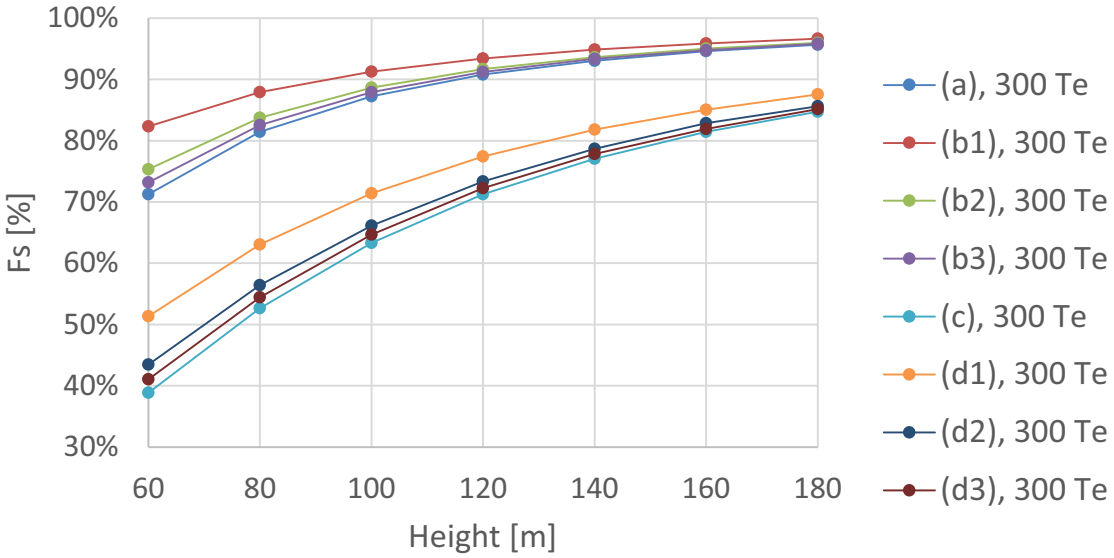

Figure 101: Horizontal load in the guy lines, as percentage of the applied horizontal load: Weak direction of the NYW section, 300 Te strand jack system.

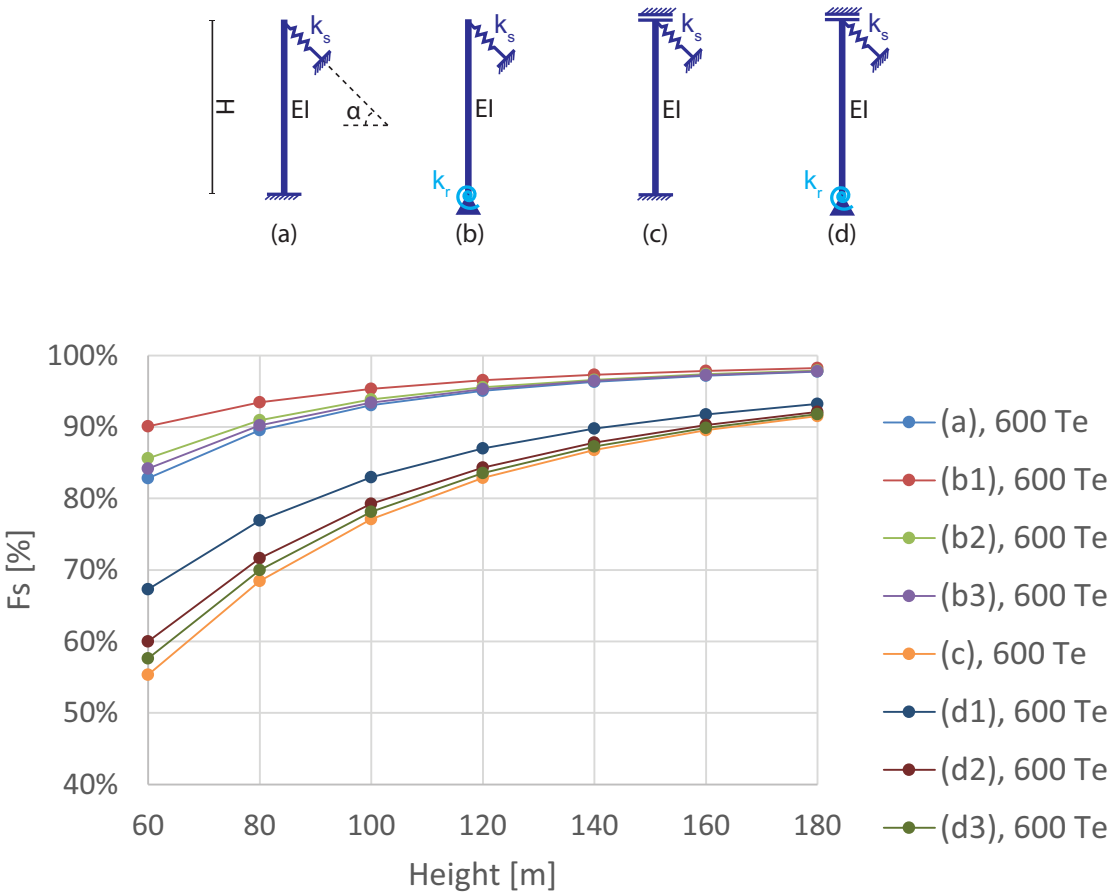

Figure 102: Horizontal load in the guy lines, as percentage of the applied horizontal load: Weak direction of the NYW section, 600 Te strand jack system.

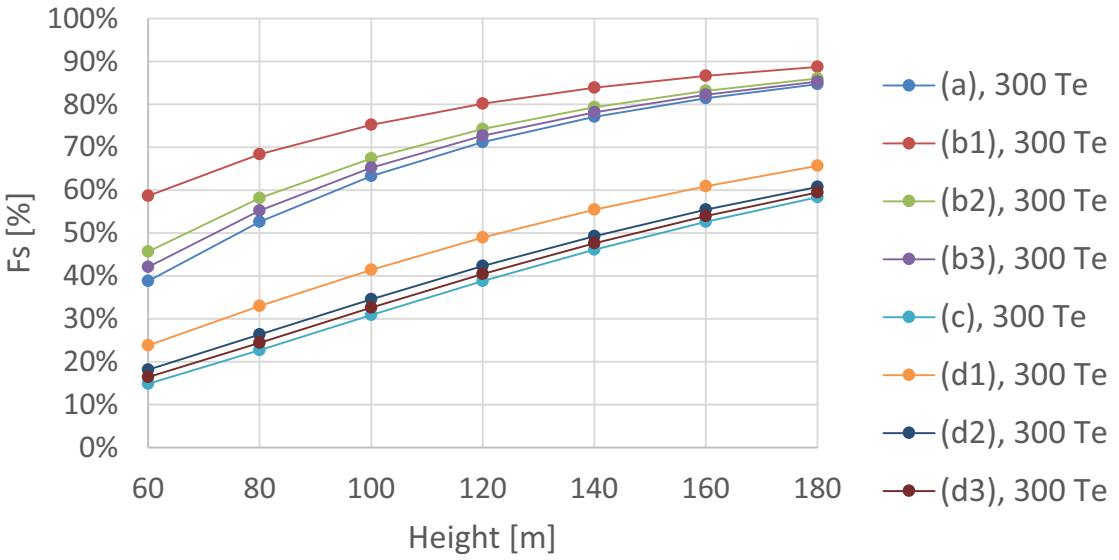

Figure 103: Horizontal load in the guy lines, as percentage of the applied horizontal load: Strong direction of the NYW section, 300 Te strand jack system.

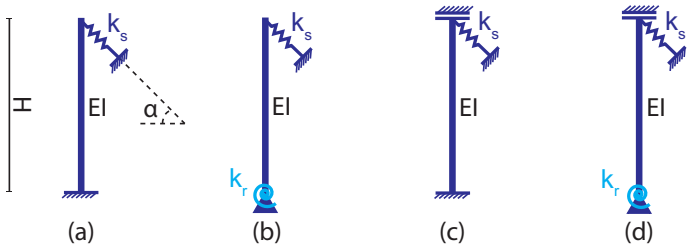

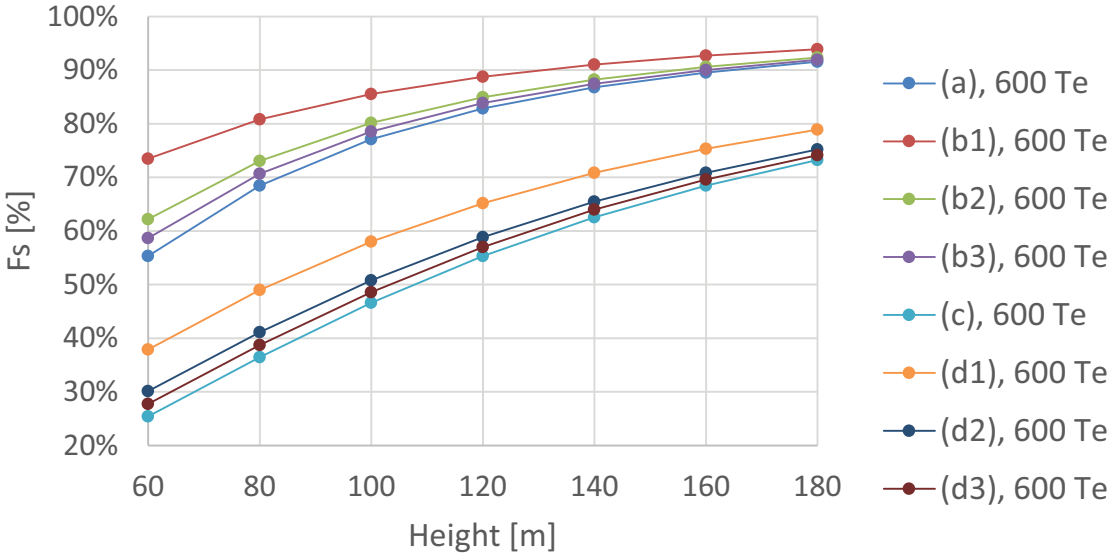

Figure 104: Horizontal load in the guy lines, as percentage of the applied horizontal load: Strong direction of the NYW section, 600 Te strand jack system.

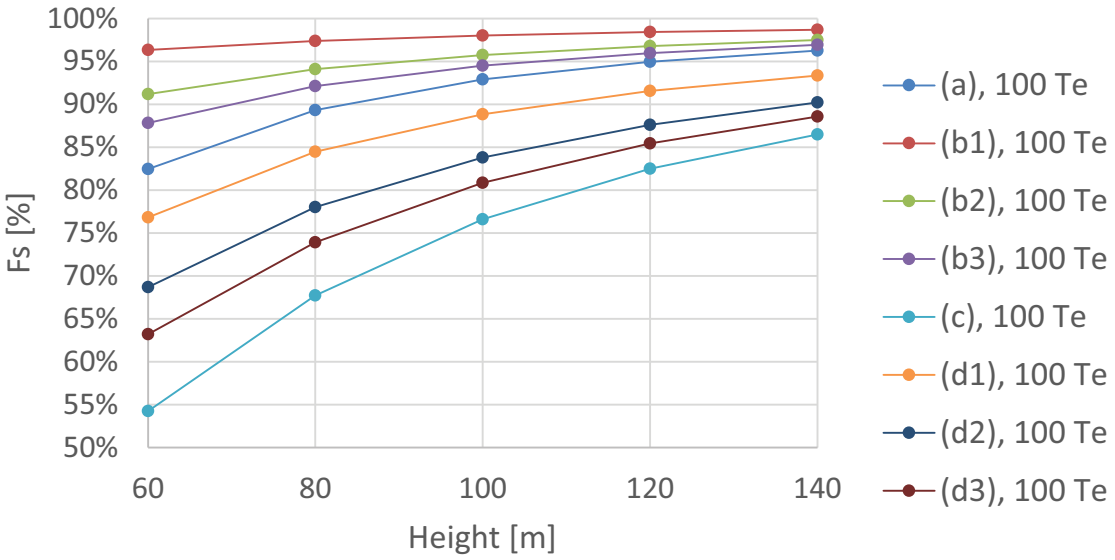

Figure 105: Horizontal load in the guy lines, as percentage of the applied horizontal load: MSG sections, 100 Te strand jack system.

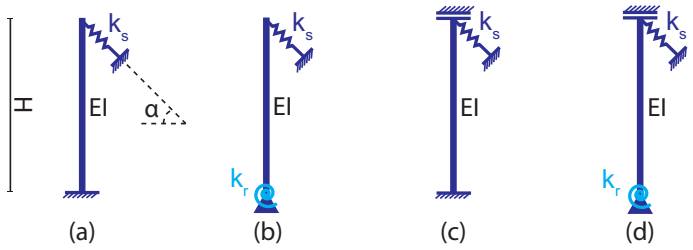

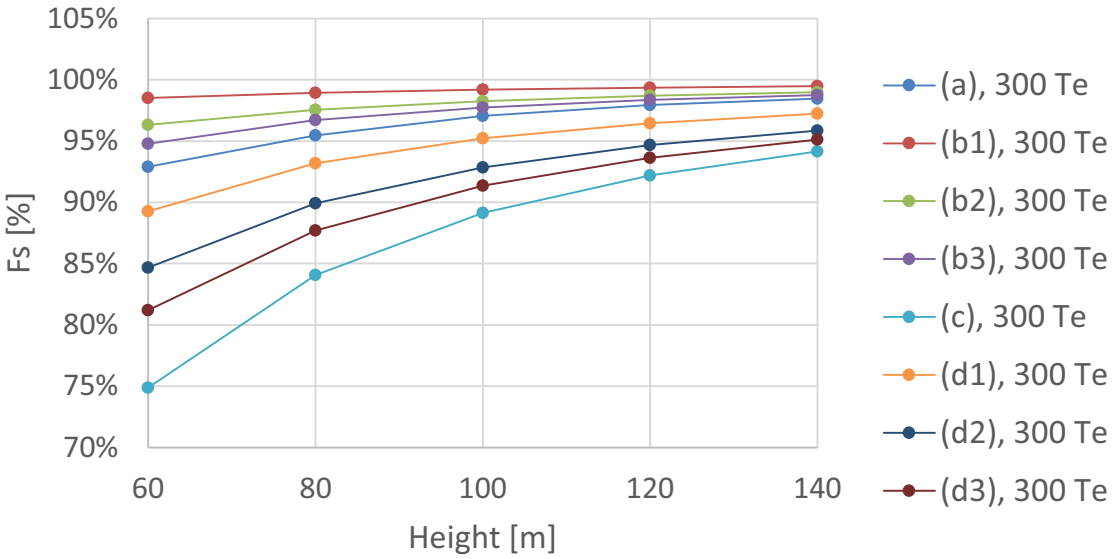

Figure 106: Horizontal load in the guy lines, as percentage of the applied horizontal load: MSG sections, 300 Te strand jack system.